

INTERFERENCE MITIGATION IN COLOCATED WIRELESS SYSTEMS

Shabbir Ahmed

B.Sc. in Computer Science

School of Engineering and Science
Faculty of Health, Engineering and Science
Victoria University

SUBMITTED IN FULFILLMENT OF THE
REQUIREMENTS FOR THE DEGREE OF
DOCTOR OF PHILOSOPHY

DECEMBER 2012



© Copyright by Shabbir Ahmed 2013
All Rights Reserved

To my family.

DOCTOR OF PHILOSOPHY DECLARATION

I, Shabbir Ahmed, declare that the PhD thesis entitled INTERFERENCE MITIGATION IN COLOCATED WIRELESS SYSTEMS is no more than 100,000 words in length including quotes and exclusive of tables, figures, appendices, bibliography, references and footnotes. This thesis contains no material that has been submitted previously, in whole or in part, for the award of any other academic degree or diploma. Except where otherwise indicated, this thesis is my own work.

Shabbir Ahmed

Date: December 14, 2012

Abstract

The placement of base station transceivers at close proximity to one another is a major challenge for RF engineers. In a colocated setting, the base station receivers have to receive weak desired signals in the presence of high-power transmit/jamming signals from colocated base station transmitters; resulting in major interference issues. The thesis identifies two major mechanism of interference for the colocated victim receiver. First, the strong jamming signals mix within the victim receiver front-end to produce intermodulation products that may fall on its desired receive channel and cause interference. The strong signals may also saturate the receiver circuits and cause desensitization. Second, large jamming signals from one colocated transmitter can radiate into the antenna system of a second colocated transmitter. The signals enter the second transmitter in the reverse direction and mix in the output stage of its power amplifier to produce intermodulation products. These ‘reverse’ intermodulation products get radiated from the antenna system and may fall on the victim receiver’s desired channel.

The thesis proposes a reference antenna based adaptive cancellation system that reduces the jammers before they hit the victim receiver’s front-end circuits, thus, mitigating intermodulation distortions and desensitization. The practicality of the system is analyzed. Practical measurements show an increased third-order intercept point (IP3) performance, implying a higher tolerance to jamming signals. This benefit comes at the expense of reduced sensitivity. The IP3 and noise figure expressions derived for the overall system reveals that the cancellation coupler in the reference path is a compromise between achieving higher IP3s and lower noise figures. Hence,

a novel signal-to-interference-and-noise (SINR) analysis is performed to find the optimum coupler value that maximizes the system SINR performance. A hardware prototype achieved a 42dB SINR improvement over a system without the canceling circuit. It managed 46dB cancellation of jammers in a controlled environment and 25dB in a realistic over-the-air setup. The jammer cancellations were enough to remove any distortions generated within the victim receiver.

Jammer reduction at the victim receiver does not mitigate the reverse intermodulation products that are radiated from the output of the colocated transmitters. Hence, the thesis proposes an architecture that regenerates an estimate of the reverse intermodulation products using the fundamental jammer components and mitigates them in a postdistortion cancellation circuit. The cancellation is done in baseband using digital signal processing techniques. A disadvantage is the wide bandwidth and high sampling rates required to receive both jammers and the corrupt desired signal in a single unit, particularly when the jammers are well out-of-band. A novel multiple-front-end receiver architecture is developed to overcome the high sample rate issue. However, this leads to a frequency offset problem in the regenerated distortion estimate. A frequency offset correction technique to mitigate the offset is incorporated within the distortion regeneration circuit. This novel technique uses signal correlation to align the frequency, phase and amplitude of the distortion estimate with the interfering reverse intermodulation product. Simulations and theoretical analysis are performed to characterize the postdistortion cancellation system. A prototype of the cancellation system demonstrates 16dB reduction of the interfering reverse intermodulation product.

Acknowledgments

First and foremost, I thank Allah (SWT) for giving me the strength, knowledge and ability to complete this thesis.

I am highly grateful and indebted to my supervisor, Prof. Mike Faulkner, for his unreserved guidance and support during the whole period of my candidature. His kindness, patience and encouragement helped me to develop as a competent researcher. This thesis would not have been possible without his research expertise and in-depth knowledge. My sincere gratitude to Dr. Stephen Collins, Lance Linton, Dr. Phillip Conder, Prof. Aladin Zayegh and Prof. Akhtar Kalam for their help and guidance.

I am most grateful to Dr. Lesley Birch, Elizabeth Smith, Sue Davies and Shukonya Benka for their continuous support over the last four years. I want to thank Victoria University for giving me the opportunity to undertake postgraduate studies here in Australia.

I want to acknowledge all my past and present colleagues in the telecommunication and microelectronics group who have always helped and encouraged me with my work, in particular, Waqas, Robab, Rahele, Shahryar, Faizan, Rizwan, Zaheer, Reza, Vandana, Micheal, Hojjat, Asyik, Hadi, Baharuddin and Andrew. A special thanks to my friend Mustafa and his family for their kind support.

Last but not the least, my deepest gratitude to my parents, two brothers, sister, and my wife for their love and support. I am ever indebted to my wife for putting up with my late-night hours in the laboratory.

Contents

Doctor of Philosophy Declaration	v
Abstract	vii
Acknowledgments	ix
Contents	x
List of Figures	xiv
List of Abbreviations	xviii
List of Symbols and Variables	xx
1 Introduction	1
1.1 Colocation	1
1.2 Interference Issues	3
1.3 Research Goals	5
1.4 Research Contributions	5
1.5 Organization of thesis	6
2 Basic Concepts	8
2.1 Noise and Noise Factor	9
2.2 RF Attenuators	10
2.3 Couplers	10
2.4 Nonlinearity	11

2.4.1	Harmonic Distortion	12
2.4.2	Intermodulation Distortion	12
2.4.3	1-dB Compression Point (P_{1dB})	14
2.4.4	Third-order Intercept Point (IP3)	15
2.4.5	Bandwidth Expansion	18
2.5	Practical Measurements	18
2.5.1	Reverse IM3	19
2.5.2	Desensitization/Blocking	21
2.6	Summary	22
3	Literature Review	23
3.1	Filtering Solutions	24
3.1.1	Knowledge-based Filtering	24
3.1.2	Passive Filtering	25
3.2	Adaptive Cancellation for Forward IM	25
3.2.1	Single Loop Narrowband Cancellation	26
3.2.2	Single Loop Wideband Cancellation	27
3.2.3	Multiple-loop Multi-band Cancellation	27
3.3	The Proposed Solution for Forward IM	29
3.4	Adaptive Cancellation for Reverse IM	30
3.4.1	Transmitter-end Solutions	30
3.4.2	Interference Cancellation Using Regenerated Distortions	31
3.4.2.1	Analog Second-order Postdistortion	32
3.4.2.2	Analog Third-order Postdistortion	32
3.4.2.3	Hybrid Analog and Digital Polynomial Postdistortion	33
3.4.2.4	Digital Polynomial Postdistortion	34
3.5	The Proposed Solution for Reverse IM	34
3.6	Summary	36
4	The Adaptive Cancellation System and its Dynamic Range	37
4.1	The Adaptive Cancellation Architecture	38

4.2	Dynamic Range of the Proposed System	39
4.2.1	Third-order Intercept Point (IP3)	39
4.2.2	Noise Analysis	41
4.2.3	Discussion	43
4.3	Experimental Results	43
4.4	Summary	46
5	Optimized Interference Cancellation	47
5.1	Derivation of SINR	48
5.1.1	Third-order Intermodulation Distortion at the Receiver	50
5.1.2	Signal and Noise at the Receiver	51
5.1.3	Signal to Interference and Noise Ratio	51
5.2	Optimum Coupling	52
5.3	Hardware Setup and Convergence	54
5.4	Results	57
5.5	Summary	60
6	An Over-the-air Adaptive Cancellation Prototype	62
6.1	Desired Signal Sample in the Reference Input	62
6.2	Experiment Results	65
6.3	Summary	68
7	Postdistortion Cancellation System for Reverse IM Products	70
7.1	Reverse Intermodulation Products	72
7.2	Proposed Architecture and Digital Signal Processing	74
7.2.1	Multiple Receivers	76
7.2.2	Nonlinear Polynomial Function: Cuber	78
7.2.3	Coarse Frequency Correction	79
7.2.4	Fine Frequency Correction	80
7.2.5	Gain-Phase Correction	81
7.2.6	Desired Signal Demodulation	81

7.3	Simulations and Analysis	82
7.3.1	Buffer/Data Processing Block Size N	82
7.3.2	Fine Frequency Correction	86
7.3.3	Improved Feedback Fine Frequency Correction	87
7.3.4	Coarse Frequency Correction	90
7.4	Practical Measurements	91
7.5	Summary	96
8	Conclusion	98
8.1	Future Work	100
8.1.1	Multi-loop Adaptive Cancellation	100
8.1.2	Cognitive Sensing and Jammer Selection	101
A	The Modulation Parameter Factor η	102
B	The Variance of \hat{f}_k^{Fine} due to Frequency Offset	104
	References	106

List of Figures

1.1	Colocation of six base stations on one roof top. Birmingham, UK.	2
1.2	Multiplexing of base station transmit signals. f_c , f_{c_1} , f_{c_2} , and f_{c_n} are carrier frequencies; Δf_1 , Δf_2 , and Δf_n are frequency offsets from f_c	3
1.3	Forward and reverse IM products.	4
2.1	Noise within a radio system component.	9
2.2	Cascaded system components (Noise factor).	9
2.3	A directional coupler.	10
2.4	Even and odd-order intermodulation products along with the fundamentals, harmonics and DC [12].	13
2.5	1dB compression point.	14
2.6	Third-order intermodulation distortion causing interference in the desired channel of a receiver [6].	15
2.7	Two-tone test results for IP3 measurement.	17
2.8	Cascaded system components (IP3).	17
2.9	Third-order intermodulation distortion causing interference in the desired channel of a receiver.	18
2.10	Reverse IM3.	19
2.11	Reverse IM3 Experiment.	20
2.12	Characterization of the reverse IM distortions.	21
2.13	Desensitization/Blocking. Spectrum at the LNA output. Desired signal at 920MHz and Jamming signal at 921MHz.	22

3.1	Passive pre and post filtering to mitigate colocated interference issues [17].	25
3.2	Transmitter leakage cancellation for a colocated GPS receiver [22]. . .	26
3.3	Interference cancellation unit for colocated radios [24].	27
3.4	A double loop cancellation adaptive duplexer [25].	28
3.5	The adaptive noise canceling concept [26].	29
3.6	Reverse IM cancellation system using direct feed phasing [28].	31
3.7	Analog second-order postdistortion [35].	32
3.8	Analog third-order postdistortion [36].	32
3.9	Hybrid analog and digital polynomial postdistortion [37].	33
3.10	Digital polynomial postdistortion [38].	34
3.11	Proposed reverse IM postdistortion solution.	35
4.1	Proposed adaptive cancellation system for colocated transceivers. . .	38
4.2	IP3 analysis of the proposed system.	40
4.3	Noise analysis of the proposed system.	42
4.4	Two-tone test on a receiver LNA with 19dB gain and 6dBm input IP3. 44	
4.5	Laboratory setup for IP3 and noise measurements.	44
4.6	Spectrum of the receiver with and without the proposed cancellation system (using -10dB coupler) during a two-tone test with an input power of -5dBm	45
5.1	An adaptive cancellation system.	48
5.2	Signal-to-interference-and-noise analysis.	49
5.3	Optimum coupler C_{opt} as a function of jammer X and the Λ value (Λ is primarily a function of the dynamic range of the components in the reference path).	53
5.4	Laboratory Setup: Signal Generator 1 generates the desired signal S and Signal Generator 2 generates the two tone jamming signal which is split into two with the Power Splitter to have equal levels of jammer X on both the Primary Path and the Reference Path.	54

5.5	Learning curve of the adaptive cancellation system during a two-tone test with an input power of -10dBm.	56
5.6	Spectrum at the receiver with and without the proposed cancellation system during a two-tone test with an input power of -10dBm; the fundamentals are at 919.75MHz and 920.25MHz, and the IM3 products are at 919.25MHz and 920.75MHz respectively. The desired signal is not included.	57
5.7	SINR vs jammer with different couplers. Noise bandwidth, $B_W = 5\text{MHz}$	58
6.1	The proposed adaptive cancellation system.	63
6.2	Experimental setup.	65
6.3	Signals, as seen by the victim receiver. Signal constellation scatter plots (LHS) and GNU radio spectrum plots (RHS). The GNU radio spectrum plots show relative scales with 75dB representing -39dBm, and on the frequency scale 0 representing 920MHz.	67
7.1	Colocated base station transceivers.	72
7.2	Proposed DSP.	75
7.3	SIR_o vs (N/OSR)	84
7.4	The effect of frequency offset f^{Fine} on the output SIR. 1bin= f_s/N Hz. ‘*’s represent theoretical results.	85
7.5	Performance with feedforward fine frequency correction. ‘*’s represent theoretical results.	87
7.6	Proposed feedback fine frequency correction.	88
7.7	Performance with feedback fine frequency correction.	89
7.8	Frequency drift tracking by \hat{f}_k^{Fine}	89
7.9	Probability of acceptable coarse frequency correction ($\Delta f - 0.25f_s/N \leq f^{Coarse} \leq \Delta f + 0.25f_s/N$) for $M = 2N$, $M = 8N$, $M = 16N$ and $M = 32N$	90
7.10	Colocated transmitters generating reverse IM3 products.	92

7.11 Frequency spectrum of the jammers and the IM3 product of concern.	93
7.12 Experiment results. Signal constellation scatter plots (LHS) and frequency spectrum plots (RHS). The spectrum plots show relative scales with 20dB representing -75dBm.	94
7.13 Frequency spectrum of the jammers.	95
7.14 Fine frequency tracking by \hat{f}_k^{Fine} . $f_s=0.5\text{Msamples/s}$, $N=4096$	95
B.1 Linear phase $\theta(= 2\pi f^{Fine} N/f_s)$ across a block.	104

List of Abbreviations

ADC	Analog-to-Digital Converter
DAC	Digital-to-Analog Converter
DC	Direct Current
DSP	Digital Signal Processing
FDD	Frequency Division Duplex
FFT	Fast Fourier Transform
FIR	Finite Impulse Response
GPA	Gain-Phase Adjuster
GPS	Global Positioning System
GSM	Global System for Mobile Communications
HSPA	High Speed Packet Access
IF	Intermediate Frequency
IM	Intermodulation
IM2	Second-order Intermodulation
IM3	Third-order Intermodulation
IP3	Third-order Intercept Point
ISM	Industrial, Scientific and Medical
LHS	Left Hand Side
LMS	Least Mean Square
LNA	Low Noise Amplifier
LO	Local Oscillator
MAC	Medium Access Control
OFDM	Orthogonal Frequency Division Multiplexing

P_{1dB}	1-dB Compression Point
PA	Power Amplifier
QAM	Quadrature Amplitude Modulation
QPSK	Quadrature Phase Shift Keying
RF	Radio Frequency
RHS	Right Hand Side
SAW	Surface Acoustic Wave
SDR	Software Defined Radio
SINR	Signal-to-Interference-and-Noise Ratio
SIR	Signal-to-Interference Ratio
UE	User Equipment
UHF	Ultra High Frequency
USRP	Universal Software Radio Peripheral
VHF	Very High Frequency
WCDMA	Wideband Code Division Multiple Access
WLAN	Wireless Local Area Network

List of Symbols and Variables

$(\cdot)^*$	Complex conjugate
$(\cdot)^A$	Signals radiated from jammer A
$(\cdot)^B$	Signals radiated from jammer B
$(\cdot)^D$	Signals radiated from remote terminal D
$(\cdot)^H$	Conjugate transpose
$(\cdot)_k$	k-th block of samples
$(\cdot)_r$	RF signals
γ	Primary to reference SIR voltage ratio
Γ	Primary to reference SIR power ratio
δ_M	FFT frequency resolution
Δf	Total frequency offset (coarse + fine)
$\Delta f_1, \Delta f_2, \dots, \Delta f_n$	Frequency offsets from f_c
ε	Error signal
η	Modulation parameter factor
θ	Linear phase across an averaging block
Λ	A function of GPA dynamic range properties
ρ	gain-phase correction factor
$\hat{\rho}$	gain-phase correction factor estimate
$\sigma_{(\cdot)}^2$	Variance of a signal
ϕ_k	Correlation between estimate $\hat{\mathbf{u}}'_k$ and primary reception \mathbf{y}_k
$\Phi(l)$	FFT of estimate \hat{u} correlated with primary reception y
1a	Coupling path coupler 1

$1b$	Through path coupler 1
$2b$	Through path coupler 2
a	Complex envelope of jammer A
$\arg(\cdot)/\angle(\cdot)$	Phase of a complex value
Amp	Amplifier
b	Complex envelope of jammer B
B_W	Noise bandwidth
C	Coupling gain of the cancellation coupler (Coupler 1)
C_{opt}	Optimum coupling value
C_ALG	FFT frequency correction algorithm
CF	Energy cost function at sampling coupler (Coupler 2)
d_1	Distance between reference antenna and jammer antenna
d_2	Distance between primary antenna and jammer antenna
$E\{\cdot\}$	Mathematical expectation
f_a	Carrier frequency of jammer A
f_b	Carrier frequency of jammer B
$f_c, f_{c_1}, f_{c_2}, \dots, f_{c_n}$	Carrier frequencies
f^{Coarse}	Coarse frequency offset
f_d	Carrier frequency of desired signal
f^{Fine}	Fine frequency offset
\hat{f}^{Fine}	Fine frequency offset estimate
f_s	Sampling frequency of SDRs
f_u, f_v	Carrier frequencies of reverse IM distortions
F, F_a, F_b, F_c	Noise factors of radio components
F_A	Amplifier noise factor
F_L	Attenuator noise factor
F_{RX}	Receiver noise factor
F_T	Effective noise factor
F_V	Vector modulator noise factor
$\mathcal{F}\{\cdot\}$	Fourier transform

LIST OF SYMBOLS AND VARIABLES

g_1	Non-linear system voltage gain
g_2	Non-linear system quadratic distortion coefficient
g_3	Non-linear system cubic distortion coefficient
g_3^A	Jammer A's power amplifier cubic distortion coefficient
g_3^B	Jammer B's power amplifier cubic distortion coefficient
g_{REF}	Reference path scaling coefficient
G, G_a, G_b, G_c	Gains of radio components
G_A	Amplifier gain
G_{CAN}	Cancellation gain
G_{CPL2}	Coupler 2 through path gain
G_e	GPA effective gain
G_L	Attenuator gain
G_{RX}	Receiver gain
G_T	Total system gain
G_V	Vector modulator gain
$h_a, h_u^A, h_b, h_u^B, h_{ba}, h_{ab}, h_d$	Channel gains
H	Jammer's gain on the ref. ant. w.r.t. the pri. ant.
I_{SYS}	IM3 distortion/interference at receiver output
IP_{1dB}	Input P _{1dB} power
$IIP3$	Input IP3 power
$IIP3_a, IIP3_b, IIP3_c$	Input IP3 powers of radio components
$IP3_A$	Amplifier input IP3
$IP3_{RX} / IIP3_{RX}$	Receiver input IP3
$IP3_T$	Effective input IP3
$IP3_V$	Vector modulator input IP3
k_B	Boltzmann's constant
l_{max}	Highest power bin in the M -point FFT
L	Attenuator
M	FFT length
N	Number of samples in an averaging block

N_s	Number of uncorrelated samples in an averaging block
N_T/ N_{SYS}	Total noise at receiver front-end
$\mathcal{N}\{\cdot\}$	Natural distribution
\mathbf{o}_k	Signal at canceler output
$OIP3$	Output IP3 power
$OIP3_A$	Amplifier output IP3
$OIP3_e$	GPA effective output IP3
OP_{1dB}	Output P_{1dB} power
OSR	Over-sampling rate of the desired signal
P_{SAT}	Saturated power output
r	Received signal at RX input
$\text{Re}[\cdot]$	Real part of a complex signal
$\text{RMSE}(\cdot)$	Root mean square error
RX	Victim Receiver
Rx0	Primary SDR front-end
Rx1, Rx2, ...	Auxiliary SDR front-ends
s	Desired signal complex envelope (primary path)
s_{REF}	Desired signal complex envelope at reference antenna
S	Desired signal power at primary antenna
S_{SYS}	Signal level at receiver output
$SINR_{SYS}$	SINR at receiver front-end
$SINR_{SYS} _{plateau}$	SINR at noise-dominated plateau region
$SINR_{SYS} _{waterfall}$	SINR at distortion-dominated waterfall region
SIR_o	output SIR
SIR_y	input SIR of primary reception (y)
SIR_{PRI}	SIR at primary antenna
SIR_{REF}	SIR at reference antenna
T_0	Standard noise temperature 290K
T_e	GPA effective output noise temperature
T_{ex}	Excess noise temperature of radio components

LIST OF SYMBOLS AND VARIABLES

T_{RX}	Receiver input noise temperature
u, v	Complex envelopes of reverse IM distortions
\hat{u}	Distortion estimate
U	IM3 distortion power at GPA output
V	Vector Modulator
x_{PRI}	Jamming signal complex envelope at primary antenna
x_{REF}	Jamming signal complex envelope at reference antenna
X_d	Design jamming level
X_{PRI}	Jamming signal power at primary antenna
X_{REF}	Jamming signal power at reference antenna
y	Received complex envelope of desired signal plus distortion
z^{-1}	Unit delay

Chapter 1

Introduction

Mobile phones have been a game-changer in the world of communications. The wireless access of information and telecommunication have changed the operational dynamics of individuals and industries across-the-board. According to recent statistics, at the end of 2011, 5.9 billion mobile phones are being used in the world [1], which constitutes about 80% of the world's population. The urbanization of population masses and limited spectrum resources have led to frequency reuse in the form of cellular network architectures. Such network architectures have lead to a diverse range of challenges.

1.1 Colocation

One such challenge is the placement of a number of radio frequency (RF) transceiver antennas at close proximity to one another, a concept known as colocation. Colocation has been a major aspect of concern in different fields of communication.

Government armed forces were the first to confront the problem. They require different wireless platforms to share a small site because of their mobile nature (e.g. battleships, aircraft, and expeditionary fighting vehicles) [2] [3] [4]. The range of wireless platforms includes VHF/UHF (very high frequency/ ultra high frequency) dual-band multi-mode terminals for voice and data communications, satellite communications transceivers, line-of-sight tactical communications equipment, global

positioning system (GPS) receivers, radars, surveillance systems, and others. They all have the potential to interfere with each other because of the close proximity of the antennas.

Lately, the advent of smart-phones and affordable mobile communication services have seen an exponential growth in the wireless subscriber base. Service providers are having to deploy a larger number of base stations every year to meet the demands. In the process, they have exhausted the most suitable locations for establishing new green field base station sites. Also, there are growing community concern in regards to visual pollution and health effects of RF radiation from base stations. As a result, multiple service providers are having to mount base station antennas on selective common sites. Fig. 1.1 shows antennas from six base stations collocated on one roof top.

Sharing a common site has economic advantages. Multiple service providers can consolidate to reduce maintenance, rental, logistics and other recurring expenses. In addition, there are RF advantages, collocation of base stations helps in reducing the near far problem at the user equipment (UE) because both desired and unwanted signals have a similar signal strength. This allows UEs to have reduced filtering and dynamic range specifications, a key requirement for reducing the cost and power



Fig. 1.1: Collocation of six base stations on one roof top. Birmingham, UK.

consumption in today's mobile devices. However, major interference challenges need to be addressed for the base station receivers.

1.2 Interference Issues

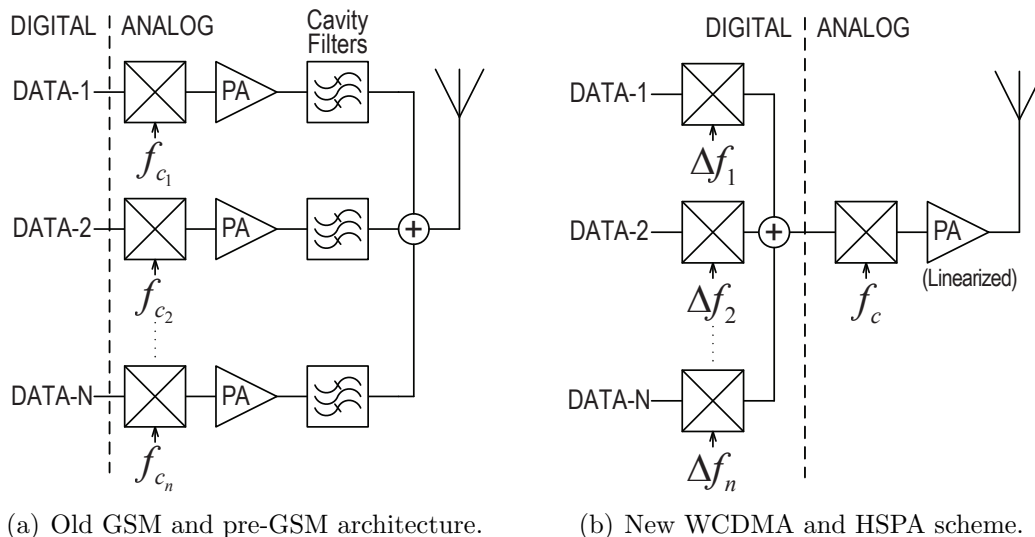


Fig. 1.2: Multiplexing of base station transmit signals. f_c , f_{c_1} , f_{c_2} , and f_{c_n} are carrier frequencies; Δf_1 , Δf_2 , and Δf_n are frequency offsets from f_c .

In a colocated setting, base station receivers have to receive weak desired signals in the presence of high-power transmit signals from neighbouring base station antennas; resulting in major interference issues. The spectrum can get congested very quickly because each additional antenna can carry many transmissions at different carrier frequencies. Multi-carrier power amplifiers (PA) or multi-coupling networks of cavity filters are often used to combine the high power signals prior to the antenna, as seen in Fig. 1.2. At the victim receiver, such high-power transmit/jamming signals, regardless of their carrier frequencies, may cause desensitization and blocking [5] [6] by forcing its circuits into saturation. A more significant concern is the formation of intermodulation (IM) distortion products. There are two major sources of IM products that fall in the desired receive channel of the victim receiver and cause interference.

1. Forward IM distortions generated within the victim receiver.

- Reverse IM distortions generated within the jammer transmitters.

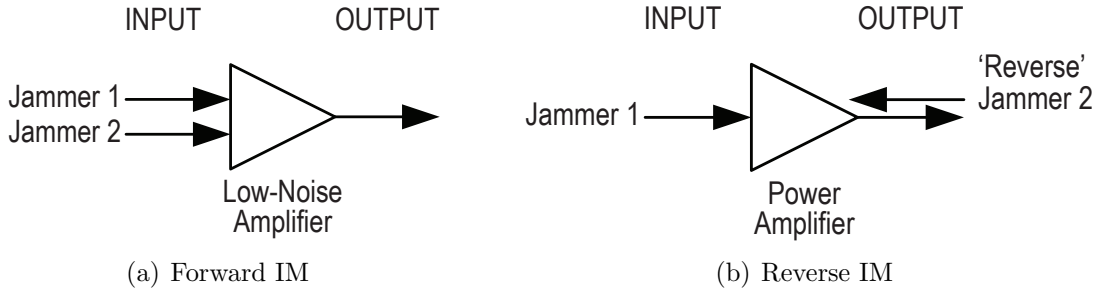


Fig. 1.3: Forward and reverse IM products.

First, the IM distortions produced within the victim receiver's front-end circuits are caused by the high power signals from colocated transmitters. The low noise amplifier (LNA) and mixer stages are most susceptible to the large jamming signals. Odd order and especially third-order intermodulation (IM3) distortions are generated and cause spectral expansion of the jamming signal into its adjacent channels, which decays with increasing frequency separation from the desired channel. If more than one high power jammer exists then intermodulation spurs are generated at multiples of the carrier separation. In this thesis, we refer to these intermodulation products as 'forward' IMs, as seen in Fig. 1.3(a), they are produced when jamming signals are applied to the input of the receiver's nonlinear circuit. The forward IMs can fall on the desired receive channel. Even-order distortions are caused by circuit imbalances or self-mixing in the mixer. In the case of a direct conversion receiver, the second-order intermodulation (IM2) distortions fall directly on the baseband irrespective of the jammer's frequency [7].

Second, the IM distortions radiated from the colocated jammer transmitters. These IM distortions are generated when a high powered jamming signal from one colocated jammer radiates in through the antenna system and mixes at the output of the power amplifier of a second colocated jammer. As seen in Fig. 1.3(b), these distortions are more precisely termed as 'reverse' IM products because of the manner in which they are produced and are specific to colocated scenarios. The distortions may fall directly in the receive channel of the colocated victim receiver. Further,

the jammers need not necessarily be in-band, they could be out-of-band and still produce distortions within the victim receiver's desired channel.

1.3 Research Goals

The goals of the research:

- Understand and quantify the mechanisms contributing to interference at base station receivers in a colocated environment.
- Develop cancellation systems that would mitigate the interference issues and allow multiple operators to coexist on one common site, keeping costs at a minimum.

1.4 Research Contributions

The research has led to the following contributions:

- S. Ahmed and M. Faulkner, "Interference Issues at Co-located Base Stations and an Adaptive Cancellation Solution," in *Proc. Electromagnetic Compatibility Symposium and Exhibition Melbourne*, September 2010.
- S. Ahmed and M. Faulkner, "An Adaptive Cancellation System for a Colocated Receiver and its Dynamic Range," in *Proc. IEEE Radio and Wireless Symposium*, January 2011.
- S. Ahmed and M. Faulkner, "Optimized Interference Canceling for Colocated Base Station Transceivers," *IEEE Transactions on Vehicular Technology*, October 2011.
- S. Ahmed and M. Faulkner, "Mitigation of Reverse Intermodulation Products at Colocated Base Stations," *IEEE Transactions on Circuits and Systems I: Regular Papers*, 2012.

- S. Ahmed and M. Faulkner, “Interference at Colocated Base Stations: A Review,” in *Proc. 23rd Annual IEEE International Symposium on Personal, Indoor and Mobile Radio Communications (PIMRC)*, September 2012.

1.5 Organization of thesis

- Chapter 2 discusses some basic concepts of noise and distortion that are required for the thesis. Some key RF components are also discussed. In addition, chapter 2 demonstrates controlled laboratory experiments verifying the generation of reverse IM products in a colocated base station setting.
- Chapter 3 provides the required background knowledge. It reviews previous solutions for the forward IM problem and proposes a reference antenna based adaptive cancellation solution for the problem. The chapter also reviews potential schemes that can be adapted to solve the reverse IM problem, and proposes a multi-front-end receiver architecture for distortion regeneration and postdistortion cancellation.
- Chapter 4 describes the proposed adaptive cancellation system for mitigating forward IM distortions. The chapter performs a dynamic range analysis cancellation system to assess its practicality.
- Chapter 5 performs a novel signal-to-interference-and-noise ratio (SINR) analysis on the adaptive cancellation system. The SINR of the system is maximized by optimizing the cancellation coupler in the reference path. The chapter then demonstrates a controlled test-bed with automated adaptive canceling, and compares SINR results from the prototype with theoretical predictions.
- The key issue of implementing an over-the-air reference antenna based cancellation system is the self-cancellation of the desired signal when the reference antenna receives a sample of the signal. Chapter 6 addresses this key challenge and demonstrates a working over-the-air prototype of the cancellation system.

- Chapter 7 addresses the reverse IM problem in its entirety. It builds on the proposed postdistortion cancellation system in chapter 3, and integrates a novel frequency offset correction circuit to mitigate offsets introduced by the multi-front-end receiver architecture during distortion regeneration. The chapter characterizes the cancellation circuit using mathematical and simulation analysis. It then demonstrates a prototype of the postdistortion cancellation system.
- Finally, chapter 8 summarize the key outcomes and findings of the thesis, and proposes future work.

The next chapter reviews the basic concepts of noise and distortion applicable to the thesis. It also demonstrates practical experiments that verify the occurrence of reverse IM products and receiver desensitization.

Chapter 2

Basic Concepts

RF front-ends are an integral part of wireless communication systems. In the transmitter front-end, the baseband modulated signals are up-converted to RF using a mixer and then power amplified before emission through the antenna system. The receiver front-end accordingly uses a low-noise amplifier to boost the weak received signals and down-converts them to baseband using a mixer. Power-amplifiers, low-noise amplifiers and mixers exhibit nonlinearity when operating at RF frequencies. They introduce unwanted signal components or nonlinear distortions. The components also add noise into the system. The distortions along with the noise degrade the overall performance of the wireless system.

In this chapter, the basic concepts of noise and distortion within wireless radio systems are discussed. The chapter then demonstrates the interference issues at colocated base station settings using laboratory measurements.

Section 2.1 discusses the basics of noise within radio systems. Sections 2.2 and 2.3 discuss the basics of radio system components, the attenuator and the coupler. Section 2.4 discusses nonlinearity and distortions within radio systems. Finally, section 2.5 demonstrates the nonlinearities (e.g., reverse IM3 and desensitization) in colocated wireless systems.

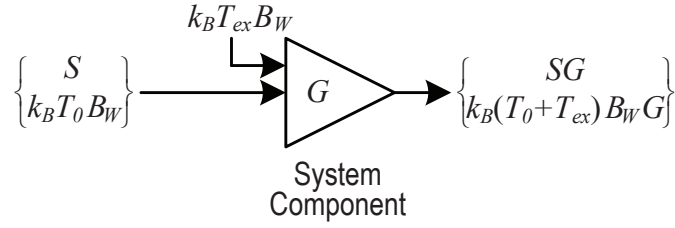


Fig. 2.1: Noise within a radio system component.

2.1 Noise and Noise Factor

The ideal transmitter or receiver component does not incorporate additional noise over the standard thermal noise power, $k_B T_0 B_W$ W, where k_B is the Boltzmann's constant, T_0 is the standard noise temperature 290K, and B_W is the noise bandwidth [8]. However, most system components are 'noisy', and add an excess noise power, $k_B T_{ex} B_W$ W, as seen in Fig. 2.1, where T_{ex} is the excess noise temperature of the component. This results in reduced sensitivity in radio receivers. Noise factor F is the performance metric that characterizes the excess noise power of the component; it is defined as the ratio of the input signal-to-noise ratio to the output signal-to-noise ratio [9] [10], given as follows,

$$F = \frac{S/k_B T_0 B_W}{SG/k_B (T_0 + T_{ex}) B_W G} \quad (2.1)$$

which can be simplified to give,

$$T_{ex} = T_0 (F - 1). \quad (2.2)$$

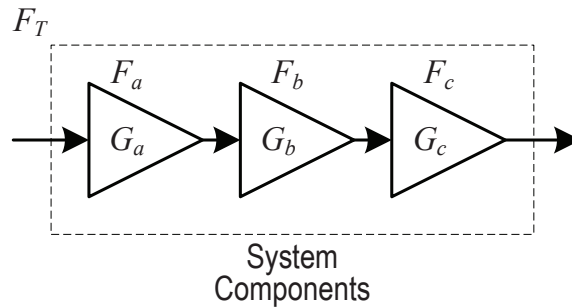


Fig. 2.2: Cascaded system components (Noise factor).

Further, given a transmitter or a receiver chain, as seen in Fig. 2.2, when individual noise factors F_a , F_b and F_c of the components are known, the overall noise factor F_T of the cascaded system is given by,

$$F_T = F_a + \frac{F_b - 1}{G_a} + \frac{F_c - 1}{G_a G_b} \quad (2.3)$$

where the total gain of the system, $G_T = G_a G_b G_c$.

Note, in this chapter, power gains and signal powers are represented with capital letters; additionally, voltage gains and signal voltages are represented with small letters.

2.2 RF Attenuators

RF attenuators work opposite to amplifiers and reduce the level of a signal by a loss factor L . The gain of the attenuator $G_L = 1/L$ and is negative when expressed in decibels (dB). Attenuators are passive devices and have a noise factor, $F_L = 1/G_L$ [11]. This implies that passive devices do not add any excess noise. At room temperature, all their input and output ports have the same noise level of $k_B T_0 B_W$ W.

2.3 Couplers

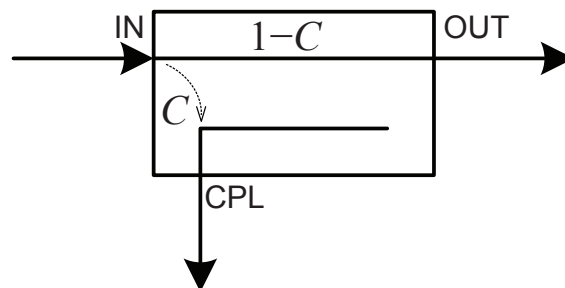


Fig. 2.3: A directional coupler.

Couplers are passive devices that can be used to sample out signals from a

transmission path or to add signals to a transmission path. They are usually three-port devices, as seen in Fig. 2.3. The coupling path (IN→CPL) has a coupling gain C ; and the through path (IN→OUT) has a gain of $1 - C$. C is within $0 < C < 1$ and is negative in decibels (dB). Effectively, the coupled (CPL) port provides a reduced level of the input signal.

Couplers are directional devices. They can be used in the opposite direction to combine signals. A signal applied to the output (OUT) port will pass through to the input (IN) port with a gain of $1 - C$, however, there will be no signal through to the coupled (CPL) port. In addition, a signal applied to the coupled (CPL) port will pass through to the input (IN) port with a gain of C , and superimpose with the signal coming from the output (OUT) port. The signal from the coupled (CPL) port will not pass through to the output (OUT) port.

Similar to an attenuator, the coupler, at standard room temperature, has a noise level of $k_B T_0 B_W$ W at all its ports.

2.4 Nonlinearity

The nonlinear devices within the RF front-ends generate different types of distortions. In this section, we discuss the major nonlinear distortions that impede the performance of the wireless system. Also, commonly used performance metrics for measuring the nonlinearity of RF devices are discussed.

For simplicity, we model a nonlinear system using the following memoryless power series,

$$y = g_1 x + g_2 x^2 + g_3 x^3 + \dots \quad (2.4)$$

where x is the input signal to the system, g_1 is the gain coefficient, g_2 and g_3 are the quadratic and cubic distortion coefficients and y is the output.

2.4.1 Harmonic Distortion

If a sinusoidal signal $x = a \cos 2\pi f_a t$ of frequency f_a was applied to a linear system the output would have been $y = g_1 a \cos 2\pi f_a t$. However, when applied to the nonlinear system in (2.4) we have,

$$y = g_1 a \cos 2\pi f_a t + g_2 a^2 \cos^2 2\pi f_a t + g_3 a^3 \cos^3 2\pi f_a t + \dots \quad (2.5)$$

or,

$$y = \frac{g_2 a^2}{2} + \left(g_1 a + \frac{3g_3 a^3}{4} \right) \cos 2\pi f_a t + \frac{g_2 a^2}{2} \cos 2\pi(2f_a)t + \frac{g_3 a^3}{4} \cos 2\pi(3f_a)t + \dots \quad (2.6)$$

Here, the second term presents the fundamental signal $\cos 2\pi f_a t$ with the original input frequency f_a . The second-harmonic distortion is given by $\cos 2\pi(2f_a)t$ and the third-harmonic by $\cos 2\pi(3f_a)t$ for harmonic frequencies of $2f$ and $3f$ respectively. There is also a second-order DC-offset given by the first term.

2.4.2 Intermodulation Distortion

Although, harmonic distortions characterize nonlinear devices, it is not a sufficient measure for systems that involve wideband or multi-carrier signals. When two or more signals of different frequencies mix within a nonlinear system they form new components that are not harmonics of the input frequencies [6]. These components are termed as intermodulation distortion products. Let us consider a two-tone input $x = a \cos 2\pi f_a t + b \cos 2\pi f_b t$ such that $f_a > f_b$, when applied to the nonlinear system in (2.4) we have,

$$y = g_1 (a \cos 2\pi f_a t + b \cos 2\pi f_b t) + g_2 (a \cos 2\pi f_a t + b \cos 2\pi f_b t)^2 + g_3 (a \cos 2\pi f_a t + b \cos 2\pi f_b t)^3. \quad (2.7)$$

Expanding the quadratic (second) term we have,

$$\begin{aligned}
 & g_2(a \cos 2\pi f_a t + b \cos 2\pi f_b t)^2 \\
 &= \frac{g_2(a^2+b^2)}{2} + \frac{g_2 a^2}{2} \cos 2\pi(2f_a)t + \frac{g_2 b^2}{2} \cos 2\pi(2f_b)t \\
 &+ g_2 ab \cos 2\pi(f_a + f_b)t + g_2 ab \cos 2\pi(f_a - f_b)t
 \end{aligned} \tag{2.8}$$

The last two terms with frequencies $f_a \pm f_b$ are the second-order intermodulation products as shown in Fig. 2.4.

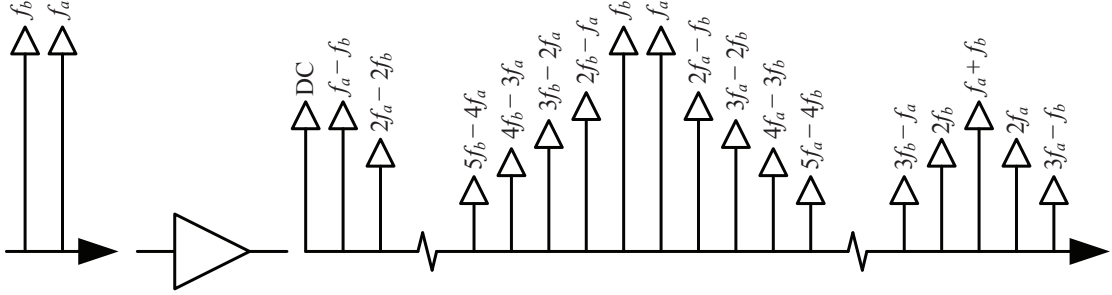


Fig. 2.4: Even and odd-order intermodulation products along with the fundamentals, harmonics and DC [12].

Next, expanding the cubic (third) term in (2.7) we have,

$$\begin{aligned}
 g_3(a \cos 2\pi f_a t + b \cos 2\pi f_b t)^3 &= \left(\frac{3g_3 a^3}{4} + \frac{3g_3 ab^2}{2}\right) \cos 2\pi f_a t \\
 &+ \left(\frac{3g_3 b^3}{4} + \frac{3g_3 ba^2}{2}\right) \cos 2\pi f_b t \\
 &+ \frac{g_3 a^3}{4} \cos 2\pi(3f_a)t + \frac{g_3 b^3}{4} \cos 2\pi(3f_b)t \\
 &+ \frac{3g_3 a^2 b}{4} \cos 2\pi(2f_a + f_b)t + \frac{3g_3 a^2 b}{4} \cos 2\pi(2f_a - f_b)t \\
 &+ \frac{3g_3 b^2 a}{4} \cos 2\pi(2f_b + f_a)t + \frac{3g_3 b^2 a}{4} \cos 2\pi(2f_b - f_a)t
 \end{aligned} \tag{2.9}$$

The last four terms with frequencies $2f_a \pm f_b$ and $2f_b \pm f_a$ are the third-order intermodulation products.

Further, higher-order intermodulation products could be generated by a n -th order power series [12] [13],

$$y = g_1 x + g_2 x^2 + g_3 x^3 + \dots + g_n x^n. \tag{2.10}$$

The n -th order intermodulation product is given at frequency $\pm n_a f_a \pm n_b f_b$ where

$|n_a| + |n_b| = n$, as seen in Fig. 2.4.

2.4.3 1-dB Compression Point (P_{1dB})

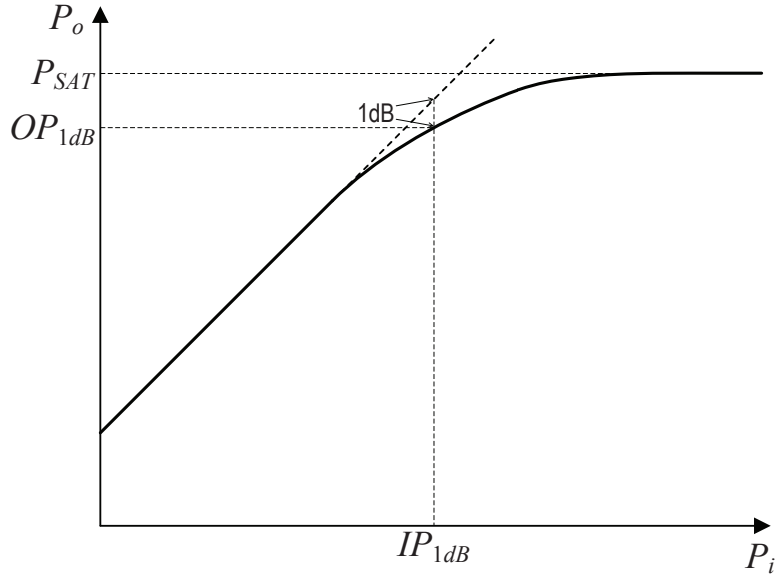


Fig. 2.5: 1dB compression point.

RF circuit gains compress and eventually saturate when the input signal reaches sufficiently high levels. From the second term of (2.6), the overall gain of the nonlinear system for the fundamental frequency f_a is $g_1 + \frac{3g_3a^2}{4}$ when the input is $x = a \cos 2\pi f_a t$. For gain compressing RF circuits g_3 is (-)ve, therefore, the overall gain decreases with increasing values of a (i.e., increasing input power $P_i = 20 \log a$). This gain compression effect is measured using the performance metric “1-dB compression point”, defined as the input signal level (or the output signal level) where the gain drops 1dB below its ideal value [6].

In practice, the 1dB compression point is measured by recording/plotting the output power, $P_o = 20 \log \left| g_1 a + \frac{3g_3 a^3}{4} \right|$, of the fundamental signal with respect to the input power P_i , as illustrated in Fig. 2.5. At the 1-dB compression point, the output power P_o falls 1dB short of the ideal output. IP_{1dB} is defined as being the input power at the 1-dB compression point and OP_{1dB} as its output power.

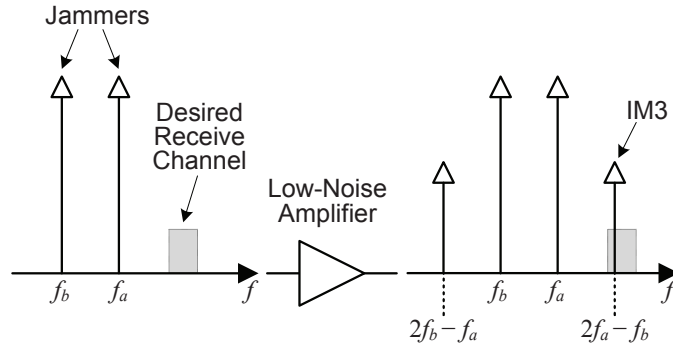


Fig. 2.6: Third-order intermodulation distortion causing interference in the desired channel of a receiver [6].

Theoretically, at the 1dB compression point, we can write [6],

$$20 \log \left| g_1 + \frac{3g_3 a^2}{4} \right| = 20 \log |g_1| - 1 \text{dB} \quad (2.11)$$

where g_1 is the ideal gain of the system. Therefore, $a^2 = 0.145 \left| \frac{g_1}{g_3} \right|$; thus,

$$IP_{1dB} = 10 \log \left(0.145 \left| \frac{g_1}{g_3} \right| \right) \quad (2.12)$$

and

$$OP_{1dB} = IP_{1dB} + 20 \log |g_1| - 1 \text{dB}. \quad (2.13)$$

Further increase of input power P_i eventually saturates the RF circuit and its overall gain goes to zero. As seen in Fig. 2.5, P_{SAT} is the saturated power output from the circuit. When RF front-end receiver circuits get hit by a strong jamming signal, regardless of its frequency, the receiver saturates and loses its overall gain. Thus, the weak desired signal is not boosted and falls below the required threshold for demodulation. This condition of the receiver is termed as receiver desensitization.

2.4.4 Third-order Intercept Point (IP3)

The most problematic of all the intermodulation distortions are the terms with frequencies $2f_a - f_b$ and $2f_b - f_a$. This is because when the difference between f_a and f_b is small the intermodulation products fall in-band close to the fundamentals. If

the fundamentals at frequencies f_a and f_b are two strong interfering jammers, as seen in Fig. 2.6, they could produce third-order intermodulation products within the low-noise amplifier of the victim receiver and corrupt the desired signal. The performance metric that characterizes nonlinear devices for such third-order intermodulation products is the “third-order intercept point” (IP3). IP3 is measured using a two-tone test with input $x = a \cos 2\pi f_a t + b \cos 2\pi f_b t$ where both tones have equal powers ($a = b$). When passed through the nonlinear system in (2.4) we have the following components of concern,

$$y(t) = (g_1 + \frac{9}{4}g_3a^2)a \cos 2\pi f_a t + (g_1 + \frac{9}{4}g_3a^2)a \cos 2\pi f_b t + \frac{3}{4}g_3a^3 \cos 2\pi(2f_a - f_b)t + \frac{3}{4}g_3a^3 \cos 2\pi(2f_b - f_a)t + \dots \quad (2.14)$$

a is chosen to be sufficiently small such that the gain is approximately equal to g_1 (i.e., $g_1 \gg \frac{9}{4}g_3a^2$) and the higher-order intermodulation products are negligible. In (2.14), as a increases the fundamentals increase in proportion to a , whereas the third-order intermodulation products increase in proportion to a^3 . Hence, when plotted in the logarithmic scale, the fundamentals grow at a gradient of 1 and the third-order intermodulation products grow at a gradient of 3, as illustrated in Fig. 2.7. IP3 is the point of intersection of these two lines. At the intersection point we have [6],

$$|g_1| a = \frac{3}{4} |g_3| a^3. \quad (2.15)$$

Thus, the input IP3,

$$IIP3 = 10 \log \left(\frac{4}{3} \left| \frac{g_1}{g_3} \right| \right) \quad (2.16)$$

and the output IP3,

$$OIP3 = IIP3 + 20 \log |g_1|. \quad (2.17)$$

In practice, the intercept point is a theoretical concept. IP3 cannot be measured by increasing the input level to reach the intercept point because of amplifier saturation. At higher levels of a , the approximation $g_1 \gg \frac{9}{4}g_3a^2$ no longer holds and the higher-order intermodulation products become prominent. Hence, as seen in

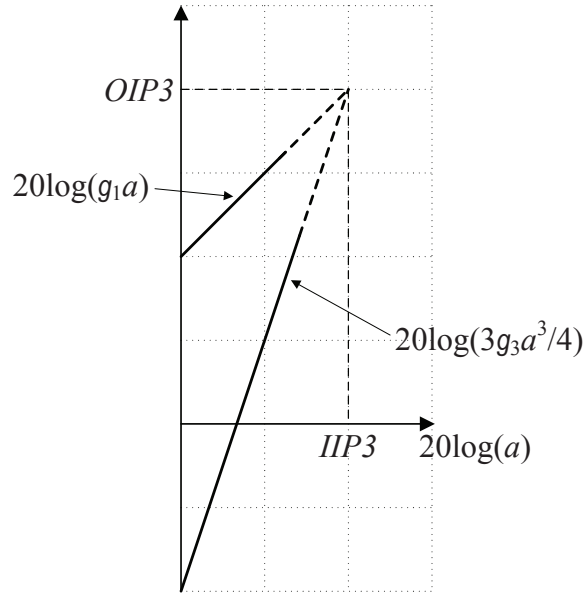


Fig. 2.7: Two-tone test results for IP3 measurement.

Fig. 2.7, the measurements are taken for small input levels of a and then the lines are extrapolated to find the intercept point.

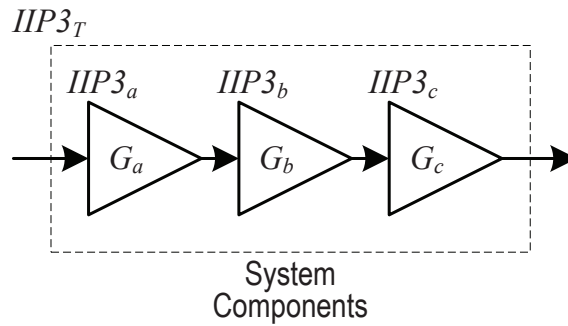


Fig. 2.8: Cascaded system components (IP3).

Fig. 2.8 shows cascaded components of a transmitter/receiver chain, similar to section 2.1. Here, the individual input IP3s $IIP3_a$, $IIP3_b$ and $IIP3_c$ of the components are known, these can be used to evaluate the overall input IP3 $IIP3_T$ of the system from the following,

$$\frac{1}{IIP3_T} = \frac{1}{IIP3_a} + \frac{G_a}{IIP3_b} + \frac{G_a G_b}{IIP3_c} \quad (2.18)$$

where the total gain of the system, $G_T = G_a G_b G_c$.

2.4.5 Bandwidth Expansion

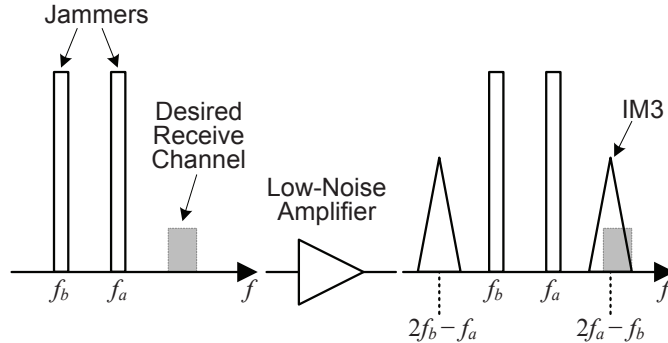


Fig. 2.9: Third-order intermodulation distortion causing interference in the desired channel of a receiver.

In real world applications, jamming signals would have modulation on them. At the victim receiver we may have $x = a(t) \cos 2\pi f_a t + b(t) \cos 2\pi f_b t$ where $a(t)$ and $b(t)$ are modulation envelopes with particular bandwidths. When the jamming signals mix within the LNA of the receiver, the IM3 product at $2f_a - f_b$ has an envelope given by $\frac{3g_3 a^2 b}{4}$ (see (2.9)). It is well known that a product in the time domain is a convolution in the frequency domain [14], i.e.,

$$\mathcal{F} \{a(t)b(t)\} = \mathcal{F} \{a(t)\} * \mathcal{F} \{b(t)\} \quad (2.19)$$

where $\mathcal{F} \{\cdot\}$ is the Fourier transform or the spectrum. Thus, the IM3 product at $2f_a - f_b$ has a bandwidth of twice the bandwidth of $a(t)$ plus the bandwidth of $b(t)$, and the IM3 at $2f_b - f_a$ has a bandwidth of twice the bandwidth of $b(t)$ plus the bandwidth of $a(t)$. Fig. 2.9 shows the bandwidth expansion of the IM3 products, these can cover many channels.

2.5 Practical Measurements

In chapter 1, we discussed that there are two major sources of intermodulation products for a base station receiver in a colocated setting. The more common of the two are the intermodulation products that are produced when large transmit

signals from neighbouring base stations combine within the low-noise amplifier (or mixer) of the victim receiver. As shown in Fig. 2.9, the intermodulation distortions may fall within the receiver's desired channel and cause interference. The second are the reverse intermodulation products that are generated at the output of power amplifiers in colocated transmitters. As illustrated in Fig. 2.10, large transmit signal

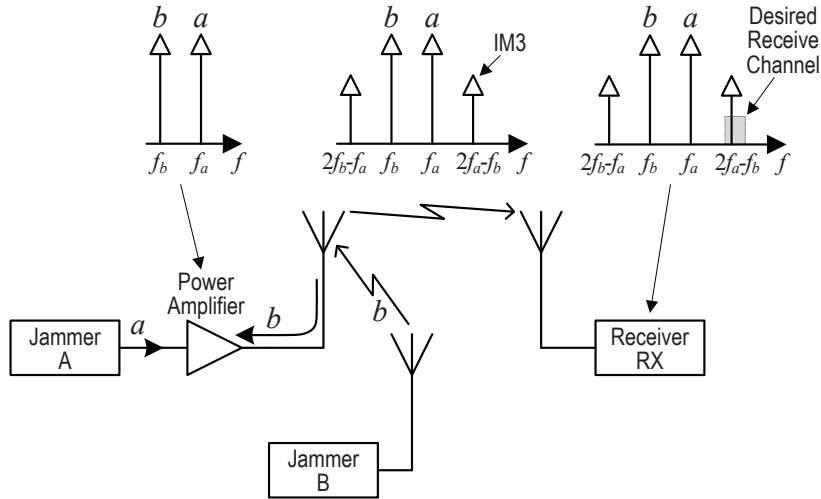


Fig. 2.10: Reverse IM3.

b from jammer B radiates into the power amplifier of jammer A and produces third-order intermodulation (IM3) products that may fall in the desired receive channel of a colocated base station receiver RX.

When jamming signal frequencies are such that the IM products do not fall directly on the desired receive channel, the high power jamming signals may still saturate the receiver front-end and cause desensitization. Such jamming signals can be at any frequency.

In this section we present laboratory measurements that we performed to demonstrate two of the above lesser known conditions, the reverse IM3s and receiver desensitization/blocking [15].

2.5.1 Reverse IM3

A laboratory setup as shown in Fig. 2.11(a) models the distortion susceptibility of a PA to an unwanted reverse signal. The device under test (PA1) is a 1 watt

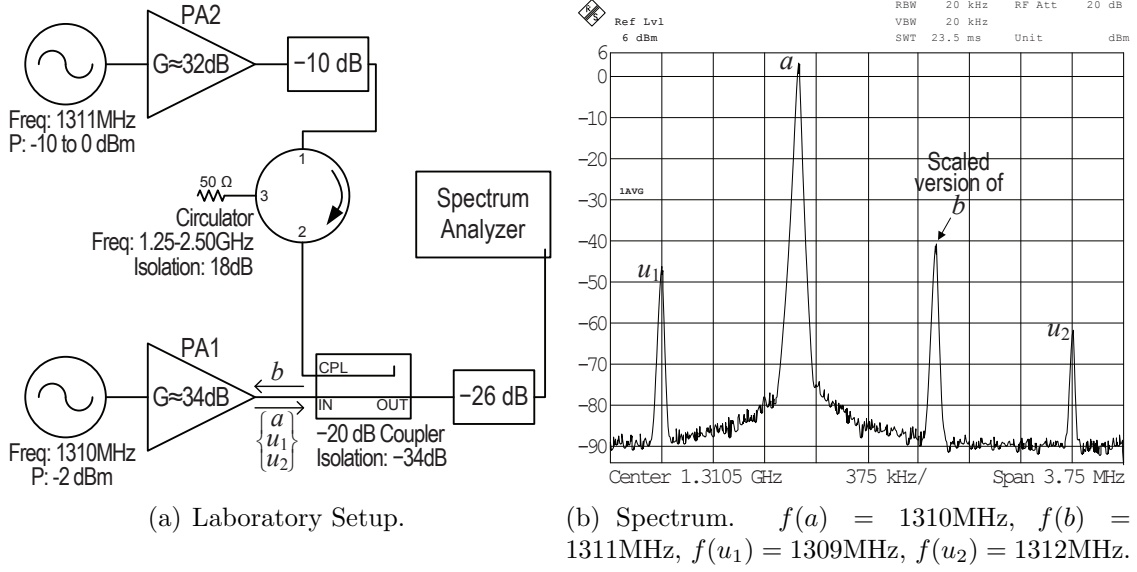


Fig. 2.11: Reverse IM3 Experiment.

power amplifier (MiniCircuits ZHL-42 [16]), which is operated at saturation. An interfering signal b is fed into its output port from the coupler. The resulting output is measured on the spectrum analyzer as seen in Fig. 2.11(b). The output consists of PA1's signal a , the distortion components u_1 and u_2 and some residual component of the interfering signal from PA2 (i.e., a scaled version of b caused by the finite reverse isolation of the coupler). The circulator and -10dB attenuator effectively stops any reverse signals into PA2. Thus the distortions produced by PA2 are negligible.

In Fig. 2.11(b), the distortion products have frequencies $f(u_1) = 2f(a) - f(b)$ and $f(u_2) = 2f(b) - f(a)$. Any other distortion product was well below the noise floor, which indicates the presence of a dominant third order distortion model. An extra 27dB (26dB for the attenuator and 1dB for the coupler and cabling loss) should be added to the magnitudes to get the signal strengths at the output of PA1.

Fig. 2.12 shows how the magnitude of the distortion products u_1 and u_2 vary with the strength of the reverse interfering signal b . The signal a from PA1 is maintained constant at the power amplifier's output saturation level. We notice that for every 1dB increase in the magnitude of b , u_2 increases by 2dB and u_1 increases by 1dB. Thus confirming that the magnitude of u_2 is proportional to $|a||b|^2$, and the magnitude of u_1 is proportional to $|a|^2|b|$. This further confirms the third-order

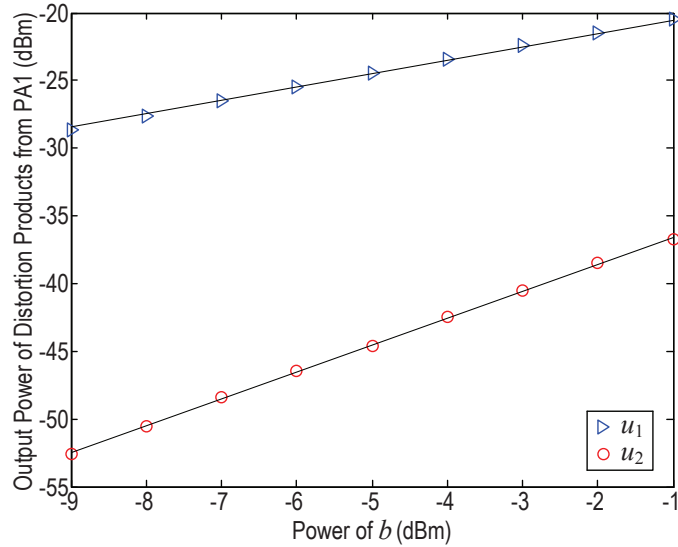


Fig. 2.12: Characterization of the reverse IM distortions.

distortion model [6].

Hence, the problem at hand is serious and the general idea of backing off by 1dB to get a 3dB reduction in distortion does not hold because increasing the isolation will only control one of the signals (b) contributing to the distortion. What is worse still is that the least responsive distortion product, u_1 , is also the largest. The isolation can be increased by either using an isolator to reduce b , or by further antenna separation between PA1 and PA2. The former introduces additional cost and insertion loss, while the latter requires more real-estate area.

2.5.2 Desensitization/Blocking

Fig. 2.13 illustrates how a strong interfering transmit signal from a colocated transmitter could desensitize/block a receiver. The experiment connects an LNA (of about 19dB gain) to two signal sources using a power combiner, one generating the desired signal and the second generating the jammer. The output of the LNA is connected to a spectrum analyzer. Initially, the figure shows the LNA output with the desired signal at -51 dBm in the presence of a small jamming signal measured at -16 dBm. On the second instance, the jamming signal has been increased by 34dB to $+18$ dBm and this forces the desired signal down to -68 dBm. The interferer has

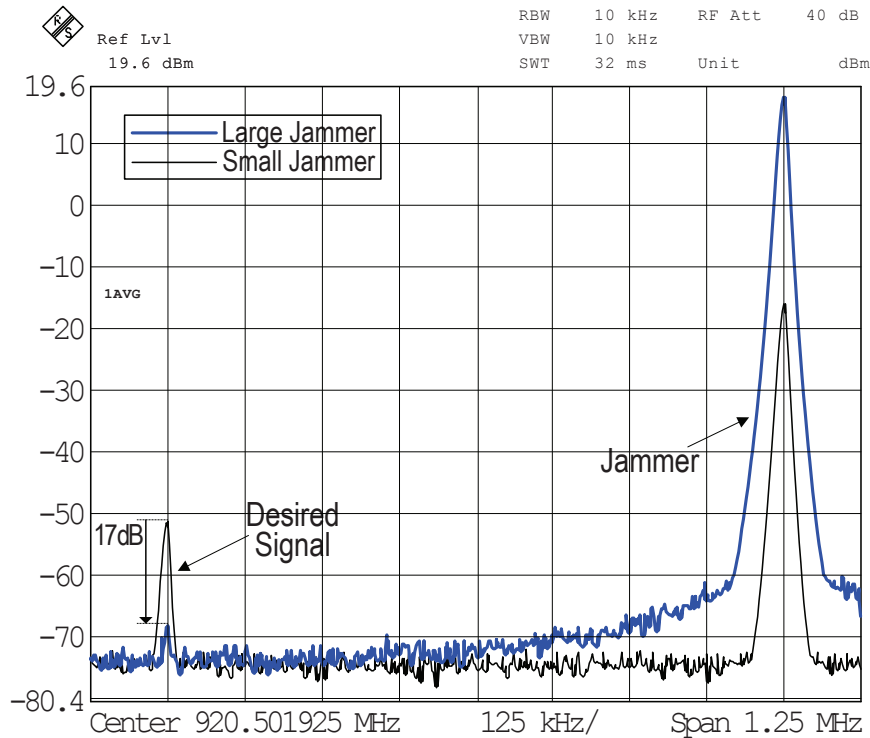


Fig. 2.13: Desensitization/Blocking. Spectrum at the LNA output. Desired signal at 920MHz and Jamming signal at 921MHz.

overwhelmed the LNA, and desensitized its gain by 17dB.

2.6 Summary

- The chapter discusses the basic concepts of noise and distortion within wireless radio systems. It defines performance metrics (e.g., noise factor, IP3, etc.) that characterize the noise and distortion properties of wireless radio systems.
- The basics of an attenuator and a directional coupler are discussed in sections 2.2 and 2.3 respectively.
- Controlled laboratory measurements are used to demonstrate reverse IM3 generation and receiver desensitization at colocated base station settings.

This chapter builds the basics required for the rest of the thesis. The next chapter investigates previously published literature and proposes potential solutions for the colocation scenario.

Chapter 3

Literature Review

Nonlinearity in RF front-ends is an ongoing challenge in the field of wireless communication. While there are many solutions that mitigate distortions and jamming signals within the receiver front-end, there is little work addressing the issues in a colocated base station receiver in its entirety. In this chapter, we discuss relevant solutions for overcoming colocation nonlinearity issues. We examine other research studies to find potential distortion mitigation techniques for the colocated receivers. Finally, we summarize our study and outline the basics of two potential solutions, one for distortions produced within the receiver front-end and the other for reverse IM distortions generated at a colocated transmitter.

One of the issues of colocation is that the early occupier of the site initially experiences no such interference problems. Distortions get generated as more transmitters are added to the site. Thus, the initial occupiers of the site would be very reluctant to adopt a new solution into their transmitters and disrupt operationally stable systems. Especially, when it incurs further capital expenditures and the victim service provider is possibly a competitor. Hence, it is less likely that the colocated victim receiver would get any collaboration from the aggressor jammers. Therefore, solutions are required that can be independently deployed by the victim receiver. Further, the victim receiver would prefer solutions that can mitigate the problem without requiring much modification to its existing hardware and incur minimum expenses.

Section 3.1 discusses different filtering solutions that are available for the collocation problem. Section 3.2 studies various adaptive cancellation schemes that could be used to mitigate forward IM products. Section 3.3 proposes an adaptive cancellation technique that mitigates forward IM products by canceling the strong jamming signals before they hit the receiver front-end circuits. Section 3.4 discusses transmitter-end solutions that have been proposed for reverse IM products, and reviews potential receiver linearization techniques that can be adapted to develop a receiver-end solution. Finally, section 3.5 proposes a receiver postdistortion cancellation technique for mitigating reverse IM products.

3.1 Filtering Solutions

This family of solutions use passive filters to reject the jamming signals before they enter the nonlinearities.

3.1.1 Knowledge-based Filtering

The authors of [3] have used computer simulations to model the collocation scenario and predict the characteristics of the jamming signals. This requires knowledge of the colocated transceiver specifications and antenna configurations. A fixed customized filter is then deployed to mitigate the interference. This makes the solution unsuitable for dynamic environments. Unfortunately, many cosite scenarios require a certain level of adaption to handle changing carrier frequencies and ON/OFF keying of transmitters.

Another approach described in [4] located the jamming signal by scanning the spectrum with a Fast Fourier Transform (FFT) and then removed it with a tunable notch filter. This adds extra filter complexity issues. Secondly, removing the jammers using such filtering techniques does not help in mitigating the reverse IM distortions produced at the transmitter-end.

3.1.2 Passive Filtering

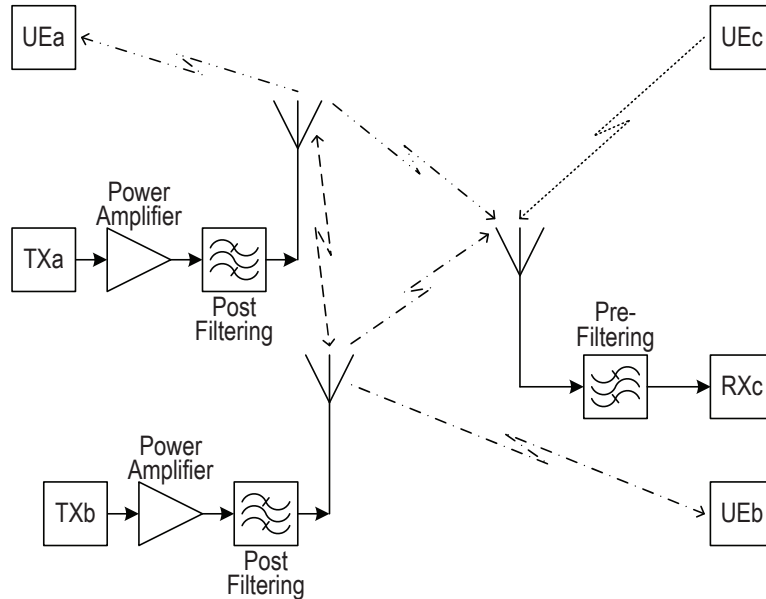


Fig. 3.1: Passive pre and post filtering to mitigate colocated interference issues [17].

Netcom proposes a brute-force solution in [17] for a military frequency hopping communication system. As seen in Fig. 3.1, it involves the placement of frequency agile band pass filters in front of receiver LNAs and after the transmitter PAs. The receiver pre-filtering stops large jamming signals and admits only the desired signal into the LNA. Likewise, transmitter post-filtering rejects any reverse signal from entering the PAs and stops IM products produced from being transmitted. However, expensive high- Q cavity filters with low insertion loss would be required to sufficiently attenuate the large transmitter signals, which, in some cases, have output powers of +47dBm (50W) [18]. In addition, frequency agility adds another dimension of complexity and cost. Overall, it is a commercially unfeasible proposition for wireless service providers.

3.2 Adaptive Cancellation for Forward IM

Colocation of multiple radio technologies is also a problem within user equipment (UE) devices. The existing solutions can be divided into the medium access control

(MAC) layer solutions and the physical layer solutions [19]. The most effective MAC layer solution is to use time slotting/sharing [20] [21]. However, such techniques reduce the overall throughput of the participating radio technologies. In contrast, physical layer solutions allow simultaneous operation of the transceivers. The ideal solution is to remove the coupled aggressor signal before it hits the victim receiver LNA/mixer circuits. Such a goal could be achieved using adaptive cancellation techniques.

3.2.1 Single Loop Narrowband Cancellation

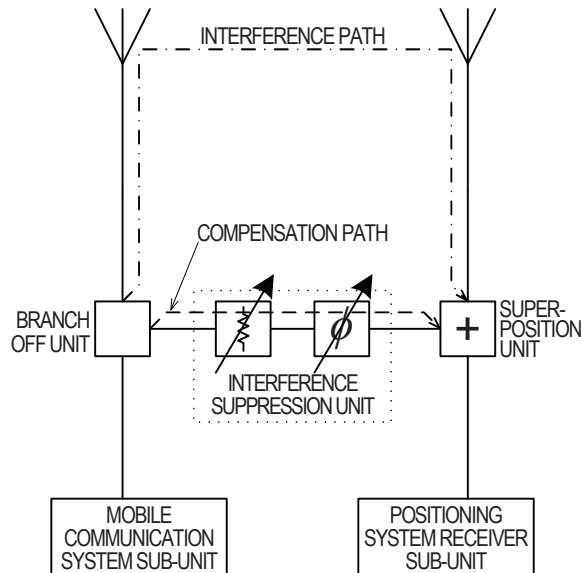


Fig. 3.2: Transmitter leakage cancellation for a colocated GPS receiver [22].

The proponents of [22] and [23] propose a single-loop adaptive cancellation system for colocating a global positioning system (GPS) receiver unit within a mobile communication UE. As seen in Fig. 3.2, the cancellation system couples out a sample of the interfering mobile communication transmit signal. The compensation path signal is then adaptively gain-phase adjusted such that it is equal in magnitude and 180° out of phase to the interference path signal when coupled back in the receive path of the GPS unit. This mitigates the interfering mobile communication transmit signal before it reaches the GPS receiver. A variable attenuator and a phase shifter

can only cancel narrow-band signals. Wideband signal cancellation would require an accurate delay match of the compensation path to the interference path.

3.2.2 Single Loop Wideband Cancellation

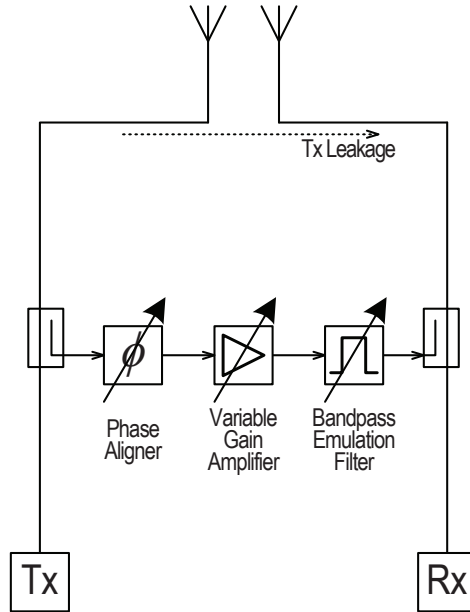


Fig. 3.3: Interference cancellation unit for colocated radios [24].

Fig. 3.3 shows how the authors of [24] add an emulation filter in their cancellation loop to estimate the transfer function of the interference path. This ensures proper delay matching and allows 15-30dB cancellation of a wideband bluetooth aggressor signal at the WLAN receiver, both colocated within the same UE.

3.2.3 Multiple-loop Multi-band Cancellation

UE devices operating in frequency division duplex (FDD) also have the problem of the transmitter acting as an aggressor on to the receiver. The regular solution is to use passive SAW (surface acoustic wave) duplexing bandpass filters. The transmit chain bandpass filter stops the radiation of transmitter noise into the receiver's desired channel. The receiver path bandpass filter stops the transmitter signal from overloading the receiver (desensitization). But these bandpass filters do not have

sufficient power handling capability when used in base station environments and are not frequency agile. An alternative approach taken by the authors of [25] propose an adaptive duplexing circuit for multi-band operation. As seen in Fig. 3.4, the adaptive duplexer uses a circulator to direct the transmit signal into the antenna port and to direct the desired signal into the receive path. However, the limited reverse isolation of the circulator allows leakage of the transmit signal and noise into the receive path. The authors use a direct feed from the transmitter in an adaptive double-loop cancellation path to create two nulls, as seen in Fig. 3.4(b), effectively removing the interfering transmit signal and transmitter noise from the receiver. Further, delay lines are used to ensure the required matching between the interference path and the cancellation path such that a 5MHz (WCDMA) wideband cancellation is achieved at the nulls. The loops achieved about 46dB cancellation of the transmit signal and 17dB reduction of the transmitter noise at the receiver.

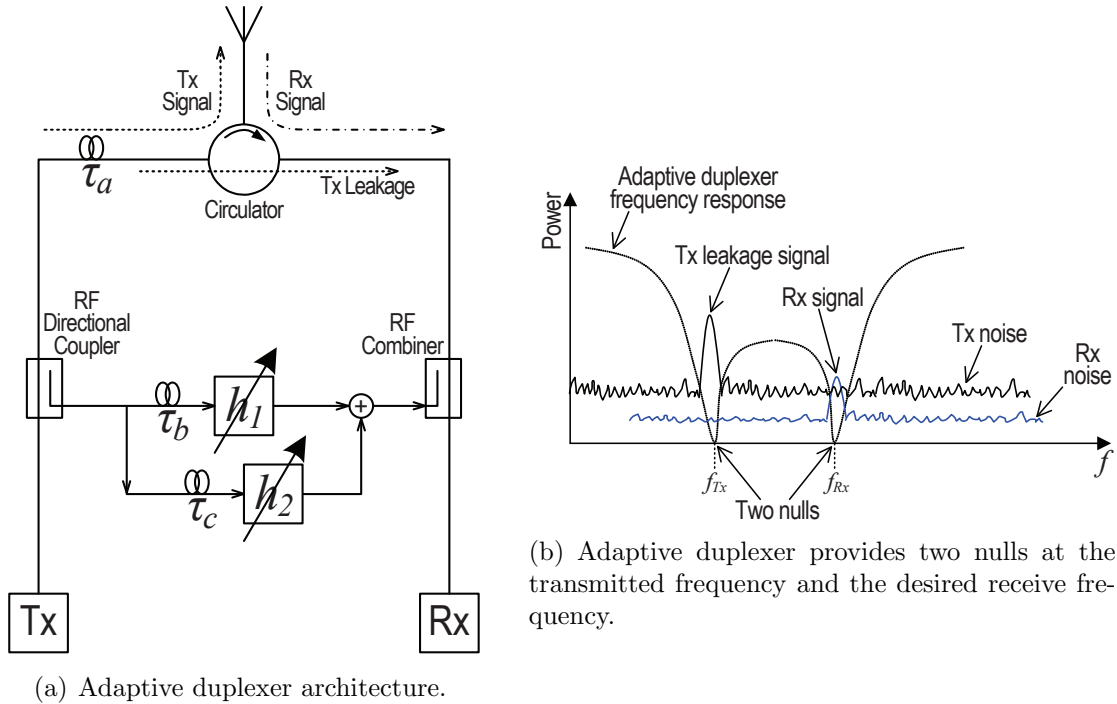


Fig. 3.4: A double loop cancellation adaptive duplexer [25].

However, in a colocated base station scenario each of the transceivers are independent and a direct feed from colocated aggressor transmitters is not likely. Further, both papers [24] and [25] publish good cancellation performance, but neither of them consider noise and distortion generated in the canceling loops themselves. This is a key factor in any practical deployment, particularly when power levels are high.

3.3 The Proposed Solution for Forward IM

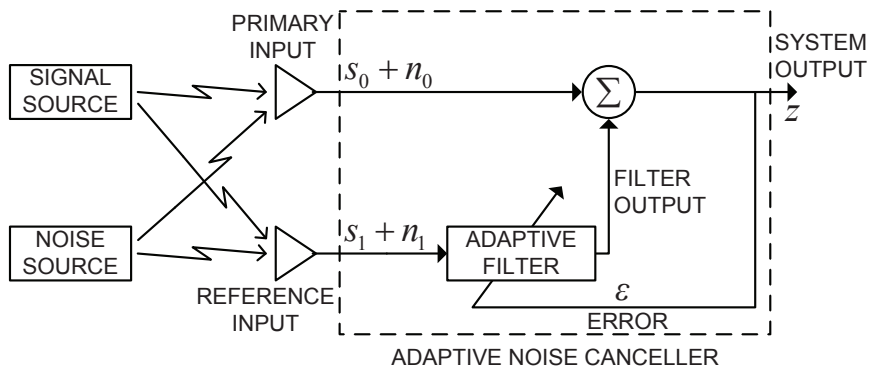


Fig. 3.5: The adaptive noise canceling concept [26].

The basis of the above mentioned techniques originates from the concept of adaptive noise canceling described in [26] and [27]. The method uses a ‘primary’ input transducer to receive the noise corrupted desired signal and a ‘reference’ transducer to acquire noise that is correlated in some way to the primary input’s noise. As shown in Fig. 3.5, the reference input is adaptively filtered and subtracted from the primary input to obtain the actual desired signal. However, a sample of the desired signal may also radiate into the reference input and result in self-cancellation. This can be overcome by placing the transducer close to the interfering noise source and achieving a sufficiently large interference-to-signal ratio in the reference input. The original application was for acoustic noise canceling, in which case, the transducers were microphones. In our work we use antennas to cancel RF jamming signals.

The technique fits our requirement, the colocated victim receiver could use a

reference antenna to pick-up the jamming signals, do the necessary gain-phase adjustment and remove them from the primary input. Mitigating the jammers before they reach the LNA would stop them from producing distortions within the receiver. The system can adapt to jamming signals over a wide range of frequencies. In chapter 4-6 of this thesis we propose such an adaptive cancellation technique and consider its practical viability, including the noise and distortion aspects of the cancellation loop.

The reverse IM problem is discussed next.

3.4 Adaptive Cancellation for Reverse IM

Reverse IM is caused when large unwanted signals enter the output of a RF power amplifier. Section 3.4.1 discusses transmitter-end cancellation solutions that have been proposed in literature. However, in this thesis we develop a receiver-end distortion regeneration technique to cancel reverse IM products. Section 3.4.2 discusses similar regeneration techniques that have been proposed for receiver linearization, this builds the basics for our proposed solution.

3.4.1 Transmitter-end Solutions

Proponents of [28] propose a transmitter-end solution for reverse IM products. The goal is to stop the reverse signal (b in Fig. 2.10) from reaching the PA, preventing the generation of IM products. As seen in Fig. 3.6, a direct feed from one jammer is gain-phase adjusted and coupled into the output of a second colocated jammer such that it is 180° out of phase to the corresponding jamming signal that radiates in through the antenna system. Since reverse IM products occur in both amplifiers, the coupling must be bidirectional. Isolators are used to achieve independent bidirectional control. The scheme gave a good 35dB reduction in reverse IM, but unfortunately it adds insertion loss to the transmit path reducing transmitter efficiency. In addition, it requires a certain level of cooperation between the operators of the two transmitters.

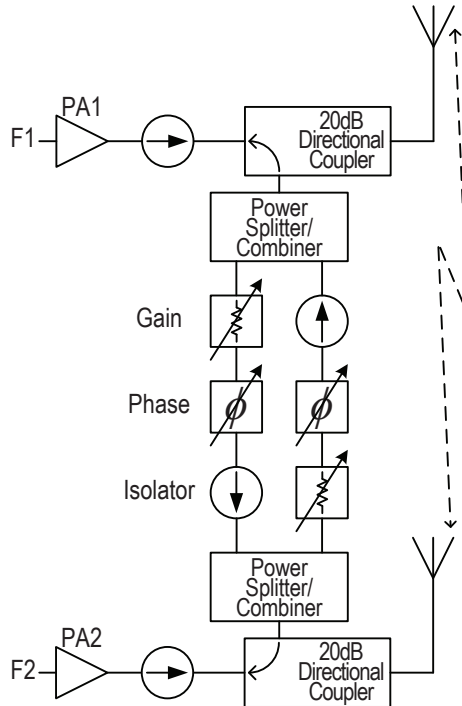


Fig. 3.6: Reverse IM cancellation system using direct feed phasing [28].

Research in the military [2] has shown that an interference cancellation technique is the best solution to such cosite distortion problems on an expeditionary fighting vehicle. However, the interference cancellation unit used in this instance takes advantage of direct feeds that are easily available from all transmitter units fitted within the vehicle.

3.4.2 Interference Cancellation Using Regenerated Distortions

An alternative philosophy is to allow the distortion to occur and then cancel it at the receiver by regenerating an estimate of the distortion using the fundamental jammers. The concept, known as postdistortion, is the inverse of predistortion which has been widely used in power amplifier linearization. The estimate of the distortions can be generated using polynomial functions. The most important of these are the second and third order distortion components. Both analog and digital techniques have been used for predistortion circuits [29]- [34]. Similar circuits can also be used

to linearize receivers and these are overviewed here.

3.4.2.1 Analog Second-order Postdistortion

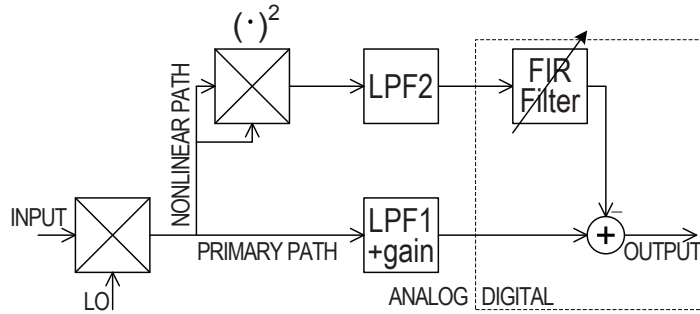


Fig. 3.7: Analog second-order postdistortion [35].

As seen in Fig. 3.7, the author of [35] has used an analog Gilbert cell multiplier as a squarer in the nonlinear path to provide an estimate of the second order distortion generated in the receiver’s down conversion mixer. The finite impulse response (FIR) filter is then adaptively equalized to remove the distortion in the primary path using the regenerated distortion estimate. An 11dB improvement in jamming margin was reported.

3.4.2.2 Analog Third-order Postdistortion

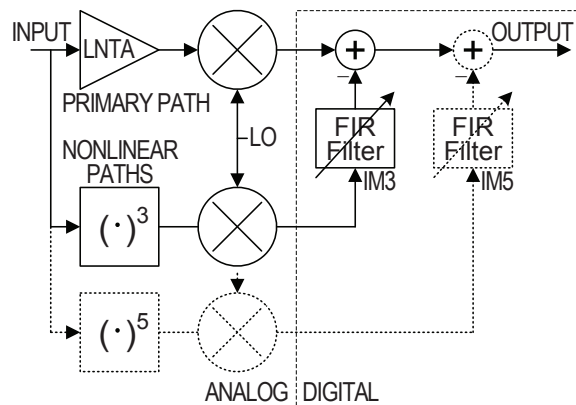


Fig. 3.8: Analog third-order postdistortion [36].

Fig. 3.8 shows the receiver architecture proposed by the authors of [36] to mitigate IM3 products produced within a receiver LNA. They use an analog cubing

circuit in the nonlinear path to produce an estimate of the IM3 products. These are down-converted to baseband before FIR filtering in the digital domain. The normalized LMS algorithm controls the FIR filter to adaptively cancel the interfering IM3 products in the primary path.

3.4.2.3 Hybrid Analog and Digital Polynomial Postdistortion

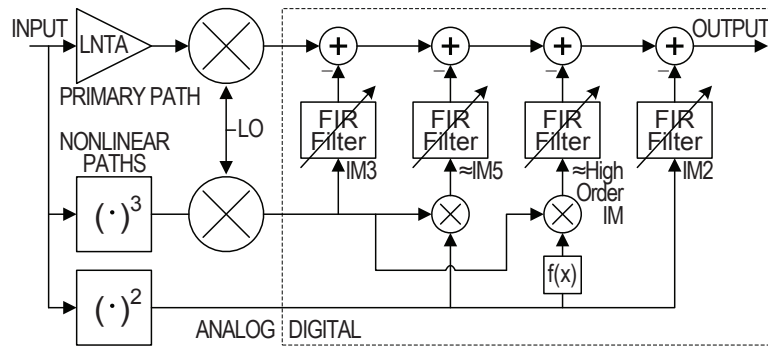


Fig. 3.9: Hybrid analog and digital polynomial postdistortion [37] .

The same authors, in [37] discuss how a polynomial extension of the scheme in Fig. 3.8 could be achieved using analog circuits capable of producing higher-order terms. However, they ascertain that complex large polynomial analog circuits would be required for such a task. In Fig. 3.9, the authors propose a hybrid analog and digital postdistortion circuit, where they produce the third-order term and the second-order term in analog, and then use polynomial functions in the digital domain to produce the required higher-order terms. Adaptive FIR filters are then used to mitigate the interfering IM products in the primary path. The circuit improved the receiver IP3 by 10dB.

Analogue squaring and cubing circuits often have inherent complexities such as direct feed-through, DC-offsets, temperature drifts and poor noise performance. Digital squaring and cubing do not have these problems; they are perfect (to within quantization noise). This leads to the next solution.

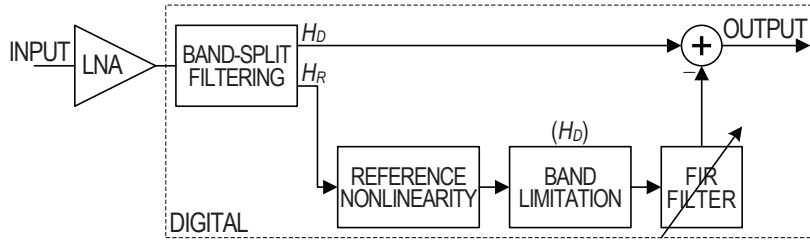


Fig. 3.10: Digital polynomial postdistortion [38].

3.4.2.4 Digital Polynomial Postdistortion

The authors of [38] performed both distortion regeneration and distortion cancellation in the digital domain. The distortion affected desired signal along with the jammers are received in the RF front-end and downconverted to digital baseband. As seen in Fig. 3.10, the desired signal band is filtered and separated from the jammers. The jammers are then processed with the appropriate polynomial function to produce the required distortion. An adaptive cancellation technique is then used to cancel the distortion from the desired signal band. However, the demonstrated system is bandlimited within the ADC's sampling rate and is unable to mitigate distortions produced by out-of-band jammers. Extremely high sampling rates are required to cater for out-of-band jammers and this is both expensive and energy consuming. The authors suggested a two-receiver solution could overcome the problem, but no further details were given.

3.5 The Proposed Solution for Reverse IM

In all the above regeneration and canceling schemes, the set of signals that generate the distortion products in the receiver circuits are exactly the same as those that generate the distortion estimate in the polynomial circuits. In the case of reverse IM, however, the set of signals that generate the distortion in the transmitter is different. The signals are likely to be the same but their relative amplitudes are different. The dominant jammers causing the reverse IM might not be the dominant jammers in the regeneration circuits. Thus a certain level of jammer selectivity is required before

regenerating the distortion estimate. A full DSP solution would give this flexibility in which case the solution of 3.4.2.4 is the best for the reverse IM problem. The cost and energy implications of the high sample rate of the ADC and processing circuits must however be addressed.

The need for multi-standard, multi-band wireless receivers has grown an increasing amount of interest in software configurable radios. Inroads have been made in developing low cost wideband software defined radios (SDRs) [39] [40]. In this thesis we take advantage of such SDR front-ends and extend the two-receiver suggestion of [38] into a multi-receiver solution using SDR front-ends. We propose a novel distortion synthesis technique for a postdistortion cancellation system. As seen in Fig. 3.11, the primary SDR front-end (Rx0) receives the corrupt desired signal (y). The auxiliary SDR front-ends (Rx1, Rx2 ...) receive the fundamental jammers ($a, b \dots$) that contributes to the interfering distortion. The fundamental jamming signals are then digitally processed to produce the required distortion estimate (\hat{u}). The additional receivers need only be of low resolution since the jamming signals are strong. The sampling rates only need to cover the signal bandwidth plus a little extra to accommodate bandwidth expansion in the regeneration circuits. The estimate is then used to remove the interfering distortion in the primary reception.

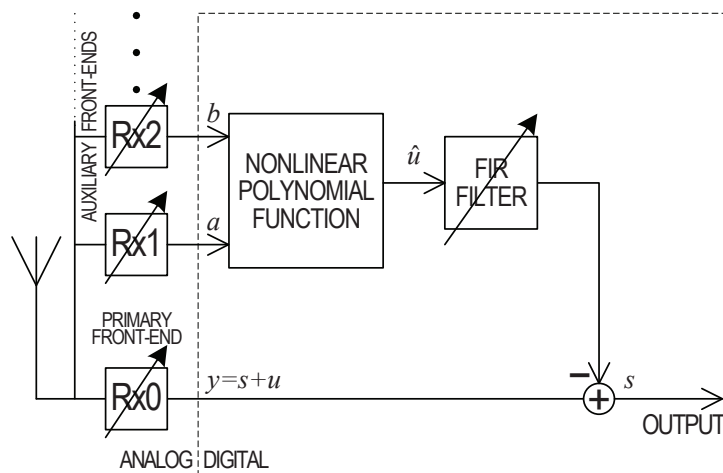


Fig. 3.11: Proposed reverse IM postdistortion solution.

3.6 Summary

- In this chapter we have discussed three different categories of solutions addressing the colocation issues. However, most solutions do not consider all aspects of the colocation problem, since they are generally targeted at the receiver distortion problem; which is not quite the same thing.
- Passive filtering solutions required high- Q and low insertion loss filters, making them difficult to implement in a frequency flexible environment at cost levels demanded by commercial equipment.
- Canceling loop solutions are a potential remedy for forward IM; they mitigate the jamming signals before they hit the nonlinear components of the receiver.
- Reverse IM solutions include canceling the reverse jammer at the transmitter output and postdistortion cancellation at the victim receiver. The former requires cooperation between service providers, and so the latter is the more suitable solution. A full DSP solution is preferred since it gives flexibility in jammer selection. A scheme that uses multiple receiver front-ends is proposed to avoid the huge sample rates of a single receiver architecture when jammers are out-of-band. It will be discussed in more detail later in the thesis (chapter 7).

The next chapter describes the proposed forward IM solution which involves jammer cancellation at RF using a separate reference antenna. This solution is an effective antidote for receiver desensitization and the production of forward IM products.

Chapter 4

The Adaptive Cancellation System and its Dynamic Range

In this chapter, we propose an adaptive cancellation system that is capable of mitigating jamming signals from a dominant colocated jammer antenna. This reduces the levels of the jamming signals hitting the nonlinear components of the victim receiver, therefore, it mitigates the generation of forward IM products and desensitization. In a modern base station site a single antenna carries many transmissions. These are normally multiplexed at baseband and then transmitted through a single linearized RF power amplifier (see section 1.2).

Further, we characterize the practical feasibility of the system by studying the effect of the cancellation loop on the receiver's dynamic range. We obtain expressions for the system IP3 and system noise factor as a function of the elements in the cancellation loop. We then use the equations to predict the performance of a hardware test bed. The test bed shows significant reduction in distortion is possible with this technique.

Section 4.1 describes the proposed adaptive cancellation system. Section 4.2 derives theoretical expressions for the IP3 and system noise factor, which formulates the upper and lower bound of the dynamic range of the system. Section 4.3 describes the laboratory setup and compares the distortion products and noise floor before and after cancellation.

4.1 The Adaptive Cancellation Architecture

The colocated scenario requires a single system that will adaptively filter all colocated high power transmit jammers and allow only the desired receive signal at the receiver. An adaptive interference cancellation system, as depicted in Fig. 4.1,

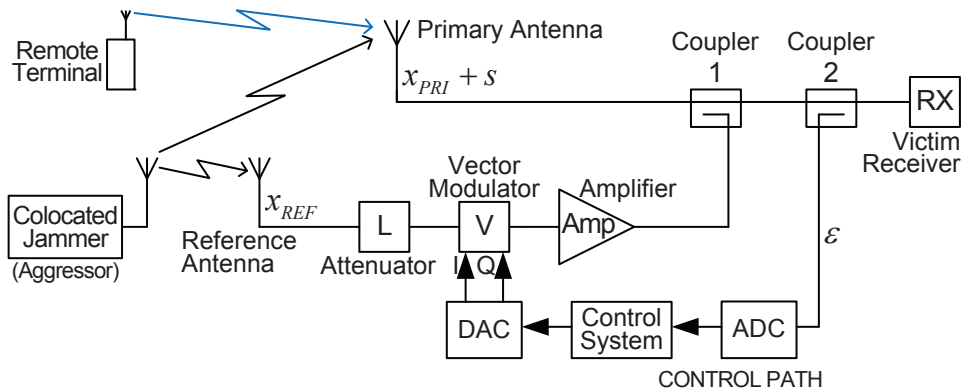


Fig. 4.1: Proposed adaptive cancellation system for colocated transceivers.

is proposed as a solution to the problem. The primary antenna picks up the desired signal s with the jamming signal x_{PRI} . The reference antenna is directed to pick only the jamming signal x_{REF} (or more practically have a much larger interference to signal ratio than the primary). The reference input is then gain and phase adjusted and coupled into the primary path to cancel the jamming signal. Ideally the additional processing elements must not generate distortion components. In reality this is not possible. The goal therefore is to limit the distortion generated by the reference path to a level that is significantly lower than the distortion of the original receiver on its own without the cancellation system. This has to be achieved with minimal degradation of the receiver noise factor. Unfortunately, it is not readily apparent how the specifications of the components such as the gain, dynamic range and coupling factor affect the system performance.

In the next section we derive expressions for the overall system IP3 and system noise factor as a function of the components in the reference path [41].

4.2 Dynamic Range of the Proposed System

Fig. 4.1 shows an I and Q vector modulator that is controlled to provide the desired phase shift and/or attenuation. Attenuation is required when the jamming signal picked on the reference antenna is sufficiently larger than that on the primary. It might be necessary to use an additional fixed attenuator ahead of the vector modulator if its signal handling capacity (dynamic range) is exceeded. The reference cancellation path also uses an amplifier to compensate for the coupler and provide the amplification needed to eliminate the jamming signal in the primary. The control system takes feedback ε from the cancellation output to provide the necessary adjustments to the vector modulator.

4.2.1 Third-order Intercept Point (IP3)

In order to analyze the circuit, the proposed system in Fig. 4.1 is redrawn with coupler 1 and coupler 2 restructured as shown in Fig. 4.2(a). In this analysis, it is to be noted that lower case variables represent complex envelope voltages which characterize both the amplitude and the phase of the signal, and uppercase variables represent respective power levels, e.g., $X_{PRI} = E\{|x_{PRI}|^2\}/2$. The diagram only represents the through-path of coupler 2, which is given a gain of G_{CPL2} . Coupler 1 has a coupling-path gain of C and a through-path gain of $(1-C)$. The attenuator (L) has a gain, G_L . G_V , G_A , and G_{RX} are the power gains of the vector modulator (V), amplifier (Amp) and the receiver (RX) respectively. $IP3_V$, $IP3_A$ and $IP3_{RX}$ are their IP3 values. The attenuator and couplers are passive linear devices and do not have IP3 values. X_{PRI} is the power of the jamming signal at the primary antenna, and X_{REF} is its power at the reference antenna. We define $H = X_{REF}/X_{PRI}$, the effective power gain of the jamming signal on the reference antenna to that on the primary antenna.

The system could be simplified and redrawn with a single input as shown in Fig. 4.2(b). At the cancellation point, the cancellation signal (x_2) is subtracted from the jamming signal (x_1) to give the resultant signal, i.e., $x_3 = x_1 - x_2$. X_3 is the

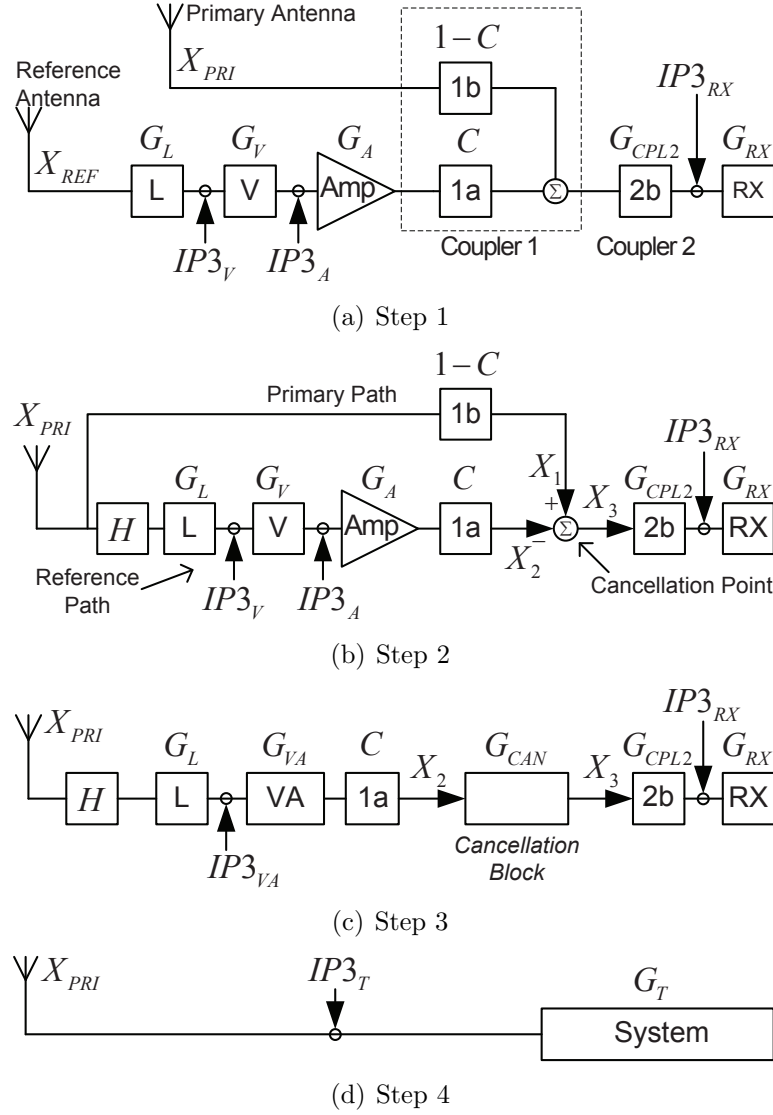


Fig. 4.2: IP3 analysis of the proposed system.

power of the resultant signal. Further, X_3 can effectively be written as a factor of X_2 . The factor is termed as the cancellation gain (G_{CAN}), it represents the amount of the jamming signal left with respect to the cancellation signal; and is evaluated as follows,

$$G_{CAN} = \frac{X_3}{X_2} = \left(\sqrt{\frac{1-C}{HG_LG_VG_AC}} - 1 \right)^2, \quad C \neq 0. \quad (4.1)$$

The diagram can be simplified further with equivalent composite blocks, as depicted in Fig. 4.2(c). The primary path and the cancellation point are represented together as the cancellation block with an effective gain of G_{CAN} . Block VA is the

composite of blocks V and Amp having a combined total gain of $G_{VA} = G_V G_A$ and a combined IP3 of $IP3_{VA}$,

$$\frac{1}{IP3_{VA}} = \frac{1}{IP3_V} + \frac{G_V}{IP3_A}. \quad (4.2)$$

Finally, Fig. 4.2(d) simplifies the system into a single block, with a total gain, $G_T = HG_L G_V G_A C G_{CAN} G_{CPL2} G_{RX}$ and an effective total IP3,

$$\frac{1}{IP3_T} = \frac{HG_L}{IP3_V} + \frac{HG_L G_V}{IP3_A} + \frac{HG_L G_V G_A C G_{CAN} G_{CPL2}}{IP3_{RX}}. \quad (4.3)$$

The study here considers that the cancellation system has converged and a perfect cancellation is achieved at the cancellation point, i.e., $G_{CAN} = 0$. Substituting Equation (4.1) in Equation (4.3) we can remove G_V and G_A . Furthermore, it is to be noted that the IP3 values in the above equations are ‘input’ IP3 values, but in practice the IP3 value for amplifiers are specified at the output. Given the output IP3 of amplifier Amp ($OIP3_A$), the following is derived,

$$\frac{1}{IP3_T} = \frac{HG_L}{IP3_V} + \frac{1 - C}{OIP3_A C}, \quad C \neq 0. \quad (4.4)$$

Equation (4.4) is used to characterize the total IP3 of the system.

4.2.2 Noise Analysis

Fig. 4.3(a) depicts the proposed system with the corresponding noise factors. The primary and the reference antenna noises are uncorrelated to one another. They are white noise and are equivalent to $k_B T_0 B_W$ W, where k_B is the Boltzmann’s constant, T_0 is the standard noise temperature (290K), and B_W is the bandwidth (Hz). Attenuator L is a passive device and has a noise factor, $F_L = 1/G_L$ [11]. F_V , F_A and F_{RX} are the noise factors of the vector modulator, amplifier and the receiver respectively. Coupler 1 is used in reverse, being a passive device, it does not add any excess noise (see section 2.3) to the input port (IN). The sampling coupler 2 is considered to have a weak coupling value (≤ -20 dB) such that it has a

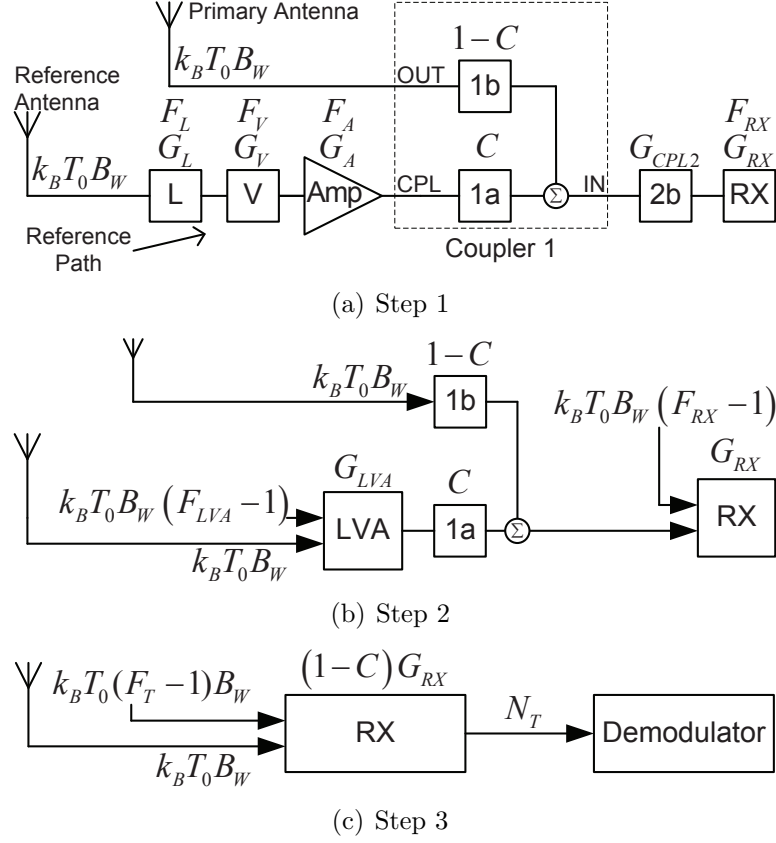


Fig. 4.3: Noise analysis of the proposed system.

negligible through-path loss (i.e., $G_{CPL2} \approx 1$) and the sensitivity of the receiver is least affected.

The system is redrawn with equivalent composite blocks, as shown in Fig. 4.3(b). The blocks are assumed to be ‘ideal’ (i.e. noiseless), with their internal noise referred to the input of the blocks. The combined noise factor of blocks L, V and Amp is

$$F_{LVA} = F_L + \frac{F_V - 1}{G_L} + \frac{F_A - 1}{G_L G_V} \quad (4.5)$$

with a corresponding total gain of $G_{LVA} = G_L G_V G_A$.

Total noise N_T at the demodulator of the receiver is given by,

$$N_T = k_B T_0 B_W G_{RX} [G_A C (F_V G_V + F_A - 1) + F_{RX} - C] W. \quad (4.6)$$

Simultaneously, as depicted in Fig. 4.3(c), the total noise of the system can be

represented in terms of the effective noise factor (F_T) of the system, as follows,

$$N_T = [k_B T_0 B_W + k_B T_0 (F_T - 1) B_W] (1 - C) G_{RX} W. \quad (4.7)$$

Therefore, from Equations (4.6) and (4.7), F_T is given by,

$$F_T = \frac{G_A C (F_V G_V + F_A - 1) + F_{RX} - C}{1 - C} \quad (4.8)$$

Equation (4.8) is used to characterize the effective noise factor of the system.

4.2.3 Discussion

It is interesting to note the effect of coupler 1. As the coupling is reduced, $C \ll 1$ the noise figure also reduces but will never go below the noise floor set by F_{RX} (4.8). On the other hand, smaller values of C reduces the $IP3_T$. Alternatively, increasing the coupling C improves $IP3_T$ (4.4). Hence, the coupling gain C works as a compromise between achieving lower noise figures and higher IP3s for the system.

4.3 Experimental Results

A low noise amplifier with a gain $G_{RX} = 19\text{dB}$, input IP3 $IP3_{RX} = 6\text{dBm}$ and a noise factor $F_{RX} = 2.7\text{dB}$ is considered as the receiver. A two-tone test demonstrates the improvement in intermodulation characteristics by the proposed cancellation system. Initially, the receiver without the cancellation system is put under investigation. A signal generator is used to produce two fundamental tones at $f_1 = 919.5\text{MHz}$ and $f_2 = 920.5\text{MHz}$ of identical amplitudes. At the output we have IM3 products at frequencies $2f_2 - f_1 = 921.5\text{MHz}$ and $2f_1 - f_2 = 918.5\text{MHz}$ along with the fundamentals at f_1 and f_2 . Fig. 4.4 shows the output power levels of the fundamentals and the IM3 products with respect to input level of the fundamentals. The fundamentals represent the jamming signals and the IM3 products are the distortions generated within the victim receiver.

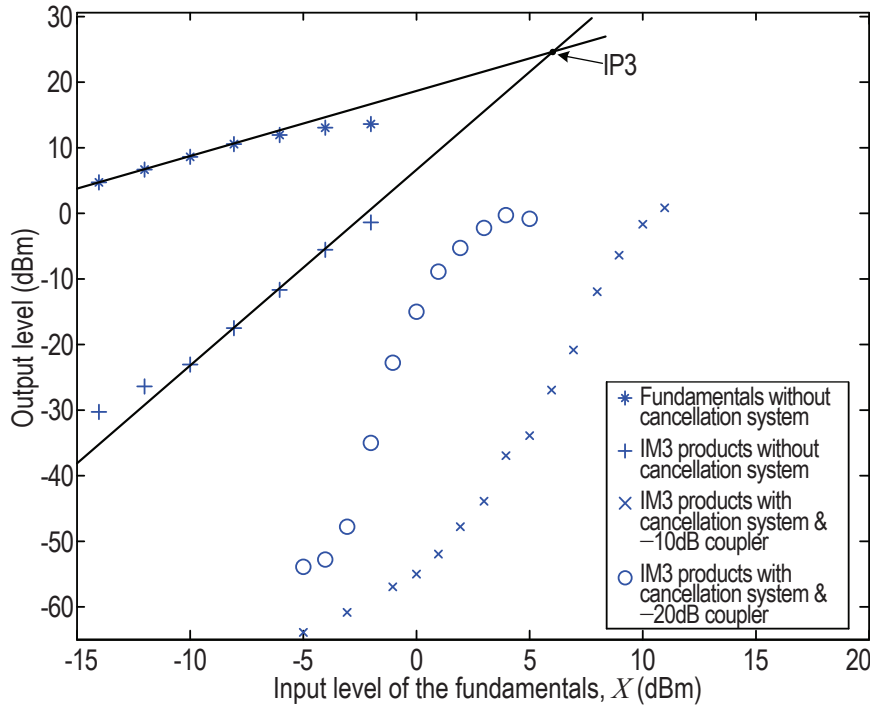


Fig. 4.4: Two-tone test on a receiver LNA with 19dB gain and 6dBm input IP3.

Fig. 4.5 shows the two tone test setup of the proposed cancellation system. We use a power-splitter at the input of the system to divide signal power equally between the primary and the reference path (i.e., $H = 1$). No attenuator is used in front of the vector modulator (i.e., $G_L = 1$). The signal in the reference path is processed through a vector modulator and an amplifier before being coupled into the primary path using coupler 1. The amplifier used has an output IP3 $OIP3_A = 40$ dBm, a

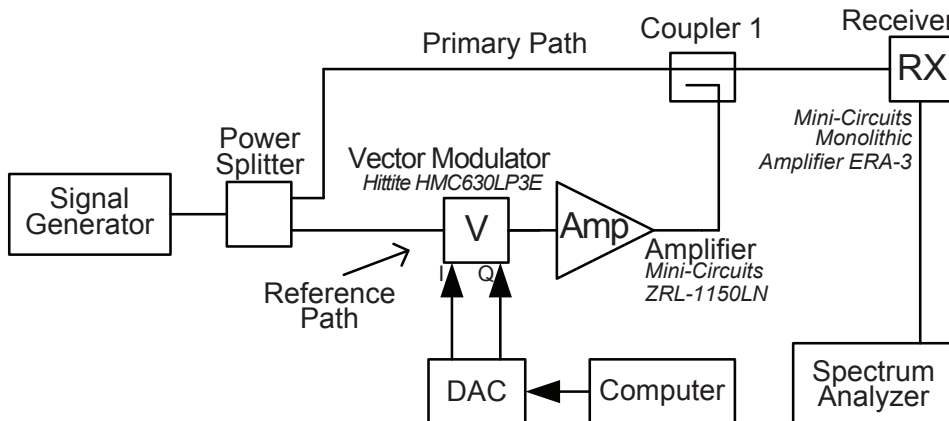


Fig. 4.5: Laboratory setup for IP3 and noise measurements.

gain $G_A = 30\text{dB}$ and a noise factor $F_A = 1.4\text{dB}$. The vector modulator has an input IP3 $IP3_V = 34\text{dBm}$, and a gain of $-50\text{dB} < G_V < -10\text{dB}$. The noise characteristics of the vector modulator varies negligibly with its gain and is defined at the output, $kT_0F_VG_V = -162\text{dBm/Hz}$. The vector modulator is adjusted to the required phase shift and attenuation for maximum cancellation. Measurements of the IM3 products with the cancellation system for both the -10dB and -20dB coupler are shown in Fig. 4.4. It is to be noted that within the unsaturated linear operating region of the receiver the IM3 products are now below the noise floor, thus showing a significant improvement in the intermodulation characteristics of the receiver. Note the increased IM3 products slopes for the -10dB and -20dB coupler is due to the over driven amplifier Amp.

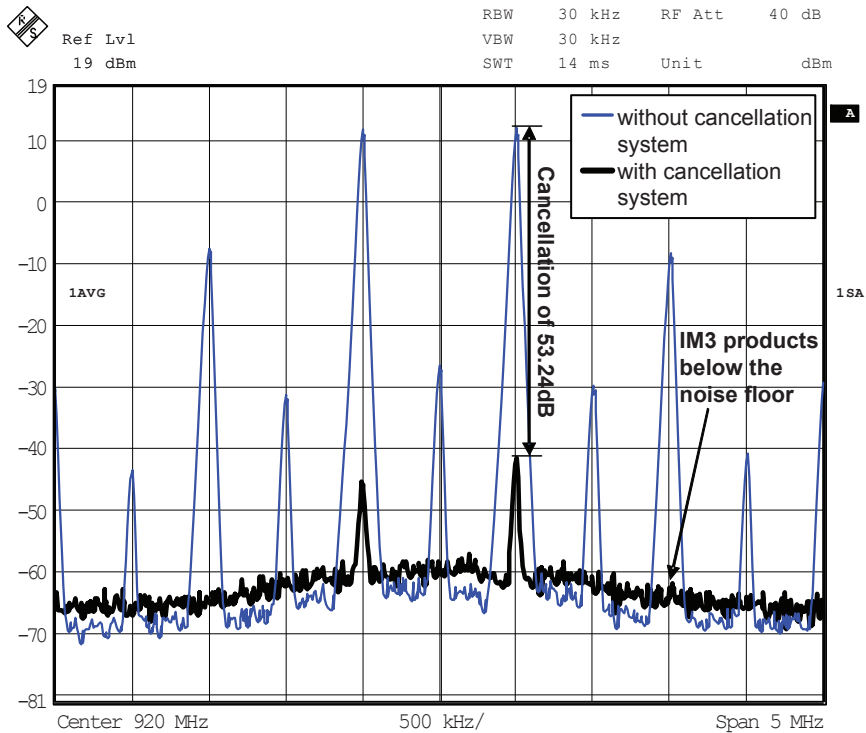


Fig. 4.6: Spectrum of the receiver with and without the proposed cancellation system (using -10dB coupler) during a two-tone test with an input power of -5dBm .

Fig. 4.6 represents the spectrum of the signal at the receiver with and without the cancellation system. Our system in the laboratory achieves a cancellation of about 53dB and brings the IM3 products down below the noise floor.

Furthermore, the canceled waveform in Fig. 4.6 has a higher noise floor due

to the canceling circuits. The measured noise floor agreed with the prediction of Equation (4.8) of -103dBm for the -20dB coupler; this could be further reduced by approximately 10dB if a lower gain version of amplifier Amp was selected. In such a case the vector modulator would not need to attenuate the signal so heavily.

4.4 Summary

- The proposed cancellation system aims at mitigating large interfering signals at the receiver and hence, it increases its capacity to handle strong signals by improving its effective IP3. However, such an increase in the upper end of its dynamic range affects the sensitivity of the receiver by degrading its noise factor.
- The chapter studies in detail the dynamic range characteristics of the proposed system. It derives theoretical expressions of the IP3 and the noise factor of the system; and concludes that the cancellation coupler (Coupler 1) is a compromise between achieving lower values of noise figure and higher values of IP3.
- The chapter then takes practical measurements and shows that the cancellation system improves the intermodulation characteristics of the receiver. It demonstrates that such a cancellation system is capable of achieving cancellations of about 53dB in practice. It also takes noise measurements and demonstrates that our derived noise expression matches very closely with practical results.

In the next chapter we build on the findings of this chapter and carry out a novel signal-to-interference-and-noise ratio analysis on the proposed cancellation system to find an optimum coupling value C .

Chapter 5

Optimized Interference Cancellation

In the previous chapter (Ch. 4), an adaptive cancellation system for mitigating forward IM products was proposed. As in most RF circuits it is possible to trade off noise for distortion and vice-a-versa. In the proposed system it is the cancellation coupler (Coupler 1) that determines the trade-off. If the coupling (C) is weak then a larger canceling signal (x_{REF}) is needed to remove the jamming signal (x_{PRI}); this toughens the IP3 requirements for the canceling branch. On the other hand a strong coupling coefficient reduces the desired signal (s) on the primary path and contributes to an increase in the receiver noise figure. The cancellation coupler is therefore a compromise between achieving higher values of IP3 and lower values of noise figure. To our knowledge no analysis has shown what the optimum coupling should be.

In this chapter we carry out a novel signal-to-interference-and-noise ratio (SINR) analysis on the proposed adaptive cancellation system for mitigating forward IM products. We develop an expression for the optimum coupler value that maximizes the SINR [42]. In addition, we describe an automated cancellation system that studies the energy at the output of the cancellation using an Universal Software Radio Peripheral (USRP) [39] and minimizes the energy using a one dimensional

iterative search algorithm. We then carry out experiments to show that our theoretical analysis aligns with practical results. A significant improvement in SINR can be achieved using the cancellation system.

Section 5.1 derives theoretical expressions for the SINR of the system and section 5.2 derives an equation for the optimum coupler value. Section 5.3 describes the hardware setup and convergence technique of the cancellation system. Section 5.4 compares SINR results from the test-bed with the theoretical predictions.

5.1 Derivation of SINR

A higher value of IP3 represents a lower level of intermodulation distortion within a receiver for a given input level. Similarly, a lower value of noise figure represents a lower level of noise within a receiver. The compromise between the level of intermodulation distortion and noise at the receiver can be evaluated simultaneously with a single parameter, i.e. the SINR. In this section, we develop expressions for the desired signal, noise and third-order intermodulation distortion from which the SINR can be evaluated.

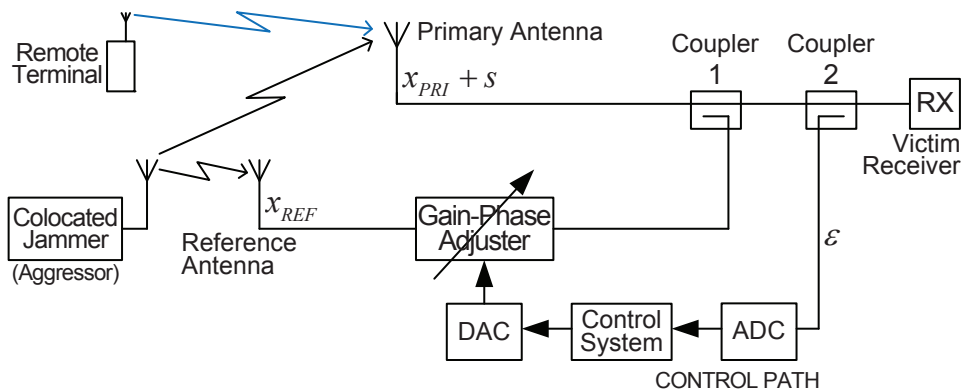


Fig. 5.1: An adaptive cancellation system.

The adaptive cancellation system described in the previous chapter (Ch. 4) is illustrated in Fig. 5.1 with a slight modification to its reference path. The reference path components, i.e., the attenuator, the vector modulator and the amplifier, are now combinedly represented as a gain-phase adjuster (GPA) for the SINR analysis.

The components can be optimized separately once the output and input characteristics of the reference arm have been decided. If manufacturers of vector modulators specify distortion or noise at the device output, then they become independent of the actual gain setting, which simplifies the analysis. Thus, the GPA is characterized with an effective gain G_e , an output IP3 $OIP3_e$ and an output noise temperature T_e . Defining the characteristics of the GPA at the output also makes our analysis compatible with data sheet specifications of some devices for our real world results.

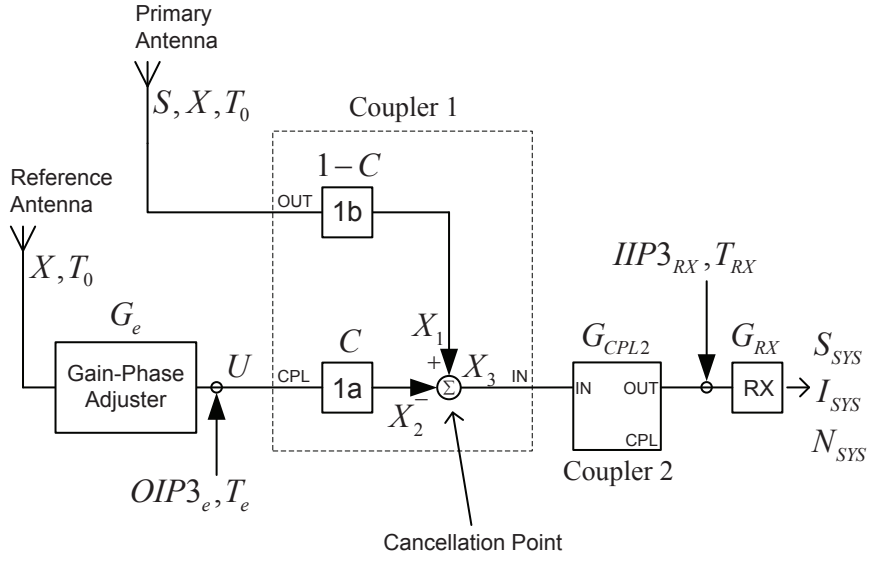


Fig. 5.2: Signal-to-interference-and-noise analysis.

In order to analyze the circuit, the proposed system in Fig. 5.1 is redrawn with Coupler 1 and Coupler 2 restructured as shown in Fig. 5.2. Here, we note that lower case variables represent complex envelope voltages which characterize both the amplitude and the phase of the signal, and uppercase variables represent respective power levels, e.g., $S = E\{|s|^2\}/2$.

The sampling Coupler 2 extracts the feedback signal for the convergence algorithm. The signal of interest for the feedback circuit is the residue of the canceled jamming signal, X_3 . This signal is not required to be totally eliminated provided it is reduced to a level that produces no significant intermodulation in the receiver (i.e., the level of the intermodulation products are below the receiver noise floor). As such the feedback signal is still large and so there is no undesirable consequences

if it is further attenuated through Coupler 2. In fact it is desirable to have a weak coupling value so that the sensitivity of the receiver to the wanted signal S is least effected. Here we assume a coupling value of $\leq -20\text{dB}$, such that it has negligible through path loss of $1 - 0.01 = 0.99$ (i.e., $G_{CPL2} \approx 1$).

Coupler 1 cancels the jammer. The coupling path gain is C , and hence, the through path gain is $1 - C$. We note that the domain of C is limited to $0 < C < 1$. Couplers are passive devices and are assumed not to produce any distortion. Further, Fig. 5.2 illustrates $OIP3_e$ and T_e of the GPA. It also shows the IP3, $IIP3_{RX}$, and the noise temperature, T_{RX} , of the receiver referred to its input. The gain of the receiver is G_{RX} .

We now develop expressions for the interference I_{SYS} , noise N_{SYS} , and signal S_{SYS} at the receiver output.

5.1.1 Third-order Intermodulation Distortion at the Receiver

For simplicity we consider that both the primary and the reference antenna pick equal powered jamming signal, i.e. $X_{PRI} = X_{REF} = X$. At the cancellation point, the cancellation signal (x_2) is subtracted from the jamming signal (x_1) to give the resultant signal ($x_3 = x_1 - x_2$). X_3 is the power of the resultant signal. The study here considers that the cancellation system has converged and perfect cancellation is achieved at the cancellation point, i.e. $X_1 = X_2$ and $X_3 = 0$. Hence, the GPA gain,

$$G_e = \frac{1 - C}{C}. \quad (5.1)$$

When $X_3 = 0$ or is insignificantly small, the receiver does not produce any third-order intermodulation distortion components, thus distortion components are only produced at the GPA. The IM3 distortion U produced at the GPA output is given by [6],

$$U = \frac{G_e^3 \cdot X^3}{OIP3_e^2}. \quad (5.2)$$

Substituting for G_e from (5.1), the IM3 distortion at the receiver output is given

by,

$$I_{SYS} = \frac{G_{RX} X^3 (1 - C)^3}{OIP_3^2 C^2}. \quad (5.3)$$

5.1.2 Signal and Noise at the Receiver

As mentioned earlier, the primary antenna is aimed at picking the desired receive signal; hence, the signal level at the receiver output is given by,

$$S_{SYS} = S(1 - C)G_{RX}. \quad (5.4)$$

The primary and the reference antenna noises are uncorrelated to one another. They are white noise and have a noise temperature of T_0 (standard noise temperature, 290K). Thus the total noise at the receiver output is given by,

$$N_{SYS} = k_B B_W G_{RX} (T_0 + T_e C + T_{RX}) \quad (5.5)$$

where k_B is Boltzmann's constant (1.38×10^{-23} J/K) and B_W is the noise bandwidth (Hz).

All of the above three equations are affected by the coupler coefficient C . Both the signal S_{SYS} and the interference I_{SYS} tend to zero as $C \rightarrow 1$. Surprisingly, the signal-to-interference ratio (SIR) improves, but unfortunately this does not apply to the SINR which includes the effect of noise.

5.1.3 Signal to Interference and Noise Ratio

Combining (5.3)–(5.5), the SINR at the receiver is given as follows,

$$SINR_{SYS} = \frac{S(1 - C)}{\frac{X^3 (1 - C)^3}{OIP_3^2 C^2} + k_B B_W (T_0 + T_e C + T_{RX})} \quad (5.6)$$

and is a function of the dynamic range of the reference path, the excess noise temperature of the receiver, the power of the jammer and coupler value. In the next section we determine the Coupler 1 value that gives the highest SINR.

5.2 Optimum Coupling

For a certain strength of the jamming signal X we can optimize the coupler value C to give the largest possible SINR. We differentiate $SINR_{SYS}$ with respect to C ,

$$\frac{dSINR_{SYS}}{dC} = \frac{S \cdot OIP3_e^2 C \left(2(1-C)^3 X^3 - k_B B_W OIP3_e^2 C^3 (T_0 + T_e + T_{RX}) \right)}{\left(k_B B_W OIP3_e^2 C^2 (T_0 + T_e C + T_{RX}) + (1-C)^3 X^3 \right)^2}. \quad (5.7)$$

Setting $\frac{dSINR_{SYS}}{dC} = 0$ for $0 < C < 1$ gives,

$$\frac{1-C}{C} = \sqrt[3]{\frac{k_B B_W OIP3_e^2 (T_0 + T_e + T_{RX})}{2X^3}} \quad (5.8)$$

which has one real root and two imaginary roots. C is a power gain and must be real; therefore there is only one extremum. Thus,

$$C_{opt} = \frac{2^{1/3} X}{\Lambda^{1/3} + 2^{1/3} X} \quad (5.9)$$

where,

$$\Lambda = k_B B_W OIP3_e^2 (T_0 + T_e + T_{RX}). \quad (5.10)$$

The optimum SINR associated with C_{opt} can be obtained by substituting (5.9) into (5.6). Inspecting (5.6), we note that SINR is always positive and has a value of 0 at both ends of C 's domain, i.e.,

$$\begin{aligned} SINR_{SYS} &> 0 \\ C \rightarrow 0, SINR_{SYS} &\rightarrow 0 \\ C \rightarrow 1, SINR_{SYS} &\rightarrow 0. \end{aligned} \quad (5.11)$$

Hence, C_{opt} gives the maximum value of $SINR_{SYS}$.

From (5.9), C_{opt} is a function of X and Λ . X is the power of the jamming signal. When X is large, C_{opt} asymptotes to 1, i.e., $C_{opt}(\text{dB}) \rightarrow 0$ in the log scale, as shown in Fig. 5.3.

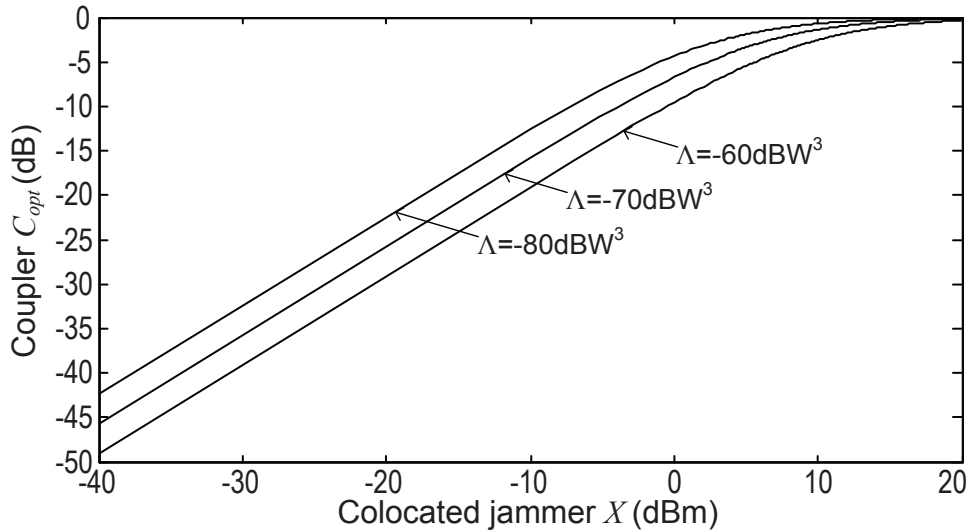


Fig. 5.3: Optimum coupler C_{opt} as a function of jammer X and the Λ value (Λ is primarily a function of the dynamic range of the components in the reference path).

Further, applying Taylor's series to (5.9),

$$C_{opt} = \frac{2^{1/3}}{\Lambda^{1/3}}X - \frac{2^{2/3}}{\Lambda^{2/3}}X^2 + \frac{2}{\Lambda}X^3 - \frac{2^{4/3}}{\Lambda^{4/3}}X^4 + \dots \quad (5.12)$$

When X is small, the first term in (5.12) dominates and there is a linear relationship between X and C_{opt} with a slope of 1 in the log scale (i.e. $C_{opt}(\text{dB})$ is proportional to $X(\text{dBW})$), as shown in figure,

$$C_{opt}(\text{dB}) = -\frac{1}{3}\Lambda(\text{dBW}^3) + X(\text{dBW}) + 1(\text{dB}). \quad (5.13)$$

Λ is a function of the dynamic range components ($OIP3_e$ and T_e) of the reference path and the noise figure (T_{RX}) of the receiver; Λ has a unit of cubic watts. Note that Λ is not dependent on $IIP3_{RX}$ since we assume perfect cancellation, and therefore, no jamming signal reaches the receiver. In the linear region, increasing Λ by 10dB decreases C_{opt} by $3\frac{1}{3}$ dB. The value of Λ characterizes the reference path and the sensitivity of the receiver. An increase in Λ makes noise in the system more dominant; a 10dB increase in Λ could either be a 10dB increase in noise, i.e., $k_B B_W (T_0 + T_e + T_{RX})$, or a 10dB increase in $OIP3_e^2$, which signifies a 10dB decrease in distortion (5.2); in either case, the noise-to-distortion ratio increases

by 10dB. Vice versa, a decrease in Λ makes distortion in the reference path more dominant.

The effect of the receiver noise figure is also covered in these equations. Receivers with low sensitivity (high T_{RX}) will have a high Λ value, implying a larger jamming signal for the same optimum coupler value. This is intuitively correct since a high effective noise floor allows higher distortion levels.

In most practical applications the coupler is an off-the-shelf item and only certain values are available (e.g., -3 , -6 , -10 , -20 dB). In such a situation, it is often necessary to know the design jamming level X_d that a given coupler will allow. Rewriting (5.9) we get,

$$X_d = \frac{\Lambda^{1/3}C}{2^{1/3}(1 - C)}. \quad (5.14)$$

5.3 Hardware Setup and Convergence

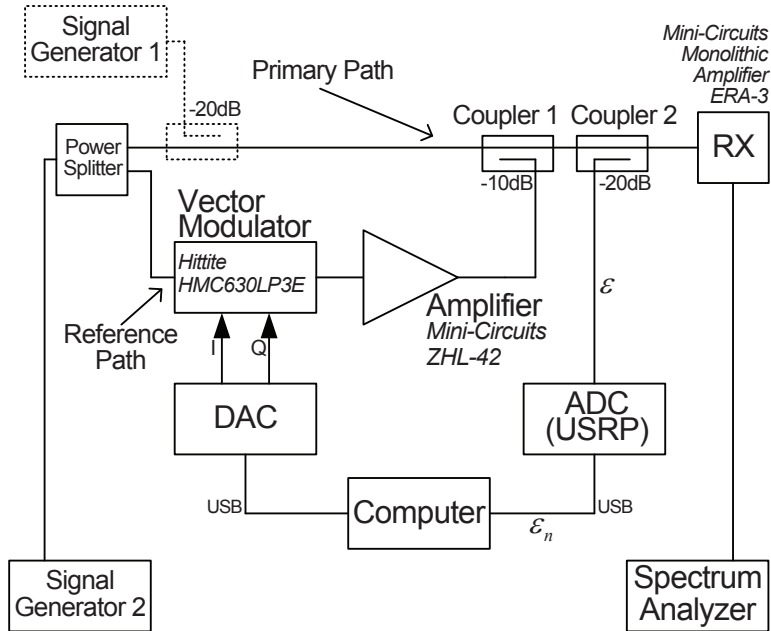


Fig. 5.4: Laboratory Setup: Signal Generator 1 generates the desired signal S and Signal Generator 2 generates the two tone jamming signal which is split into two with the Power Splitter to have equal levels of jammer X on both the Primary Path and the Reference Path.

A two-tone test is carried out on the proposed cancellation system to further study the SINR characteristics of the system and verify theory with practical results.

In order to have a controlled experiment that focuses on the actual SINR performance of the cancellation scheme, signals were all directly coupled into the system, no antennas were used. Fig. 5.4 shows the two tone test setup of the proposed cancellation system. The gain-phase adjuster is realized with the use of a vector modulator [43] and an amplifier [16]. The vector modulator provides the required attenuation on the reference path when the jamming signal is larger than that of the primary. The amplifier provides the gain required to compensate for the coupler and the amplification required to eliminate the jammer in the primary path. An attenuator in front of the GPA might also be required if the copy of the jamming signal on the reference path is high.

The adaptive cancellation process works by learning the energy at the output of the cancellation and minimizing it. We use a -20dB coupler (Coupler 2) to couple out a sample from the cancellation output; a USRP is used to measure the sample in IQ components within a computer, then an algorithm evaluates the energy of the sample, the algorithm takes the energy as a cost function and minimizes it by iteratively changing the input voltage to the vector modulator using a DAC. The cost function is given by,

$$CF = \sum_{n=1}^{1500} \varepsilon_n \varepsilon_n^* \quad (5.15)$$

where ε_n is a complex baseband sample from the USRP working as an ADC. If we assume the noise, signal and the distortion products are uncorrelated then,

$$CF = \left(\frac{\left((1 - C) + G_e C - 2\sqrt{G_e (1 - C) C} \right) X}{+ \frac{S_{SYS} + I_{SYS}}{G_{RX}} + k_B B_W (T_e C + T_0)} \right) C_2 \quad (5.16)$$

where the coupling path gain of Coupler 2, $C_2 = -20\text{dB}$, and reaches a global minimum of,

$$CF_{min} = \left(\frac{S_{SYS} + I_{SYS}}{G_{RX}} + k_B B_W (T_e C + T_0) \right) C_2 \quad (5.17)$$

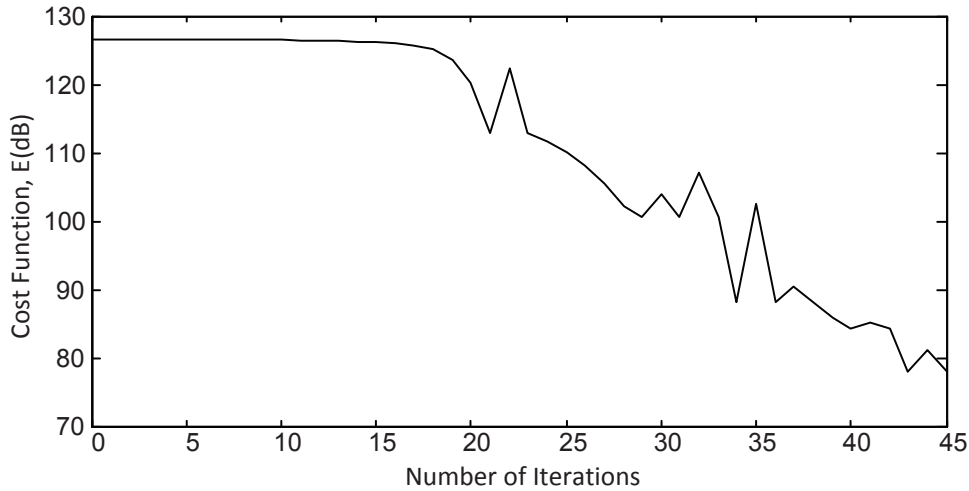


Fig. 5.5: Learning curve of the adaptive cancellation system during a two-tone test with an input power of -10dBm.

when (5.1) applies.

The DAC has a resolution of 1mV, the algorithm iterates and minimizes energy (CF) in steps of 100mVs and then 10mVs and finally 1mV. Fig. 5.5 shows such a learning curve during a two-tone test. The cost function takes about 45 iterations to reach its minimum value. Each iteration takes $187.5\mu\text{s}$ to obtain 1500 samples for the CF estimate at a USRP sample rate of 8M samples/s. The total convergence time is a respectable 8.4375ms.

Fig. 5.6 illustrates the spectrum at the receiver with and without the cancellation system. The IM3 products are reduced below the noise floor of the spectrum analyzer. The automated cancellation system achieves a cancellation of about 46dB, which is 7dB less than what was achieved with a manual cancellation system in the previous chapter [41]. One of the causes is a large noise component, i.e., $k_B B_W (T_e C + T_0) C_2$, in the CF due to the wide bandwidth of the measuring system (in this case, 8MHz). A wide-band receiver is needed in the feedback loop since the exact frequency of the jamming signal is unknown. An alternate solution using a frequency scanning narrowband receiver would also work.

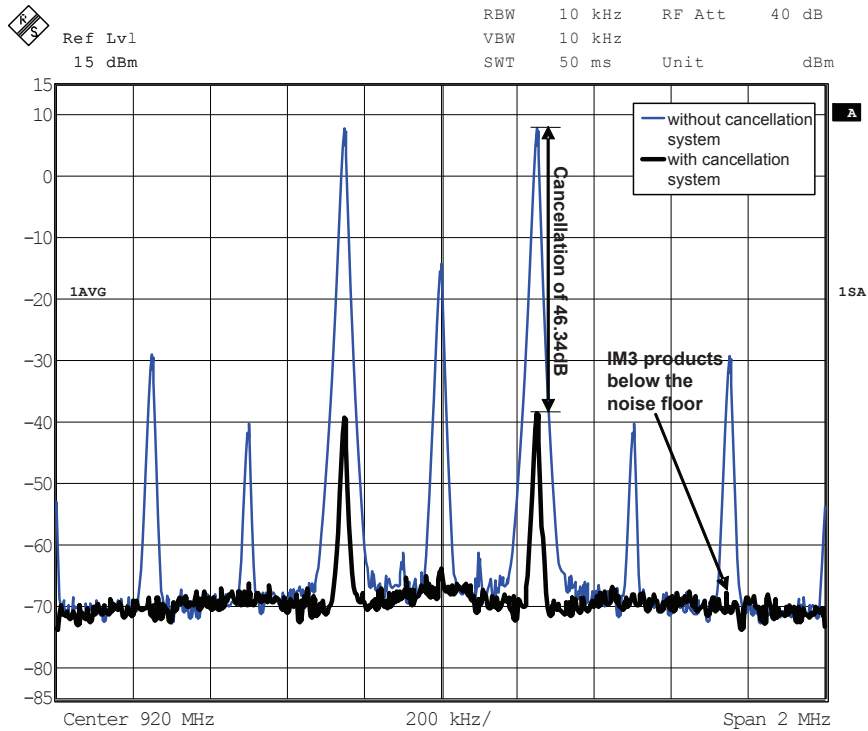


Fig. 5.6: Spectrum at the receiver with and without the proposed cancellation system during a two-tone test with an input power of -10dBm ; the fundamentals are at 919.75MHz and 920.25MHz , and the IM3 products are at 919.25MHz and 920.75MHz respectively. The desired signal is not included.

5.4 Results

Fig. 5.7 compares the SINR of the receiver without the cancellation system (from hereon referred to as the “do-nothing” system) to the receiver with the cancellation system over a range of colocated jammers from -40dBm to 10dBm . The theoretical calculations are based on a receiver with $G_{RX} = 19\text{dB}$, input IP3 $IIP3_{RX} = 6\text{dBm}$ and a noise figure $NF_{RX} = 2.7\text{dB}$ ($NF_{RX} = 10 \log_{10} F_{RX}$); these specifications align with the Mini-Circuits Monolithic Amplifier ERA-3 [44] that we use for our practical measurements. Similarly, for the $OIP3_e$ value and the T_e value of the GPA we refer the combined specification values of the vector-modulator (Hittite HMC630LP3E) and amplifier (Mini-Circuits ZHL-42) to the amplifier output.

At low jamming levels the “do-nothing” system has better SINR performance than the proposed cancellation system. This is because of additional noise from the

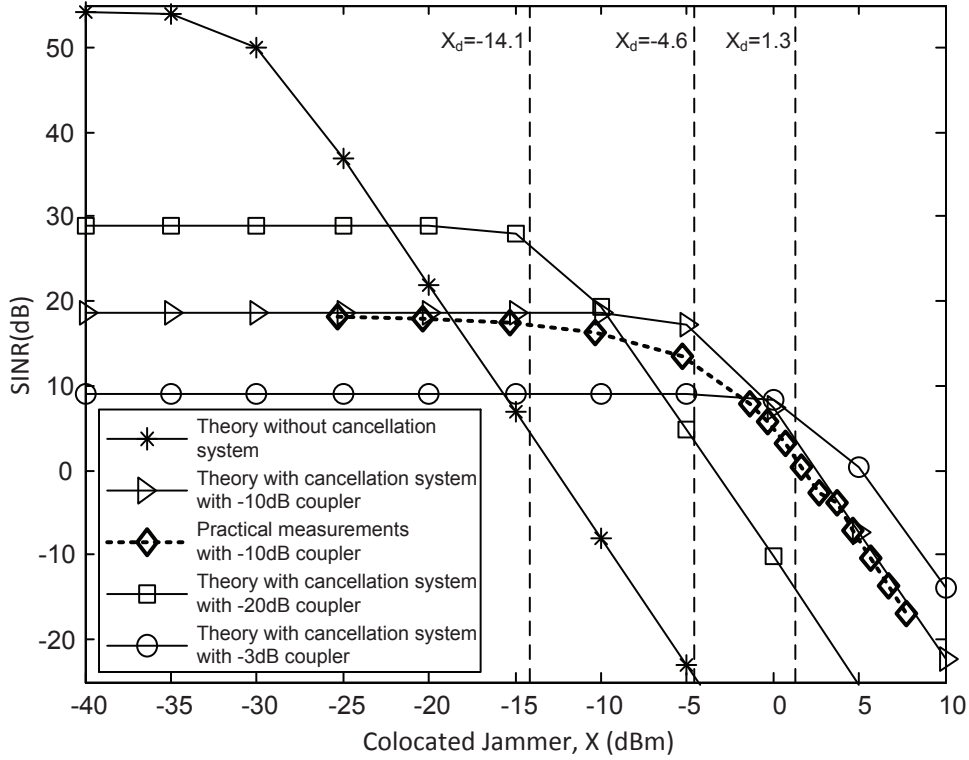


Fig. 5.7: SINR vs jammer with different couplers. Noise bandwidth, $B_W = 5\text{MHz}$.

reference path and the reduction in signal amplitude caused by the coupler. However, at higher jamming levels, increasing receiver distortion in the “do-nothing” system causes its SINR to fall below that of the cancellation system. The cancellation system removes the jamming signal on the primary path before the receiver, and hence, there is no receiver distortion. The distortion in the system then depends on the combined IP3 properties of the components in the reference path. Eventually, reference path distortion becomes dominant as X continues to increase and the cancellation system enters the waterfall region. The slope of all curves in the waterfall region are the same; thus, despite worsening SINRs, the canceling system always outperforms the “do-nothing” system.

The coupler is a compromise between the noise and distortion introduced at the receiver. It determines the onset of the waterfall region. From (5.14), the coupler optimizes the system for a design jamming level X_d . Jamming levels lower than X_d generate negligible distortion, and the SINR is dominated by the noise term. From

(5.6), the $SINR_{SYS}$ value forms a plateau at,

$$SINR_{SYS}|_{plateau} \approx \frac{S(1-C)}{k_B B_W (T_0 + T_e C + T_{RX})}. \quad (5.18)$$

As the jamming levels start getting larger, i.e. $X > X_d$, the distortion component dominates the SINR value, i.e.,

$$SINR_{SYS}|_{waterfall} \approx S(1-C) / \frac{X^3(1-C)^3}{OIP3_e^2 C^2} \quad (5.19)$$

and we have the waterfall region on the logarithmic graph with a slope of 3.

Fig. 5.7 also compares the SINR performance values with different coupler values. Consider the middle curve that is optimized for a jammer of $X_d = -4.6\text{dBm}$ and uses a -10dB coupler (i.e., $C = -10\text{dB}$). A higher coupling factor on Coupler 1 requires less gain on the GPA for the cancellation. Hence, smaller distortions are produced for the same level of the jammer. This is illustrated by the -3dB coupler line, optimized for $X_d = 1.3\text{dBm}$. Better SINR performance is obtained for $X > 0\text{dBm}$. However, this performance enhancement comes at a price, i.e., higher coupling allows more noise from the reference path, and hence, the noise-dominated plateaus are at lower SINR levels. The figure illustrates the plateau of the -3dB coupler at a 9dB SINR, which is less than the plateau of the -10dB coupler at an 18.6dB SINR. Vice versa, a -20dB coupler that optimizes for $X_d = -14.1\text{dBm}$ gives lower SINR performance than the -10dB coupler system for $X > -10\text{dBm}$; and has a plateau at a 29dB SINR better than an 18.6dB SINR of the -10dB coupler.

The noise plateaus will degrade the overall receiver performance when jammers are not present. Hence, there should always be an option of disabling the canceling circuits in such scenarios. Only the small insertion loss of Coupler 1 ($\approx 0.5\text{dB}$ for a -10dB coupler) will then effect receiver sensitivity.

SINR measurements were performed on the hardware test-bed to corroborate the analysis results. A -10dB cancellation coupler (Coupler 1) was used. The spectrum analyzer was used to measure the signal, noise, and distortion components at the output of the receiver's LNA. The two tone jamming signal was generated, with

powers ranging from -25dBm to 8dBm to measure the IM3 products. The above were used to calculate the SINR and plotted against the input jamming signal levels X , as shown by the dotted line of Fig. 5.7. Our practical measurements fell slightly short of the theoretical results of the system; this is because of distortion products produced by the signal generator themselves and difficulties of measuring distortion levels close to the spectrum analyzer's own noise floor. These extra distortion products affect the result mostly in the transition region from a noise-dominated plateau to a distortion-dominated waterfall, where neither the noise nor the distortion from our system is dominant. Apart from the transition region, the results agreed with the analysis in the plateau region and waterfall region to within 1dB.

5.5 Summary

- Colocation introduces undesired interference that produces distortion in the victim receiver. An adaptive cancellation system is used to overcome the interference and the performance improvement is optimized using an SINR analysis. The coupler value (C_{opt}) that optimizes the SINR is derived. C_{opt} is linear with X in the logarithmic scale for many practical values of X ($< 0\text{dBm}$, Fig. 5.3).
- The reference path becomes a source of noise and distortion in the cancellation system. The design jamming level X_d , represents the transition between distortion-dominated and noise-dominated operation. In the absence of any jammer we can turn OFF the cancellation path and revert back to the original sensitivity of the receiver.
- An experimental prototype achieved a significant 42dB SINR improvement over the basic “do-nothing” system at the designed jamming level of $X_d = -4.6\text{dBm}$. This means that the tolerated jamming signal can be 15dB larger compared to the basic “do-nothing” system for the same SINR. Results agreed with the theoretical predictions.

- The system was made adaptive by reducing the energy at the cancellation output. An iterative search routine reduced the jamming signal by 46dB in 8.4ms. If faster convergence is necessary, then it should be possible to borrow algorithms from the extensive signal processing literature on null steering, phased array antennas, direction of arrival estimation and acoustic noise canceling [45] [46] [47].

This chapter demonstrates a significant SINR performance enhancement using the proposed adaptive cancellation system. However, the practical measurements were done under controlled conditions; in particular the reference path used a direct feed from the jammer, and therefore, contained no trace of the desired signal. In a real world application, it is impossible to isolate the reference antenna from the desired signal. The presence of the desired signal on the reference input can result in self-cancellation on the primary path. A sufficiently large interference-to-signal ratio is required in the reference input to minimize any self-cancellation, and this can be achieved by the use of directional antennas or by judicious antenna placement. In the next chapter, we demonstrate such an over-the-air prototype.

Chapter 6

An Over-the-air Adaptive Cancellation Prototype

The major challenge for the practical realization of the proposed adaptive cancellation system is to resolve the issue where the reference antenna receives a copy of the desired signal. A sample of the desired signal in the reference input can result in self-cancellation. In this chapter we implement an over-the-air practical prototype of the cancellation system. The implementation examines the level of noise in the victim receiver and minimizes the effect of the cancellation loop on the overall noise figure of the system. The improvement in desired signal reception is shown using data constellation scatter plots.

Section 6.1 discusses the scenario where the reference antenna picks a copy of the desired signal. Section 6.2 describes our experimental setup and demonstrates performance results.

6.1 Desired Signal Sample in the Reference Input

Fig. 6.1 shows the adaptive cancellation system where the reference antenna receives a copy of the desired signal s_{REF} (shown dotted in Fig. 6.1) along with the copy of the jamming signal x_{REF} . The component of the desired signal (s_{REF}) in the reference path may cause the cancellation of the desired signal (s) at the receiver.

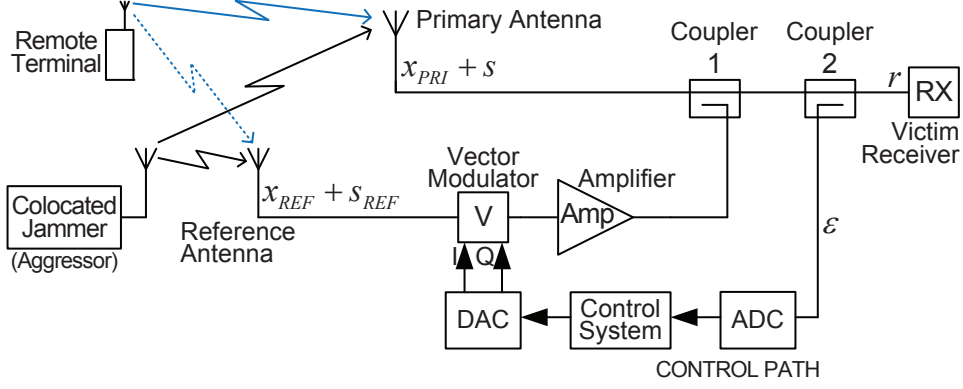


Fig. 6.1: The proposed adaptive cancellation system.

As such, the scheme requires the signal-to-interference ratio on the primary antenna ($SIR_{PRI} = S/X_{PRI}$) to be sufficiently more than the signal-to-interference ratio on the reference antenna ($SIR_{REF} = S_{REF}/X_{REF}$) to avoid any major cancellation of the desired signal [26].

At the receiver, after the reference path is scaled by the coefficient g_{REF} and subtracted from the primary path, the received signal is,

$$r = x_{PRI} - g_{REF} x_{REF} + s - g_{REF} s_{REF}. \quad (6.1)$$

Note, the lower case variables represent complex envelope voltages which characterize both the amplitude and the phase of the signals.

When g_{REF} is scaled to remove the jamming signal components, then the received signal strength is given by,

$$r = s - g_{REF} s_{REF}, \quad \text{where} \quad g_{REF} = \frac{x_{PRI}}{x_{REF}}. \quad (6.2)$$

Now, if we have $SIR_{PRI} > SIR_{REF}$ by a factor of $\Gamma = |\gamma|^2$, i.e.,

$$\frac{SIR_{PRI}}{SIR_{REF}} = \Gamma \Rightarrow \frac{s}{x_{PRI}} / \frac{s_{REF}}{x_{REF}} = \gamma \quad (6.3)$$

which is further evaluated using (6.2),

$$\frac{x_{PRI}}{x_{REF}} = g_{REF} = \frac{s}{\gamma s_{REF}}. \quad (6.4)$$

Thus, using (6.4) the received signal is,

$$r = s(1 - 1/\gamma). \quad (6.5)$$

The phase of γ determines whether or not the received signal r is canceled or boosted. This phase is determined by the uncontrolled incoming components of the desired signal. The worst case phase angle $\arg(\gamma) = 0$ is assumed. The nulling of the jammer will not affect the received signal if Γ (the difference between the SIRs) is large. This could be achieved by the use of a directly coupled signal from the aggressor's antenna feed cable, avoiding the need for a reference antenna. Alternatively, since this is not likely, we take advantage of the fact that the desired signal is generally weak and far away from the base station, in which case its average signal strength will be the same on both the primary and the reference antennas. Therefore, the SIRs can be changed by altering their distances to the aggressor antenna; normally, we decrease the SIR on the reference antenna by mounting it closer to the aggressor than the primary antenna. Alternatively, the reference antenna could be made directional and pointed at the aggressor. In the prototype of Fig. 6.2 we use omni-directional disccone antennas and mount the reference antenna $d_1 = 0.15\text{m}$ from the aggressor, whereas the primary/victim antenna is mounted $d_2 = 1.15\text{m}$ from the aggressor to give an SIR ratio of $\Gamma = (d_2/d_1)^2 = 59$ (based on the $1/d^2$ path-loss model when operating in the far-field of the antennas, i.e., $r_{far} \geq 2D^2/\lambda = 3\text{cm}$ at frequency 920MHz, wavelength $\lambda = 32.6\text{cm}$ and the largest dimension of the antennas $D = 7\text{cm}$ [48]). According to (6.5), the worst case cancellation on the desired signal S is limited to a maximum value of -1.2dB . And in the best case the desired signal could gain by $+1.06\text{dB}$. It is to be noted that in most commercial deployments the primary antenna is directional and covers a sector of 120 degrees. The gain/directivity on the primary antenna comes as an advantage to the cancellation

system. It improves the SIR on the primary antenna. However, in the worst case scenario, where the aggressor and the desired UE are in the same line of reception to the primary antenna, the reference antenna has to be placed closer to the aggressor to have a sufficiently reduced SIR in comparison to the primary antenna.

6.2 Experiment Results

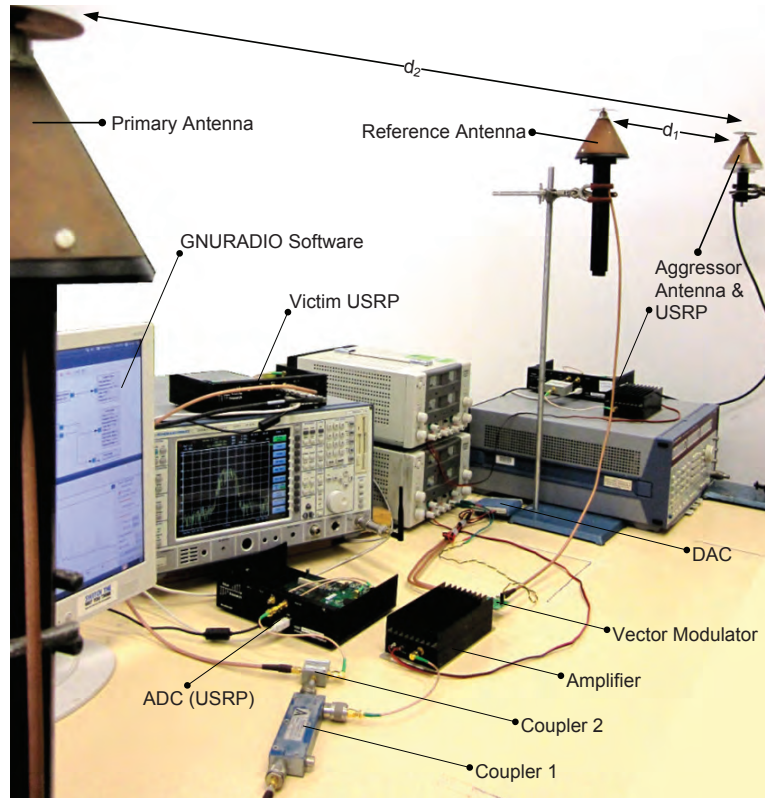


Fig. 6.2: Experimental setup.

Fig. 6.2 shows the over-the-air experimental setup. This is in accordance with the block diagram in Fig. 6.1. The transmitter and the receiver for the desired signal in the experiment are USRP units using GNU radio software. The colocated aggressor is also a USRP unit transmitting two large jamming signals with the help of an amplifier (Mini-Circuits ZHL-42 [16]). The cancellation loop on the reference path uses a -20dB coupler (Coupler 1) with 13dB net amplification (Minicircuits ZX60-33LN [49] + -6dB attenuator) and a vector modulator (Hittite HMC630LP3E

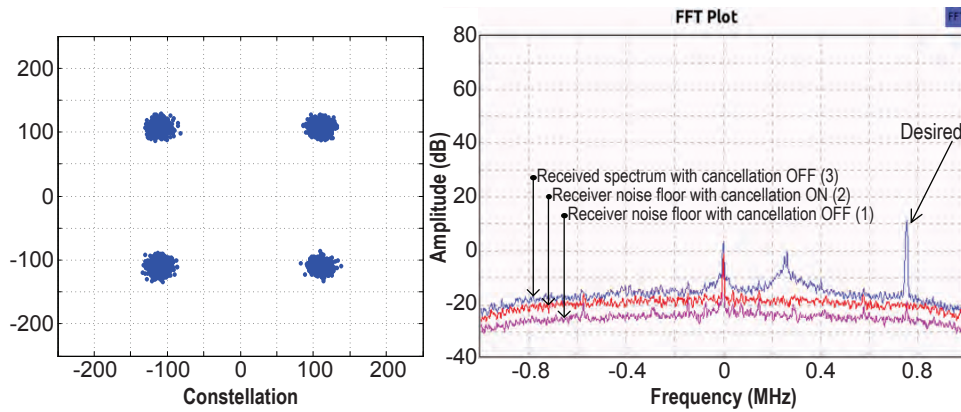
[43]). The lower net amplification reduces cancellation loop noise, but is still high enough to cancel the jammers.

To demonstrate the performance of the system with modulated signals we use a narrow band (12.5kHz) QPSK modulated signal for both the desired and aggressor signals. The symbol rate is 7.8125ksymbols/sec and filtered with a Nyquist filter with 50% excess bandwidth.

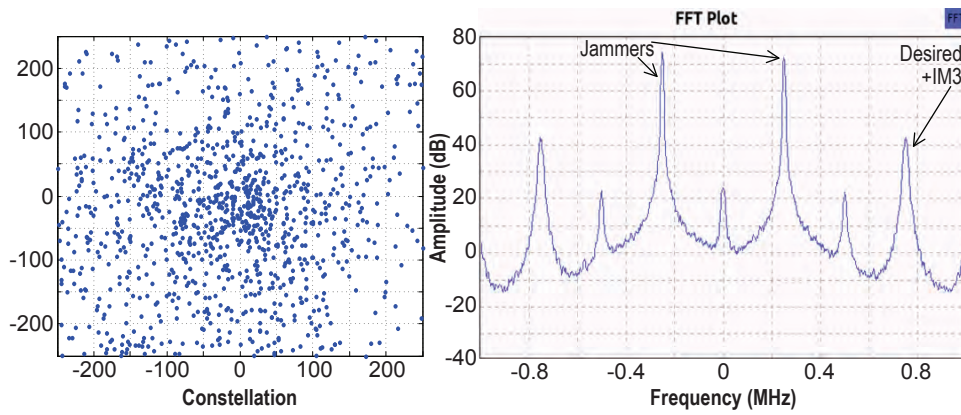
Fig. 6.3 shows the four constellation points of the received desired signal, along with a 2MHz frequency spectrum centered at 920MHz showing the jammers, the intermodulation products and the desired signal.

Fig. 6.3(a) shows three spectrum traces. Trace 1 (purple) at the bottom represents the noise floor with a 50Ω termination replacing the antenna at the primary input and the cancellation loop turned off (i.e., the components of the cancellation loop switched off adding zero noise to the overall system). The noise figure of the receiver without the cancellation loop is measured to be 2.2dB. Trace 2 (red) in the middle represents the noise floor of the total system with the cancellation loop turned on and 50Ω terminations at the primary and reference antenna inputs. The noise figure of the receiver with the cancellation loop turned on is measured to be 7.2dB. The increase of 5dB in the receiver noise figure is due to the noise added by the components of the cancellation loop.

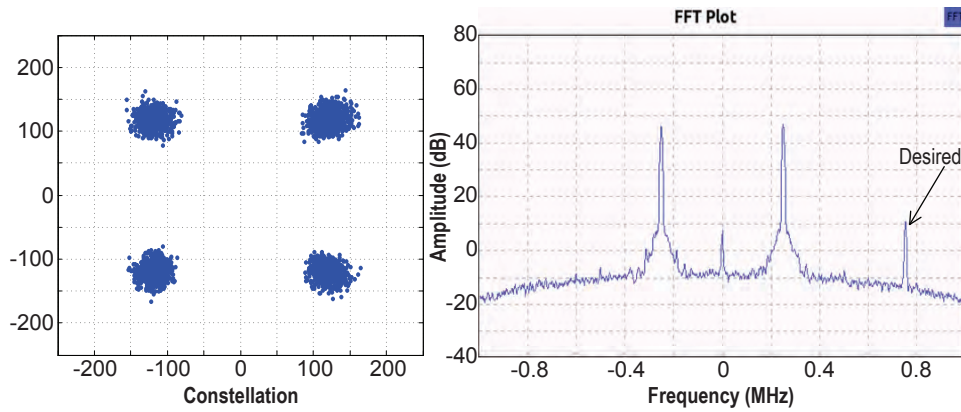
Trace 3 on the top (blue) shows reception from the primary antenna without any jammer and the cancellation circuit turned off. The low power transmitter for the desired signal is mounted in the next room and its spectrum is shown by the peak at 920.75MHz (shown as an offset of 0.75MHz on the figure, with 0 representing 920MHz). The scatter plot on the left hand side shows the received QPSK constellations at a signal to noise ratio of about 26dB. The spur at 920.27MHz is an unrelated weak external transmission picked up through the antenna and has no influence on the experiment. The spur in the middle is the LO leakage of the relatively inexpensive USRP receivers. A point to note is the overall radiated noise received in the 900MHz industrial, scientific, and medical (ISM) band dominates the receiver noise (Trace 1) by about 7dB. This noise floor will dilute the effect of



(a) Without jammers



(b) With jammers



(c) With jammers and cancellation system

Fig. 6.3: Signals, as seen by the victim receiver. Signal constellation scatter plots (LHS) and GNU radio spectrum plots (RHS). The GNU radio spectrum plots show relative scales with 75dB representing -39dBm, and on the frequency scale 0 representing 920MHz.

a 5dB rise in the receivers noise figure when the cancellation loop is activated.

The aggressor transmitter carries two equal power transmissions at 919.75MHz

and 920.25MHz. These couple into the victim USRP receiver at an aggregate jamming strength of -36dBm; enough to generate intermodulation products including the two dominant components at the third order frequencies of 919.25MHz and 920.75MHz. The latter falls directly on to the channel of our desired signal and causes interference. Fig. 6.3(b) shows the constellations are unrecognizable as a result of the interference. The spectrum shows the jammers, the desired signal and the odd- and even-order intermodulation products. The desired signal is completely masked by the distortion products. Note, the integrity of the transmitted spectrum from the jammer was verified using a spectrum analyzer; no intermodulation products were produced by the jammer.

Fig. 6.3(c) illustrates the performance of the system with interference canceling switched on. The system canceled the jammers by a margin of 25dB. Theoretically, this would be sufficient to reduce the third-order intermodulation products by 75dB; well below the noise floor. The constellations are improved, but not to the extent of the original signal without interference. The constellation blooms are about 4dB larger. A detailed investigation shows that the 4dB rise in noise floor is partly due to the additional noise of the canceling loop (≈ 2.1 dB) and partly to the noise transmitted from the jammers themselves. The latter can be fixed by better transmitter filtering (e.g., the duplexing filters and/or RF filtering before the final power amplifier stage).

As for the desired signal itself, its amplitude has hardly changed. In this instance γ has a phase almost perpendicular to our desired signal, causing a small cancellation of approximately 0.3dB.

6.3 Summary

- In this chapter we demonstrated that, in practice, the reference-antenna based system can achieve a significant cancellation of the jamming signals with negligible self-cancellation of the desired signal.

- The over-the-air demonstration in the 900MHz ISM band showed a 25dB reduction in jammer power and the elimination of all distortion products.
- The trade-off was a 5dB increase in receiver noise figure. In a quiet site, this directly transforms into a loss of receiver sensitivity. However sites that operate in an interference limited mode (urban cellular sites or ISM sites for example) will be degraded less by the loss in noise figure. Further, the trade-off is insignificant in comparison to the distortions that generate when hit by large jammers. In the absence of any jammer we can turn OFF the cancellation path and stop noise penalties.

Chapters 4, 5 and 6 have demonstrated the feasibility of adaptive cancellation as a counter measure to forward IM generation in a multi-operator colocated site. Mathematical derivations showed that the cancellation loop components dominated the system's overall dynamic range. The performance was highly dependent on the choice of the cancellation coupler. The optimum coupler value was derived for a designed jamming level. An automated scheme for controlling the reference path was demonstrated and an over the air prototype showed real life performance with modulated signals similar to those expected in today's private mobile radio systems.

The next chapter describes a solution for the second cause of interference in a colocated environment; that of reverse intermodulation generated in the transmitters themselves. The postdistortion solution uses multiple SDR front-ends and a novel distortion synthesis technique.

Chapter 7

Postdistortion Cancellation

System for Reverse IM Products

The discussion in chapter 3 showed that reducing the jammers entering the victim receiver front-end does not help in mitigating the reverse IM products. These are generated at the colocated transmitters. Transmitter-end solutions can reduce the reverse jammer at the aggressor transmitter, thus, mitigating the generation of reverse IM products [17] [28]. However, in a commercially competitive scenario such transmitter-end access for a colocated victim receiver is less likely. Therefore, a solution that could be independently deployed by the victim receiver is desired. Section 3.4.2 reviewed previously published postdistortion linearization circuits for receiver generated IM products. However, the dominant jammers causing the reverse IMs at the transmitter might not be the dominant jammers at the victim receiver. This sets the need for jammer selectivity for the regeneration circuits at the receiver. A new multiple SDR front-end receiver was then proposed (Fig. 3.11) for jammer selection, IM regeneration and mitigation of the interfering reverse IM products.

The primary SDR front-end (Rx0) receives the corrupt desired signal and converts it to digital baseband (y). The auxiliary SDR front-ends (Rx1,Rx2,..) are each tuned to a jamming signal that contributes to the interfering reverse IM distortion. These signals are also converted to digital baseband where they are described by their complex envelope representation ($a,b,..$). All subsequent processing is digital

using DSP. The fundamental jamming signals are processed to produce an estimate \hat{u} of the required reverse distortion product u . This is then subtracted from the primary received signal after appropriate gain and phase scaling.

The scheme relies on the exact match in amplitude, phase and frequency of the distortion estimate \hat{u} with the distortion u in the received signal y . This can only be achieved if the frequency of the jamming signals are known. In practice, this assumption might not be valid, and even if the frequencies are known (e.g., from database look-up), component tolerances, aging and temperature drifts in the transceiver reference crystals produce unknown frequency offsets. If the jammer modulation is known the offset can be estimated using coherent detection. For example, carrier frequency offset [50] correction using pilots, cyclic prefix and signal statistics is well known for OFDM signals [51] [52].

The solution proposed here does not require knowledge of these offsets or knowledge of the jamming signals' modulation. No spectral or time domain information about the jammers is assumed. However what is assumed, is the jammers are large and can be identified by a scanning receiver using simple energy detection. The frequency estimates are therefore very coarse and must be corrected as part of the distortion synthesis process. A novel two part frequency correction technique is described in this chapter. It involves a combination of FFT and signal correlation to correct the frequency offset in the synthesized distortion.

Section 7.1 discusses a colocated base station model and the reverse IM products that cause interference. Section 7.2 describes the novel distortion synthesis technique with frequency correction and the proposed postdistortion cancellation architecture. Section 7.3 characterizes the cancellation system using simulations and mathematical analysis. Section 7.4 presents a practical prototype of the cancellation system, measurements and results.

7.1 Reverse Intermodulation Products

A model of three colocated base stations along with a remote terminal is shown in Fig. 7.1. Terminal D transmits the desired signal $s_r^D(t)$ ¹ over channel gain $h_d(t)$ to base station receiver RX. The spectrum of the output at terminal D shows the desired signal $s_r^D(t)$ at frequency channel f_d .

A high powered signal $b_r^B(t)$ from jammer B propagates through a channel gain of h_{ba} into the colocated power amplifier of jammer A and produces reverse IM3 products $u_r^A(t)$ and $v_r^A(t)$; with $u_r^A(t)$ at f_u , overlapping receiver RX's desired channel

¹Radio frequency signals have the subscript 'r'. $s_r^D(t) = \text{Re} [s^D(t)e^{j2\pi f_d t}]$, where $s^D(t)$ is the complex envelope.

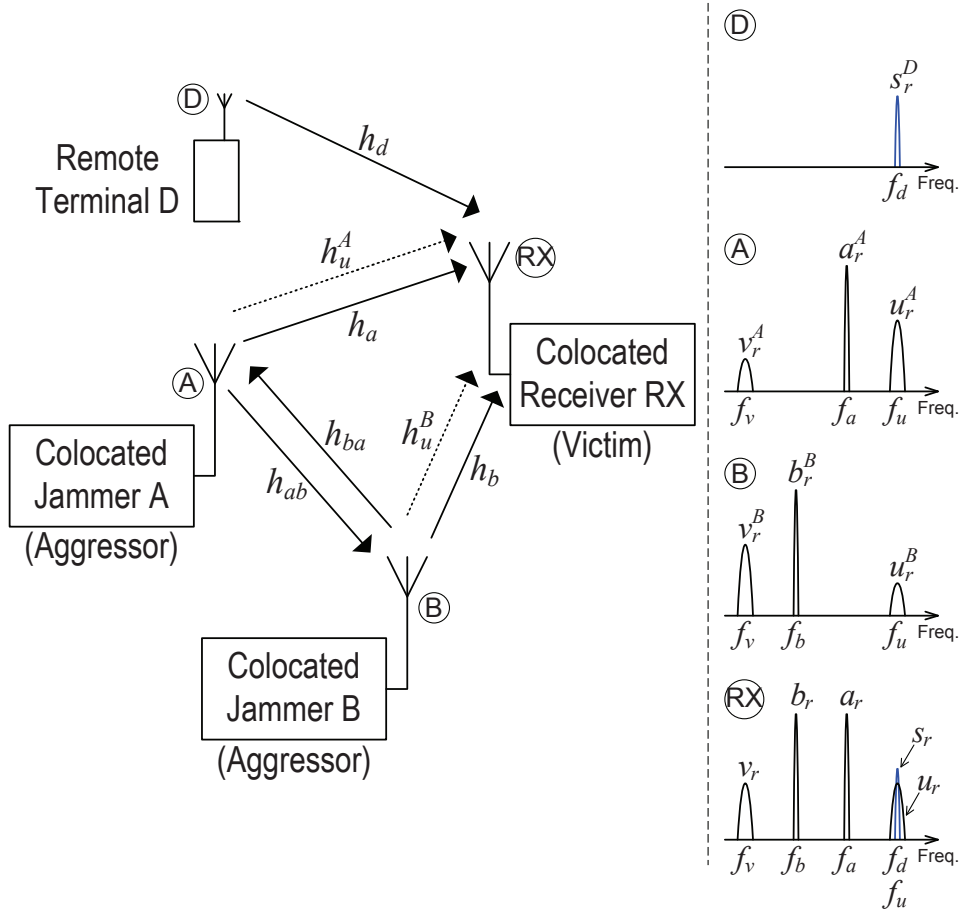


Fig. 7.1: Colocated base station transceivers.

frequency f_d , and $v_r^A(t)$ is at frequency f_v , given as follows,

$$f_u = 2f_a - f_b \quad (7.1)$$

$$f_v = 2f_b - f_a \quad (7.2)$$

where f_a and f_b are the transmit frequencies of $a_r^A(t)$ and $b_r^B(t)$ respectively. The IM3 products $u_r^A(t)$ and $v_r^A(t)$ are radiated from jammer A along with its own transmission. Spectrum A shows the output at jammer A.

Similarly, signal $a_r^A(t)$ from jammer A propagates over a channel gain of h_{ab} to generate reverse IM3 products $u_r^B(t)$ and $v_r^B(t)$ at jammer B. Spectrum B shows the output at jammer B.

Spectrum RX shows the signals $v_r(t)$, $b_r(t)$, $a_r(t)$, $u_r(t)$ and $d_r(t)$ received at receiver RX after propagating through their respective channel gains. Reverse IM3 product $v_r(t)$ does not affect desired channel f_d and is not of concern.

Large transmit signals $a_r(t)$ and $b_r(t)$ could be of considerable concern if they exceed the dynamic range levels of receiver RX as discussed in chapters 4-6. However, in this chapter we consider them to be within receiver RX's dynamic range and so do not contribute to the distortions within the receiver's front-end.

Reverse IM3 product $u_r(t)$ falls directly on to the desired signal channel f_d and causes interference for receiver RX. The IM3 product $u_r(t)$ has two components $u_r^A(t)$ and $u_r^B(t)$ given by,

$$u_r(t) = \text{Re} \left[\left(h_u^A u^A(t) + h_u^B u^B(t) \right) e^{j2\pi f_u t} \right] \quad (7.3)$$

where h_u^A and h_u^B are the respective channel gains through which $u_r^A(t)$ and $u_r^B(t)$ propagate to receiver RX (Note: These gains are different from h_a and h_b because they are at different carrier frequencies); $u^A(t)$ and $u^B(t)$ are the complex envelopes.

The IM3 product $u_r^A(t)$ is linearly affected by the channel gain h_{ba} , its magnitude is given as follows,

$$|u_r^A(t)| = g_3^A |a^A(t)|^2 |h_{ba}| |b^B(t)| \quad (7.4)$$

where g_3^A is the cubic distortion coefficient of jammer A's power amplifier and is related to its output IP3 [6]. However, the magnitude of the IM3 product $u_r^B(t)$ depends on the square of the channel gain h_{ab} , as given below,

$$|u_r^B(t)| = g_3^B |h_{ab}|^2 |a^A(t)|^2 |b^B(t)| \quad (7.5)$$

where g_3^B is the cubic distortion coefficient of jammer B's power amplifier. If both transmitter amplifiers are similar then the distortion coefficients $g_3^A \sim g_3^B$. Thus, $u_r^B(t)$ is usually very small and is considered negligible throughout this chapter.

A point to note, although the channel gain $h_d(t)$ is time varying, the other gains shown in Fig. 7.1, h_a , h_u^A , h_b , h_u^B , h_{ba} and h_{ab} are all considered to be quasi-static given the close proximities and fixed nature of the colocated antennas A, B and C.

7.2 Proposed Architecture and Digital Signal Processing

The proposed architecture (Fig. 7.2) has an antenna feeding three software defined radio (SDR) front-ends and a common DSP that synthesizes the interfering reverse IM3 product and removes it from the contaminated desired signal before the demodulator.

If the cancellation is to be effective the synthesized distortion must have the correct amplitude, phase, timing and frequency. In this work timing accuracy is obtained by using the same sampling clock for all three receivers. Frequency locking is obtained using a correction algorithm and gain-phase correction is obtained by adaptive adjustment.

The sample rates have to be reasonably high because of frequency offsets and the bandwidth expansion that occurs on the nonlinear jamming signals. For example the distortion u_r has a bandwidth of twice the bandwidth of the a_r signal plus the bandwidth of the b_r signal (see 2.4.5). A large over sampling rate will handle most contingencies as well as give reasonable timing fidelity in the cancellation. Note, the

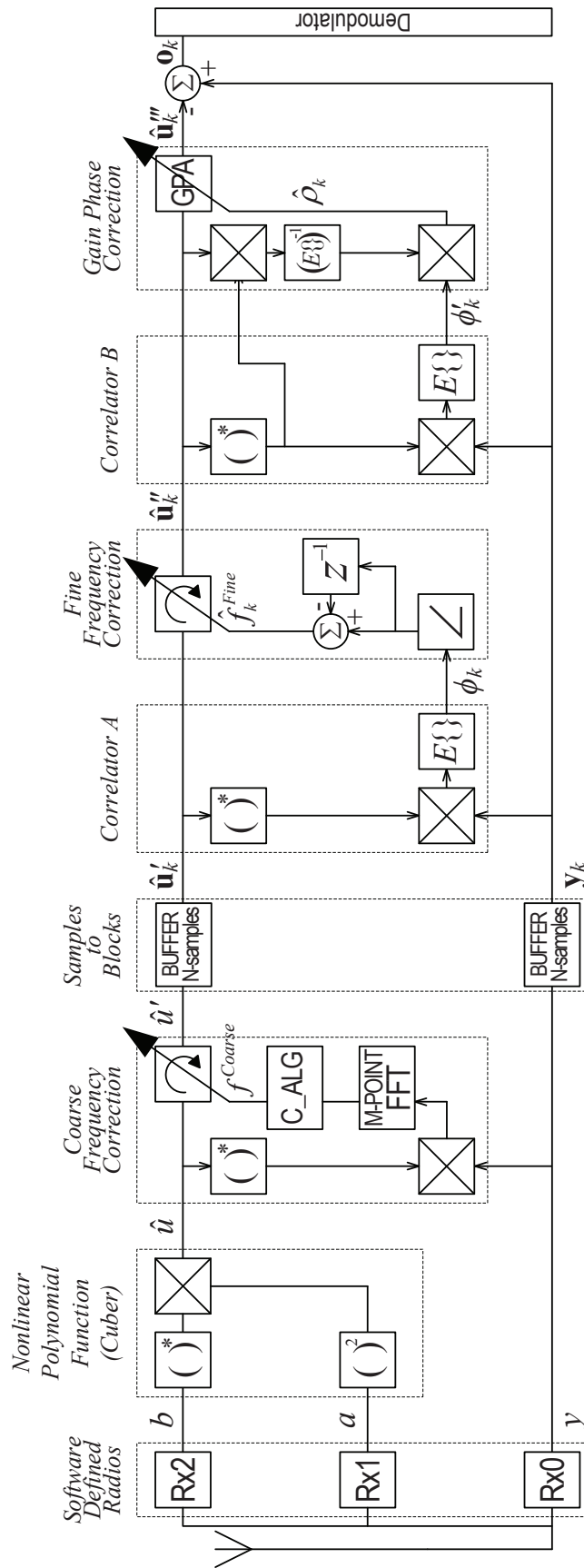


Fig. 7.2: Proposed DSP.

sample rate is still much less than a single wideband receiver covering all jamming and desired signals.

The next subsections describe the major modules in the system.

7.2.1 Multiple Receivers

The victim receiver has multiple independently tuned RF front-ends. The primary receiver front-end Rx0 is tuned to receive at the desired signal frequency f_d . It receives the desired signal $s_r(t)$ along with the interfering reverse IM3 product $u_r(t)$. The received signal,

$$y_r(t) = s_r(t) + u_r(t) \quad (7.6)$$

where,

$$s_r(t) = \text{Re} \left[h_d(t) s^D(t) e^{j2\pi f_d t} \right] \quad (7.7)$$

with $s^D(t)$ being the complex envelope of $s_r(t)$, and,

$$u_r(t) = \text{Re} \left[g_3^A h_u^A h_{ba} \{b^B(t)\}^* \{a^A(t)\}^2 e^{j2\pi(2f_a - f_b)t} \right]. \quad (7.8)$$

with $a^A(t)$ and $b^B(t)$ being the complex envelopes of $a_r^A(t)$ and $b_r^B(t)$ respectively and $\{b^B(t)\}^*$ is the conjugate of $b^B(t)$. As discussed the non-linear IM3 products have expanded bandwidths and can cover many channels. The center frequency of $u_r(t)$ could therefore have a frequency offset Δf_u of more than one channel from f_d (i.e. $2f_a - f_b = f_d + \Delta f_u$) and still cause interference to $s_r(t)$. Thus, $u_r(t)$ could be rewritten and expressed as follows,

$$u_r(t) = \text{Re} \left[g_3^A h_u^A h_{ba} \{b^B(t)\}^* \{a^A(t)\}^2 e^{j2\pi(f_d + \Delta f_u)t} \right] \quad (7.9)$$

The complex envelope of the received signal $y_r(t)$ is $y(t)$ at receiver Rx0's operating frequency f_d . After sampling and analog-to-digital conversion the digital baseband signal is given by,

$$y_n = s_n + u_n \quad (7.10)$$

where s_n is the desired signal component,

$$s_n = h_{d,n} s_n^D \quad (7.11)$$

and u_n is the IM3 distortion component,

$$u_n = g_u \{b_n^B\}^* \{a_n^A\}^2 e^{j2\pi\Delta f_u n/f_s} \quad (7.12)$$

with $g_u = g_3^A h_u^A h_{ba}$, and f_s is the sampling frequency of the software defined radios.

The auxiliary receiver front-ends Rx1 and Rx2 scan for the out-of-band jammers $a_r(t)$ and $b_r(t)$ respectively. These jammers are the fundamental components of the interfering IM3 product $u_r(t)$ and can be used to digitally synthesize the IM3 product at baseband. A relatively simple energy detection technique could be used to scan for the high powered jammers, since, an exact lock onto their carrier frequencies is not necessary. As such, the carrier frequencies f'_a and f'_b of their respective receiver front-ends Rx1 and Rx2 are at certain frequency offsets Δf_a and Δf_b from the jammer frequencies f_a and f_b , given as follows,

$$f_a = f'_a + \Delta f_a \quad (7.13)$$

$$f_b = f'_b + \Delta f_b. \quad (7.14)$$

The following are the received signals at Rx1 and Rx2 respectively in terms of the complex envelope components of the jammers,

$$a_r(t) = \text{Re} \left[h_a a^A(t) e^{j2\pi(f'_a + \Delta f_a)t} \right] \quad (7.15)$$

$$b_r(t) = \text{Re} \left[h_b b^B(t) e^{j2\pi(f'_b + \Delta f_b)t} \right] \quad (7.16)$$

which at digital baseband are as follows,

$$a_n = h_a a_n^A e^{j2\pi\Delta f_a n/f_s} \quad (7.17)$$

$$b_n = h_b b_n^B e^{j2\pi\Delta f_b n/f_s}. \quad (7.18)$$

The aim is to use these baseband jammer components a_n and b_n to synthesize a duplicate of the received distortion u_n and remove it from y_n .

7.2.2 Nonlinear Polynomial Function: Cuber

The cuber module, as shown in Fig. 7.2, starts the synthesization process. It produces a sample of the required IM3 distortion by taking a_n and b_n as inputs, conjugating b_n and then multiplying with the square of a_n to give,

$$\hat{u}_n = b_n^* a_n^2 = g_{\hat{u}} \{b_n^B\}^* \{a_n^A\}^2 e^{j2\pi\Delta f_{\hat{u}} n/f_s} \quad (7.19)$$

where $g_{\hat{u}} = h_b^* h_a^2$ and $\Delta f_{\hat{u}} = (2\Delta f_a - \Delta f_b)$.

A comparison between Equations (7.12) and (7.19) shows that the synthesization process would further require a frequency offset Δf correction such that,

$$\Delta f_{\hat{u}} - \Delta f = \Delta f_u \quad (7.20)$$

and a gain-phase correction ρ such that,

$$\rho g_{\hat{u}} = g_u. \quad (7.21)$$

Hence, u_n is given as follows,

$$u_n = \rho \hat{u}_n e^{-j2\pi\Delta f n/f_s} \quad (7.22)$$

and y_n can be reformatted as,

$$y_n = s_n + \rho \hat{u}_n e^{-j2\pi\Delta f n/f_s}. \quad (7.23)$$

Further, the frequency tuning is a two part process. Where \hat{u} is rotated for a coarse

correction of f^{Coarse} and then tracked in blocks and finely tuned by f^{Fine} , i.e.,

$$\Delta f = f^{Coarse} + f^{Fine}. \quad (7.24)$$

7.2.3 Coarse Frequency Correction

To do coarse frequency correction we must first find the distortion signal \hat{u} within y . To do this we use correlation.

$$\Phi = E \{ \hat{u}_n^* y_n \} \quad (7.25)$$

where $E\{\cdot\}$ is the expectation operator. Substituting for y_n from (7.23) gives

$$\Phi = E \{ \hat{u}_n^* s_n \} + E \left\{ \rho \hat{u}_n^* \hat{u}_n e^{-j2\pi \Delta f n / f_s} \right\}. \quad (7.26)$$

The first term is zero since \hat{u}_n is uncorrelated to s_n . The product of $\hat{u}_n^* \hat{u}_n$ is always real and averaging gives its power. However, the frequency offset term $e^{j2\pi \Delta f n / f_s}$ rotates the products and their average will tend to zero since most products would be balanced out with another product 180° out of phase. Thus, a second rotator is needed to reverse the frequency offset rotation prior to averaging. The FFT provides a bank of such rotators all rotating at different frequencies. It also provides the summation function for the averaging, and hence, it gives,

$$\Phi(l) = \sum_{n=0}^{M-1} \left\{ \hat{u}_n^* s_n + \rho \hat{u}_n^* \hat{u}_n e^{-j2\pi \Delta f n / f_s} \right\} e^{-j2\pi \frac{ln}{M}}, \quad l = 0, 1, \dots, M-1. \quad (7.27)$$

The correction algorithm C_ALG uses $\Phi(l)$ to find the highest power bin l_{max} in the M -point FFT, i.e., $l_{max} = \arg \max_l \Phi(l)$. Which gives f^{Coarse} as follows,

$$f^{Coarse} = \delta_M l_{max} \quad (7.28)$$

where the frequency resolution is $\delta_M = f_s / M$. Large values of M are preferred in order to get an accurate frequency estimate as well as to minimize the noise

contribution caused by the desired signal in the first term of (7.27).

Finally, the rotator in the coarse frequency correction module is set to correct \hat{u}_n by frequency f^{Coarse} such that,

$$\hat{u}'_n = \hat{u}_n e^{-j2\pi f^{Coarse} n/f_s}. \quad (7.29)$$

The correction is only accurate within half a bin size $\delta_M/2$. The small difference in rotation left between \hat{u}'_n and u_n in y_n is then adjusted by the fine frequency correction module. Generally, coarse frequency estimation is only performed once at switch ON.

7.2.4 Fine Frequency Correction

The stream of samples \hat{u}'_n and y_n is now buffered into blocks of N -samples, the k -th block is defined below,

$$\hat{\mathbf{u}}'_k = [\hat{u}'_{0,k} \ \hat{u}'_{1,k} \ \dots \ \hat{u}'_{(N-1),k}]^T \quad (7.30)$$

$$\mathbf{y}_k = [y_{0,k} \ y_{1,k} \ \dots \ y_{(N-1),k}]^T. \quad (7.31)$$

The blocks $\hat{\mathbf{u}}'_k$ and \mathbf{y}_k are then fed as inputs to correlator A.

Correlator A evaluates the correlation (ϕ_k) of $\hat{\mathbf{u}}'_k$ with \mathbf{y}_k ,

$$\phi_k = E\{\hat{u}'_{n,k}^* y_{n,k}\} \approx (\hat{\mathbf{u}}'^H_k \mathbf{y}_k) / N \quad (7.32)$$

and forwards it to the fine frequency correction module. The parameter of interest is the phase of ϕ_k ($\angle\phi_k$).

It is to be noted that \mathbf{y}_k has an IM3 distortion component \mathbf{u}_k and a desired signal component \mathbf{s}_k , i.e., $\mathbf{y}_k = \mathbf{u}_k + \mathbf{s}_k$. The aim is to align $\hat{\mathbf{u}}'_k$'s frequency rotation with \mathbf{u}_k . $E\{\hat{u}'_{n,k}^* y_{n,k}\}$ calculates the average of all the angle differences between each sample of $\hat{\mathbf{u}}'_k$ and \mathbf{u}_k . Hence, $\angle\phi_k$ holds the relative angle of the block $\hat{\mathbf{u}}'_k$ to \mathbf{u}_k . And $\angle\phi_{k-1}$ holds the relative angle of the previous block $\hat{\mathbf{u}}'_{k-1}$ to \mathbf{u}_{k-1} . The difference in

the two angles,

$$\Delta\angle\phi = \angle\phi_k - \angle\phi_{k-1} \quad (7.33)$$

gives the extra phase rotation that $\hat{\mathbf{u}}'_k$ obtains due to the fine frequency offset over N -samples. The fine frequency estimate then becomes,

$$\hat{f}_k^{Fine} = \Delta\angle\phi f_s/2\pi N. \quad (7.34)$$

The rotator uses \hat{f}_k^{Fine} to back rotate $\hat{\mathbf{u}}'_k$ with $\Delta\angle\phi/N$ radians/sample over the block.

$$\hat{u}''_{n,k} = \hat{u}'_{n,k} e^{-j2\pi\hat{f}_k^{Fine} n/f_s}. \quad (7.35)$$

This tunes $\hat{\mathbf{u}}''_k$ to the same frequency as \mathbf{u}_k in \mathbf{y}_k .

7.2.5 Gain-Phase Correction

We use Bussgang's theory [53] to identify the coefficient estimate $\hat{\rho}_k$ which is the amount of $\hat{\mathbf{u}}''_k$ in \mathbf{y}_k , i.e.,

$$\hat{\rho}_k = \frac{E\{\hat{u}''_{n,k} y_{n,k}\}}{E\{\hat{u}''_{n,k} \hat{u}''_{n,k}\}} \approx \frac{(\hat{\mathbf{u}}''_k^H \mathbf{y}_k)}{(\hat{\mathbf{u}}''_k^H \hat{\mathbf{u}}''_k)}. \quad (7.36)$$

Further, $\hat{\mathbf{u}}''_k = \hat{\rho}_k \hat{\mathbf{u}}''_k$ is subtracted from \mathbf{y}_k to give us the desired signal \mathbf{s}_k which forms the input to the radio demodulator.

7.2.6 Desired Signal Demodulation

The received signal \mathbf{y}_k is essentially intact/unaltered until the distortion estimate $\hat{\mathbf{u}}''_k$ gets subtracted at the input to the demodulator. Therefore, no modifications (e.g., frequency offset and gain-phase adjustment) are imposed on the desired signal \mathbf{s}_k . A standard receiver demodulator can be used. The demodulator would do the normal receiver functions of time synchronization, frequency synchronization, channel estimation and demodulation. Note, frequency synchronization here centers

the desired signal modulation to DC. There is no relation between this and the frequency correction applied to the distortion estimate.

7.3 Simulations and Analysis

In practice, a certain level of interference \mathbf{z}_k remain at the output of the system. Thus at the canceler output \mathbf{o}_k becomes,

$$\mathbf{o}_k = \mathbf{y}_k - \hat{\mathbf{u}}_k''' = \mathbf{s}_k + \mathbf{z}_k. \quad (7.37)$$

This section identifies the different sources of interference that cumulate to give \mathbf{z}_k at the output. The investigation works backward from the canceler output to isolate and identify each of the interference sources.

7.3.1 Buffer/Data Processing Block Size N

First, under investigation is the gain-phase correction module along with its correlator B that process data in blocks of N -samples; the preceding fine and coarse frequency correction modules are perfectly adjusted. Substituting for \mathbf{y}_k in equation (7.36), we have,

$$\hat{\rho}_k = \rho + \frac{E\{\hat{u}_{n,k}''^* s_{n,k}\}}{E\{\hat{u}_{n,k}''^* \hat{u}_{n,k}''\}}, \quad (7.38)$$

the latter term is zero, but, when the expectation takes the form of an average over N_s uncorrelated samples, the output approximates a normal distribution,

$$\hat{\rho}_k = \mathcal{N} \left\{ \rho, \frac{\sigma_s^2 \sigma_u^2}{N_s \sigma_u^4} \right\} \quad (7.39)$$

where the desired signal power $E\{|s_{n,k}|^2\} = \sigma_s^2$, and the distortion estimate power $E\{|\hat{u}_{n,k}|^2\} = \sigma_u^2$. Simplifying (7.39), we have,

$$\hat{\rho}_k = \mathcal{N} \left\{ \rho, \frac{\sigma_s^2}{N_s \sigma_u^2} \right\} \quad (7.40)$$

where the first term is the mean and the second term is the variance of a normal distribution. Since, the signals are over sampled we approximate $N_s = \eta N / OSR$ where OSR is the over-sampling rate of the desired signal and equal to $f_s / \text{bandwidth of } s$. The factor η is dependent on the modulation parameters of the signals a , b and s . We show in appendix A, $\eta = (3/2)^2$ when all three fundamental signals are Gaussian in nature and have a rectangular spectrum. Substituting $\hat{\mathbf{u}}_k''$ in (7.37) with $\hat{\rho}_k \hat{\mathbf{u}}_k''$, we have,

$$\mathbf{o}_k = \mathcal{N} \left\{ \mathbf{s}_k, \frac{\sigma_s^2 \sigma_{\hat{\mathbf{u}}}^2}{N_s \sigma_{\hat{\mathbf{u}}}^2} \right\} \quad (7.41)$$

which is further simplified to give,

$$\mathbf{o}_k = \mathcal{N} \left\{ \mathbf{s}_k, \frac{\sigma_s^2}{N_s} \right\}. \quad (7.42)$$

Hence, output signal-to-interference ratio (SIR),

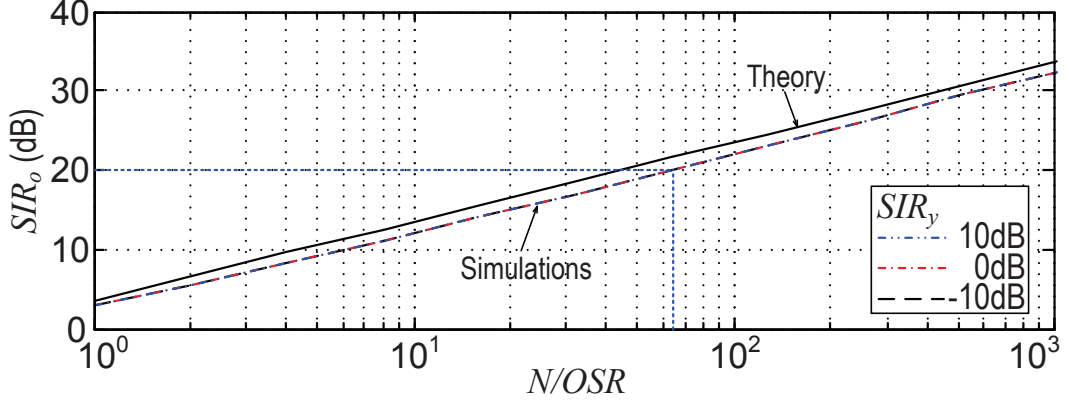
$$SIR_o = \sigma_s^2 / \frac{\sigma_s^2}{N_s} \quad (7.43)$$

which gives,

$$SIR_o = N_s. \quad (7.44)$$

We note, the SIR_o of \mathbf{o}_k is independent of the input SIR (SIR_y) of \mathbf{y}_k . The improvement in SIR in dB is $N_s(\text{dB}) - SIR_y(\text{dB})$ can be very large for heavily jammed signals, but can go negative if the input interference \mathbf{u}_k is weak! It is important therefore to switch the canceling off if the SIR_y is better than N_s . N_s sets the target SIR into the demodulator and is plotted in Fig. 7.3. Simulations verify the theoretical analysis and show a difference of about 1.5dB corresponding to the Gaussian assumption for the QPSK signals. Further, three SIR_y s (10dB, 0dB, -10dB) were taken, all produced the same curve, indicating the independence of SIR_o from SIR_y .

The simulations used QPSK modulated signals for the desired signal (s) and jammer signals (a and b). The symbols were Nyquist filtered with 50% excess bandwidth, and oversampled by $OSR = 64$.


 Fig. 7.3: SIR_o vs (N/OSR) .

In what follows, the analysis considers a block size $N = 2^{12} = 4096$ giving $N/OSR = 64$, and hence, $SIR_o = 20\text{dB}$ (as shown by the blue dotted lines in Fig. 7.3). This is sufficient for 16-QAM demodulation.

The analysis above assumes no frequency offset for the $\hat{\mathbf{u}}_k''$ signal. A small frequency offset will add a linear phase component to $\hat{\mathbf{u}}_k''$. In the absence of the fine frequency correction block the signal,

$$\hat{u}_{n,k}''' = \hat{\rho} \hat{u}_{n,k}'' e^{j(-\theta/2 + \theta n/N)} \quad (7.45)$$

where the phase change over the block,

$$\theta = 2\pi f^{Fine} N/f_s. \quad (7.46)$$

After the final subtraction the error caused by the offset is given by $\rho \hat{u}_{n,k}''' - \hat{u}_{n,k}''$, and can be approximated for small θ to give,

$$o_{n,k} = s_{n,k} + \rho \hat{u}_{n,k}'' - \hat{\rho}_k \hat{u}_{n,k}'' \left(1 + j \left(-\frac{\theta}{2} + \frac{\theta n}{N} \right) \right) \quad (7.47)$$

which includes the error contribution from $\hat{\rho}_k$ given by (7.40). The variance term is now

$$\sigma_z^2 \approx \frac{\sigma_s^2}{N_s} + \frac{1}{N} \sum_1^N \hat{\rho}_k^2 \hat{u}_n''^2 \left(-\frac{\theta}{2} + \frac{\theta n}{N} \right)^2 \quad (7.48)$$

expanding the brackets and considering only the dominant terms (since N is large) and approximating,

$$\sigma_z^2 \approx \frac{\sigma_s^2}{N_s} + \frac{\hat{\rho}_k^2 \sigma_u^2 \theta^2}{12} \quad (7.49)$$

where the first term is the variance from the error in ρ and the second term is the variance caused by the frequency offset. Substituting for θ and further approximating $\hat{\rho}_k^2 \sigma_u^2 \approx \sigma_s^2 / SIR_y$ we have,

$$\mathbf{o}_k = \mathcal{N} \left\{ \mathbf{s}_k, \frac{\sigma_s^2}{N_s} + \frac{(f^{Fine} N / f_s)^2 \pi^2 \sigma_s^2}{3SIR_y} \right\}. \quad (7.50)$$

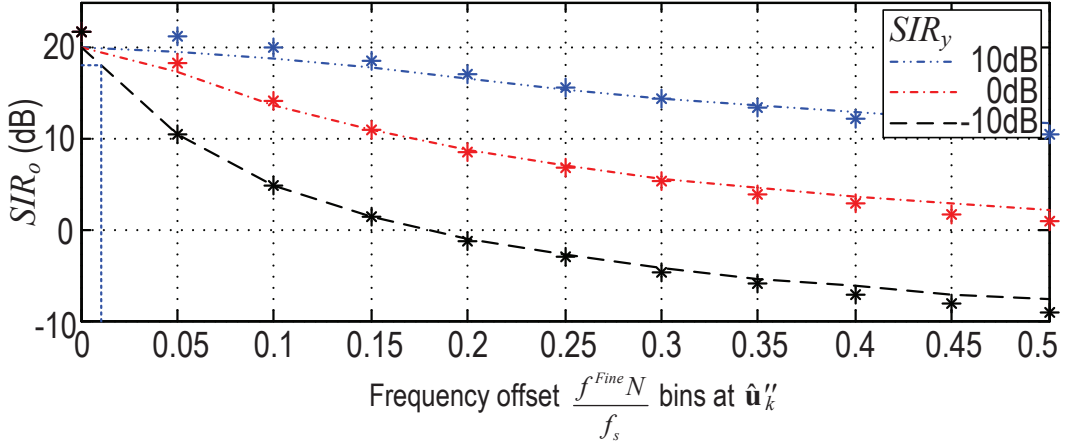


Fig. 7.4: The effect of frequency offset f^{Fine} on the output SIR. 1bin= f_s/N Hz. ‘*’s represent theoretical results.

Fig. 7.4 shows how the output SIR is degraded with frequency offsets measured in bins (equivalent to an N -point FFT bin size of $f_{bin} = f_s/N$ Hz). The discrepancy between the simulations and theoretical is caused by the error in the first term as previously explained and the loss of the low angle assumption at larger f^{Fine} s. It is to be noted that SIR_o deteriorates with small frequency offsets, especially when \mathbf{y}_k has a significant interference component \mathbf{u}_k . Frequency offset should be less than 0.01 bins (i.e., $f^{Fine} < 0.01 f_s/N$ Hz), if $SIR_y = -10$ dB, and the implementation loss is to be restricted to less than 2dB (as shown by the blue dotted lines in Fig. 7.4). This is the goal of the fine frequency correction discussed next.

7.3.2 Fine Frequency Correction

The fine frequency correction module removes any remaining offsets after the initial coarse correction stage. The module is designed to operate within offsets of ± 0.5 bins (i.e., $f^{Fine} < |0.5f_s/N|$ Hz). There are two factors that affect the accuracy of the estimate \hat{f}_k^{Fine} ,

- a) the level of desired signal \mathbf{s}_k in \mathbf{y}_k that acts as interference to the estimation process, and
- b) the absolute value of frequency offset f^{Fine} on the input signal $\hat{\mathbf{u}}'_k$.

Expanding (7.32) by splitting y into its signal and distortion components and then using equation (7.22) and (7.29), gives,

$$\phi_k = \frac{1}{N} \sum_{n=1}^N s_{n,k} \hat{u}'_{n,k} + \frac{1}{N} \sum_{n=1}^N \rho \hat{u}'_{n,k} \hat{u}_{n,k} e^{-j(\psi_k - \frac{\theta}{2} + \frac{\theta n}{N})}. \quad (7.51)$$

The linear phase shift is caused by the residual frequency offset f^{Fine} , and ψ_k is the mean phase offset of the block. The mean $\bar{\phi}_k \approx \rho \sigma_{\hat{u}}^2 e^{-j\psi_k}$ comes from the second term, and is accurate when θ is small. The variance of the first term is $\sigma_{\phi_{k,1}}^2 = \sigma_s^2 \sigma_{\hat{u}}^2 / N_s$. This variance is circularly symmetric and so the contribution to the phase error is a half of this value. The variance of the phase due to the first term is therefore,

$$\sigma_{\angle \phi_{k,1}}^2 = \frac{1}{2} \frac{\sigma_s^2 \sigma_{\hat{u}}^2}{\rho^2 \sigma_{\hat{u}}^4 N_s} = \frac{SIR_y}{2N_s}. \quad (7.52)$$

After the angles have been subtracted (i.e., $\Delta \angle \phi = \angle \phi_k - \angle \phi_{k-1}$), the fine frequency estimate \hat{f}_k^{Fine} is obtained from (7.34). The variance \hat{f}_k^{Fine} due to the first term in (7.51) becomes,

$$\sigma_{\hat{f}_{k,1}^{Fine}}^2 = \frac{SIR_y}{4\pi^2 N_s} \left(\frac{f_s}{N} \right)^2. \quad (7.53)$$

The second term of (7.51) contributes an additional variance when $f^{Fine} \neq 0$ resulting in a linear phase shift θ over the block. This makes the phase of ϕ_k dependent on the amplitudes of the individual $\hat{u}'_{n,k}$ samples. The variance of \hat{f}_k^{Fine} due to frequency offset is derived in the appendix B and the overall estimate \hat{f}_k^{Fine}

becomes,

$$\hat{f}_k^{Fine} = \mathcal{N} \left\{ f^{Fine}, \frac{SIR_y}{4\pi^2 N_s} \left(\frac{f_s}{N} \right)^2 + \frac{(f^{Fine})^2}{24N_s} \right\}. \quad (7.54)$$

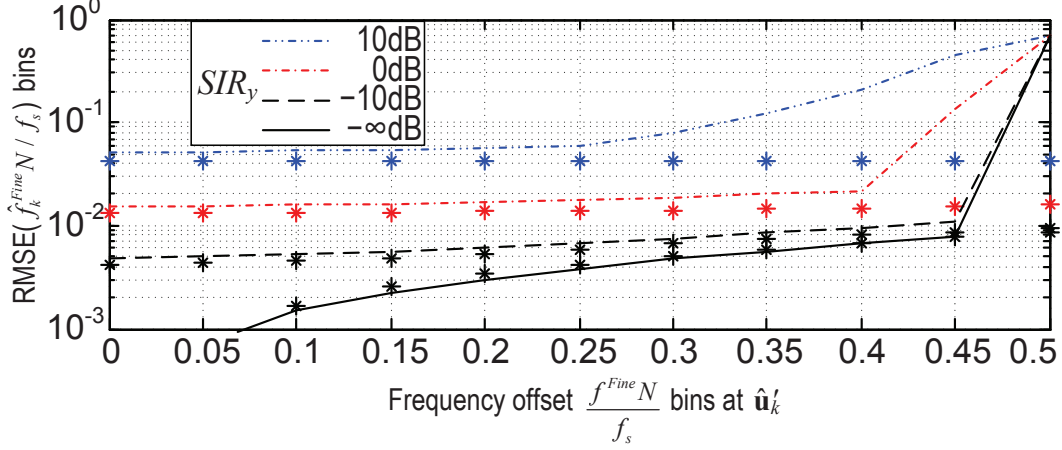


Fig. 7.5: Performance with feedforward fine frequency correction. “*”s represent theoretical results.

Fig. 7.5 shows the root mean square error of \hat{f}_k^{Fine} (i.e., $\text{RMSE}(\hat{f}_k^{Fine}) = \sqrt{E\{(\hat{f}_k^{Fine} - f^{Fine})^2\}}$) as a function of the actual frequency offset f^{Fine} . The solid black line represents an input \mathbf{y}_k without any \mathbf{s}_k (i.e. $\mathbf{y}_k = \mathbf{u}_k$ and $SIR_y = 0$). The increase in $\text{RMSE}(\hat{f}_k^{Fine})$ with frequency offset is from the second term only. When $SIR_y \neq 0$ the minimum $\text{RMSE}(\hat{f}_k^{Fine})$ level is set by the first term of (7.51). There is good agreement between simulations and theory for frequency offsets below 0.25 bins (i.e., $f^{Fine} < 0.25f_s/N$ Hz). When the frequency offset f^{Fine} goes beyond 0.5 bins ($0.5f_s/N$ Hz) the phase difference $\angle\phi_k - \angle\phi_{k-1}$ crosses π and the estimate \hat{f}_k^{Fine} jumps from 0.5 bins to -0.5 bins, a catastrophic situation. In the diagram the variance in the phase $\angle\phi_k$ causes \hat{f}_k^{Fine} to jump prematurely at lower frequency offsets, indicated by the steep rise in RMSE. This scheme will only work if the residual frequency offset f^{Fine} after the coarse correction is $\ll 0.5$ bins (i.e., $f^{Fine} \ll 0.5f_s/N$ Hz).

7.3.3 Improved Feedback Fine Frequency Correction

An improved architecture with a feedback fine frequency correction is proposed to reduce the probability of exceeding the discontinuity at $f^{Fine} = 0.5$ bins ($0.5f_s/N$

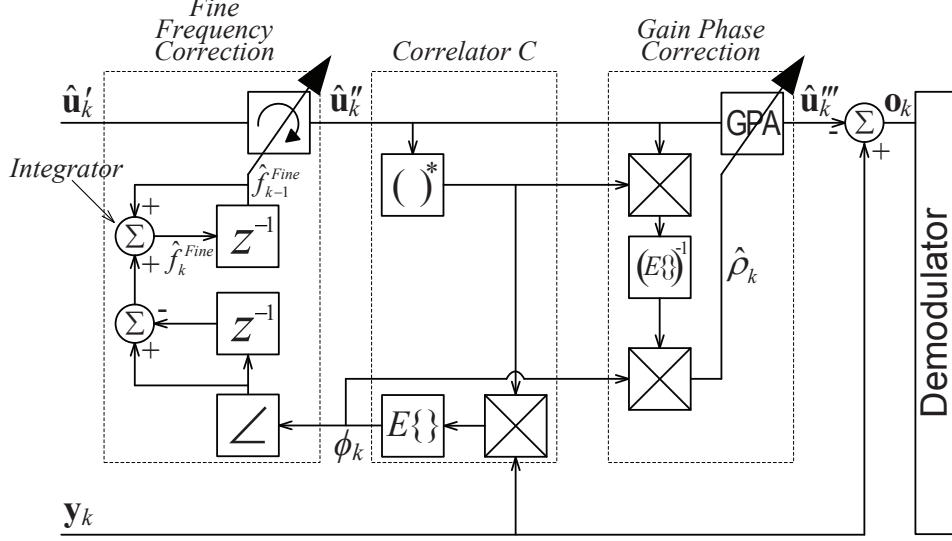


Fig. 7.6: Proposed feedback fine frequency correction.

Hz) as well as reduce the averaging error caused by frequency offsets in (7.54). We correct the frequency offset prior to estimating $\angle\phi_k$, as shown in Fig. 7.6,

$$\hat{u}_{n,k}'' = \hat{u}_{n,k}' e^{-j2\pi\hat{f}_{k-1}^{Fine}n/f_s}. \quad (7.55)$$

The correlator C now only has to calculate the change in f^{Fine} between blocks. An integrator holds the total estimate \hat{f}_k^{Fine} ,

$$\hat{f}_k^{Fine} = \hat{f}_{k-1}^{Fine} + \Delta\angle\phi f_s/2\pi N. \quad (7.56)$$

The scheme relies on any drift in frequency offset being slow. However, drifts that take the frequency offset beyond 0.5 bins ($0.5f_s/N$ Hz) can now be catered for. The key requirement is that the change in frequency per block must be $\ll 0.5$ bins. Fig. 7.7 shows the improved performance with respect to f^{Fine} , the contribution from the second term in (7.54) is nearly eliminated. Fig. 7.8 compares the two schemes tracking a frequency drift of magnitude 10^{-5} bins per sample ($10^{-5}f_s^2/N$ Hz/sec). The feedforward scheme fails to track the frequency offset once it drifts beyond 0.5 bins (in line with previous observations in Fig. 7.5). This is because the feedforward scheme calculates the total frequency offset of $\hat{\mathbf{u}}_k'$ relative to \mathbf{u}_k in

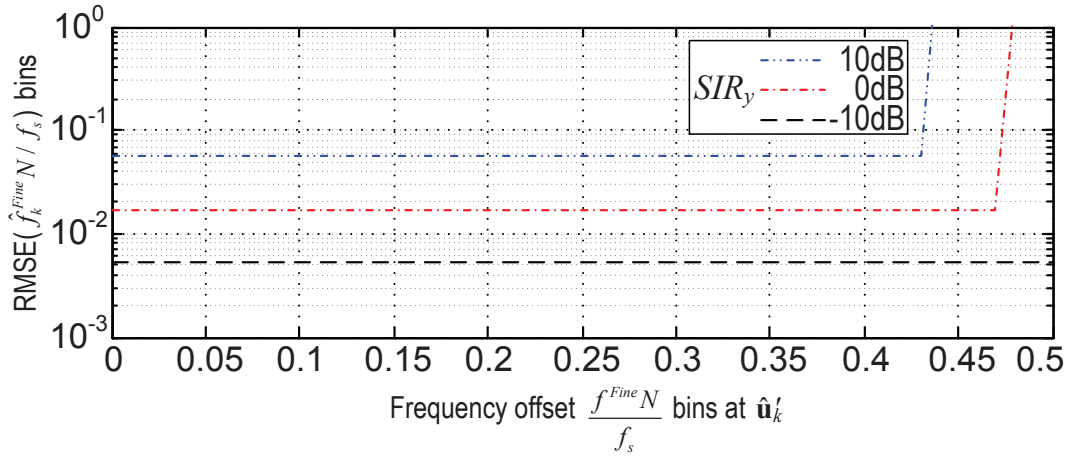


Fig. 7.7: Performance with feedback fine frequency correction.

each block stage. In contrast, the feedback scheme continues to track without any failures, since it only estimates the extra frequency offset that the current block has after correcting it with \hat{f}_{k-1}^{Fine} (which is the total tracked frequency offset at the

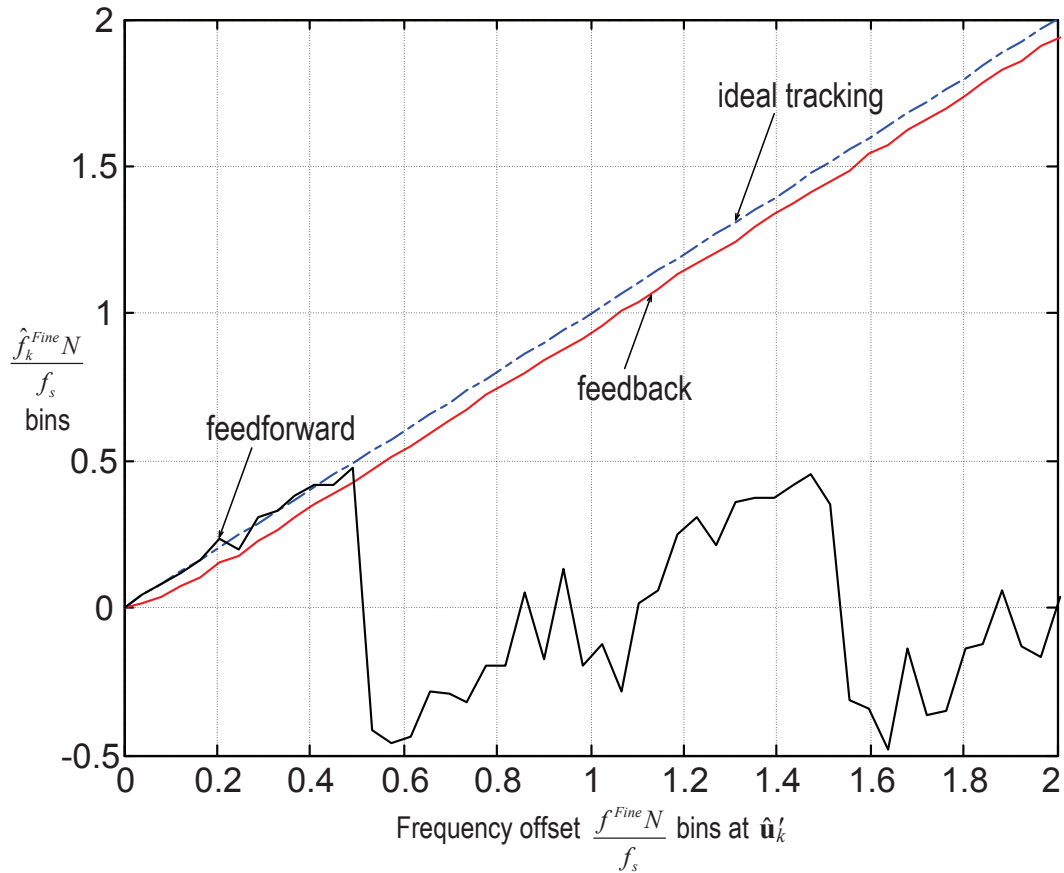


Fig. 7.8: Frequency drift tracking by \hat{f}_k^{Fine} .

previous block). However, the feedback design of the scheme makes \hat{f}_k^{Fine} to fall short of tracking the exact offset, because the offset keeps increasing with every sample; as demonstrated in the figure, the feedback scheme's tracking runs below the ideal tracking line.

Finally, it is to be noted that the feedback scheme can only track frequency drifts when it starts with small frequency offsets less than 0.5 bins ($0.5f_s/N$ Hz) depending on SIR_y . As observed earlier in Fig. 7.7, it can fail to track when starting with frequency offsets that are too high (e.g., 0.43 bins for $SIR_y = 10$ dB).

7.3.4 Coarse Frequency Correction

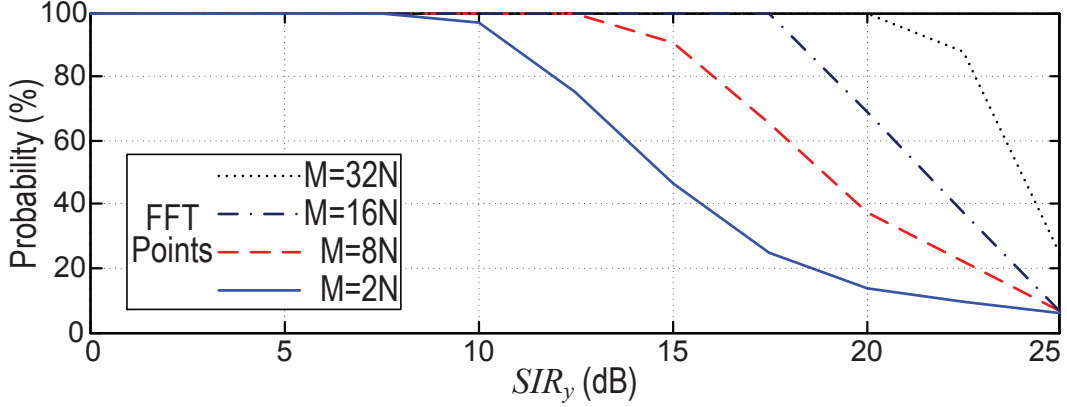


Fig. 7.9: Probability of acceptable coarse frequency correction ($\Delta f - 0.25f_s/N \leq f^{Coarse} \leq \Delta f + 0.25f_s/N$) for $M = 2N$, $M = 8N$, $M = 16N$ and $M = 32N$.

A good target for the coarse frequency correction module is to reduce the residual frequency offset f^{Fine} on $\hat{\mathbf{u}}'_k$ to within 0.25 bins (i.e. $f^{Fine} \leq 0.25f_s/N$ Hz). Hence, from (7.24) we have,

$$\Delta f - 0.25f_s/N \leq f^{Coarse} \leq \Delta f + 0.25f_s/N. \quad (7.57)$$

As discussed earlier in section 7.2.3, the coarse correction module is accurate within 0.5 bins of the M -point FFT (equivalent to $0.5f_s/M$ Hz). Hence, evaluating $0.25f_s/N = 0.5f_s/M$ gives the required number of FFT points on the coarse correction module $M = 2N$ (8192).

However, the M -point FFT can be forced into error by the presence of s in y . In the worst case scenario where the frequency offset is on a bin boundary, the target residual offset ($f^{Fine} \leq 0.25f_s/N$ Hz) is achieved if the highest power bin l_{max} is one of the two bins on either side of the offset bin boundary. The solid line (blue) Fig. 7.9 shows the probability of l_{max} being one of the two bins for increasing powers of s (i.e increasing SIR_y). At $SIR_y = 10$ dB, the probability of f^{Coarse} being within range (7.57) is 97%. But SIR_y s greater than 10dB forces l_{max} outside the two expected bins and the probability falls exponentially.

The performance at higher SIR_y s can be improved by increasing the number of FFT points M . This reduces the FFT bin sizes and its susceptibility to noise. It also increases the number of frequency bins that result in acceptable coarse correction. For example, a $M = 8N$ -point FFT results in $0.125f_s/N$ Hz bin sizes and l_{max} could be any one of 4 bins (two on either side of the offset bin boundary). Fig. 7.9 further illustrates the probability of f^{Coarse} being within range (7.57) for $M = 8N$, $M = 16N$ and $M = 32N$.

7.4 Practical Measurements

In this section, a practical setup in accordance to Fig. 7.1 is used to demonstrate that two out-of-band jammers at a colocated setting generate reverse IM3 products causing major interference for the victim receiver. Further, a practical implementation of our proposed receiver architecture is demonstrated using Universal Software Radio Peripherals (USRPs) [39] as SDR front-ends. The signals are data-logged and processed in MATLAB.

Fig. 7.10 shows the two jammer antennas (A and B) colocated at close proximity to one another. Each jammer is a signal generator, QPSK modulated with an USRP and amplified by a power amplifier (Mini-Circuits ZHL-42W [16]), transmitting with an omni-directional dipole antenna. A small separation of 40cm is required to generate a considerable reverse IM3 product at the low transmitting powers in the laboratory setting. Jammer A transmits a 0.5W signal at 922MHz and jammer

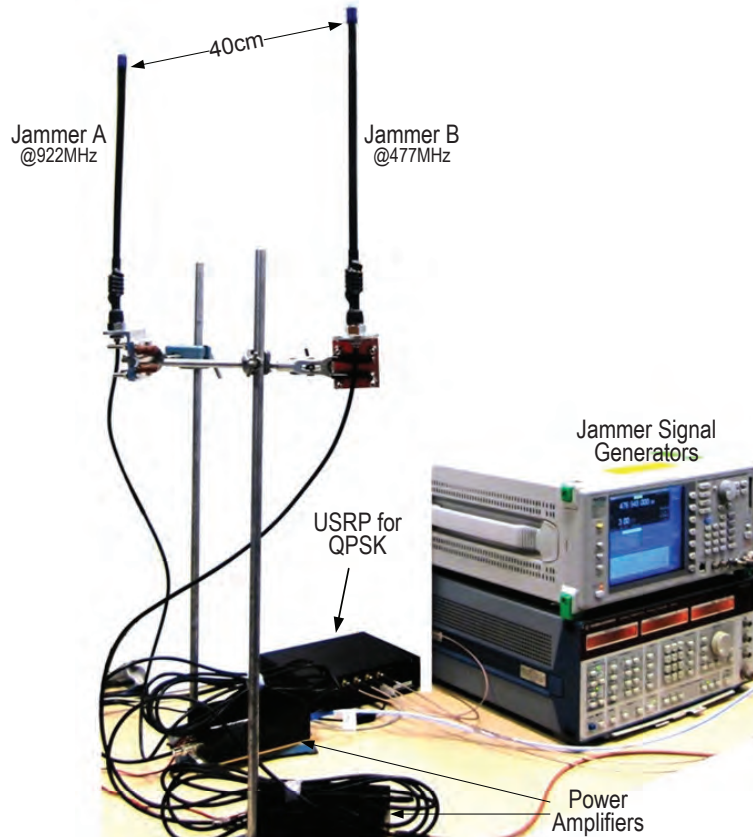


Fig. 7.10: Colocated transmitters generating reverse IM3 products.

B transmits a 1W signal at 477MHz, this propagates into the power amplifier of jammer A and produces a reverse IM3 product at 1367MHz. Fig. 7.11 shows the frequency spectrum at the victim receiver RX's antenna. Adjacent to the 1367MHz reverse IM3, the spectrum shows the 1399MHz (922MHz+477MHz) reverse second-order intermodulation (IM2) product and the 1431MHz (3x477MHz) third harmonic, these signals are at sufficient separation and do not affect our experiment.

Victim receiver RX is setup in accordance to our proposed receiver architecture using three crystal locked USRP units Rx0, Rx1 and Rx2 as seen in Fig. 7.2. The victim antenna is placed 3m from the out-of-band jammers A and B to ensure that they do not overload the receiver front-ends. To demonstrate the performance of the receiver system a narrow-band 12.5 kHz QPSK modulated signal is used for both the desired and jammer signals. The symbol rate is 7.8125 ksymbols/s and filtered with a Nyquist filter with 50% excess bandwidth. Fig. 7.12 shows the constellation

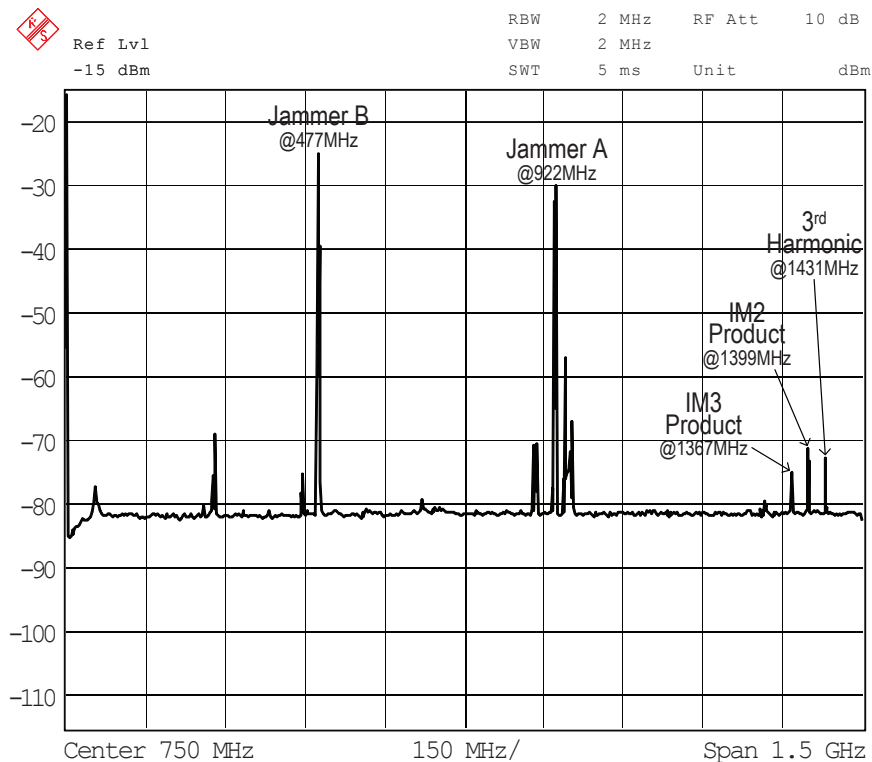


Fig. 7.11: Frequency spectrum of the jammers and the IM3 product of concern.

of the desired signal and a 0.5MHz baseband spectrum received at Rx0.

Fig. 7.12(a) shows the reception of the desired signal at Rx0 without any jammers and interference. The receiver is operated at low IF to avoid any DC offset issues. The low-powered transmitter for the desired signal is mounted in an adjacent room. The scatter plot on the left hand side shows the four QPSK constellation points of the received desired signal at a signal-to-noise ratio (SNR) of about 38dB.

Fig. 7.12(b) shows the spectrum at Rx0 with the out-of-band colocated jammers turned on. The reverse IM3 product from jammer A falls directly on the desired signal frequency (1367MHz) and completely masks the signal causing major interference. The constellations are unrecognizable as a result of interference.

Fig. 7.12(c) shows the spectrum after DSP correction. The inset compares the spectrum (black) of the DSP corrected signal with the spectrum (blue) of the IM3 distorted signal. Error vector magnitude measurements on the constellation diagrams indicate that the IM3 distortion has been canceled by 16dB, leaving the desired signal with a SNR of about 18dB. The DSP is implemented in MATLAB

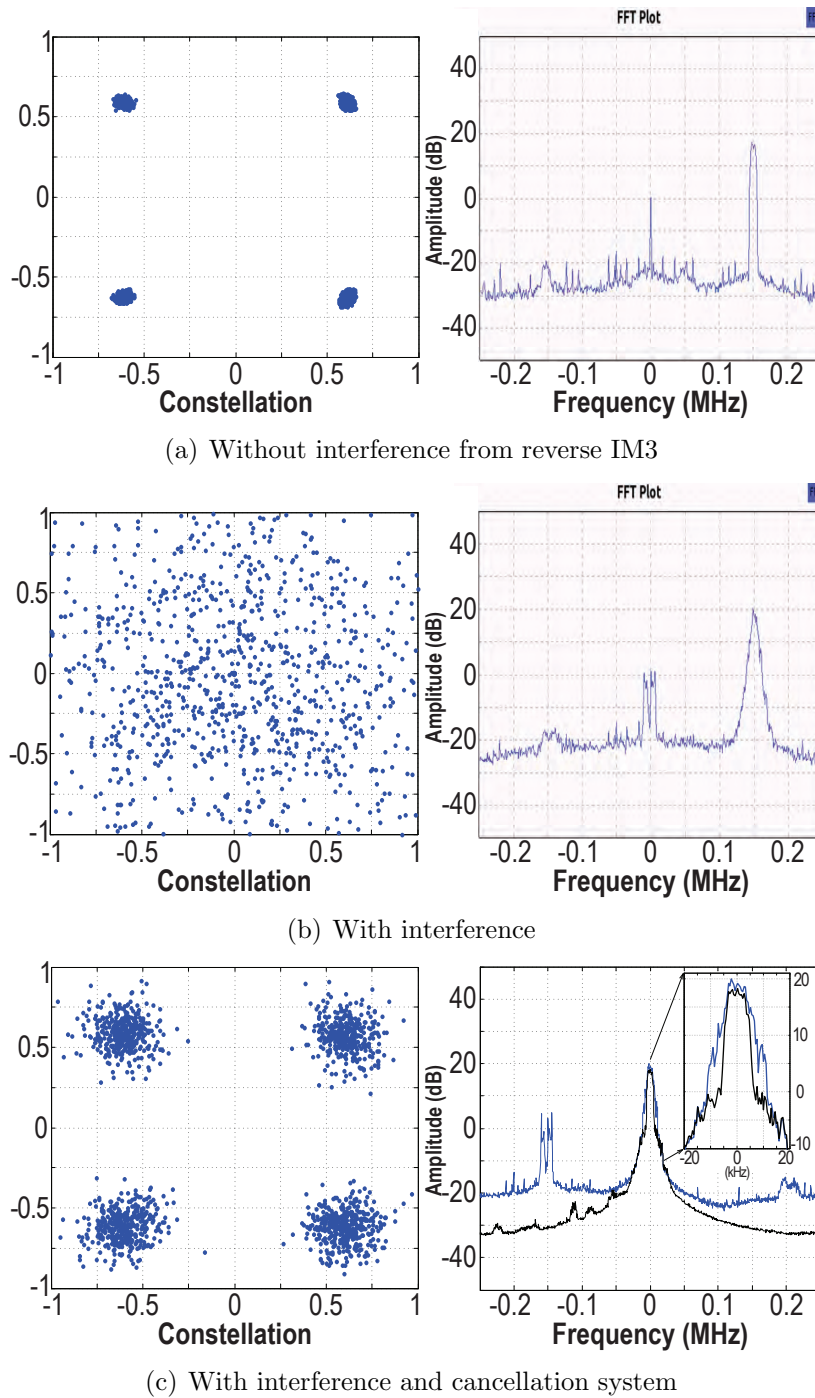


Fig. 7.12: Experiment results. Signal constellation scatter plots (LHS) and frequency spectrum plots (RHS). The spectrum plots show relative scales with 20dB representing -75dBm.

in accordance to our simulation settings with $N = 4096$ and $M = 2N$. As in Fig. 7.2, the DSP takes inputs from Rx1 and Rx2, synthesizes a copy of the IM3 and

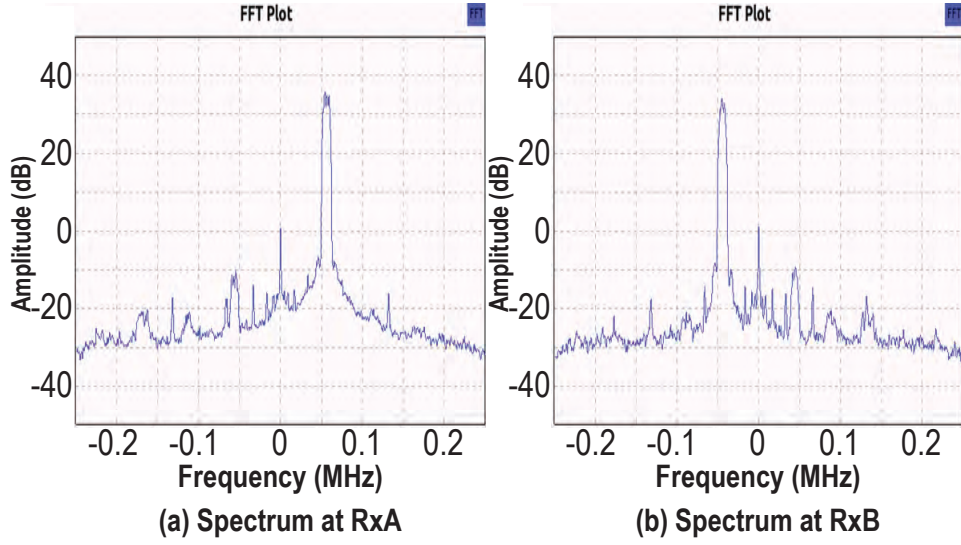


Fig. 7.13: Frequency spectrum of the jammers.

removes it from the primary reception at Rx0. The 18dB SIR achieved is in close agreement to the 20dB output SIR achieved in our simulations (Fig. 7.3).

Fig. 7.13(a) and (b) show the baseband frequency spectrums on Rx1 and Rx2 respectively. Rx1 receives the 922MHz jammer A at a frequency offset of 55kHz and Rx2 receives the 477MHz jammer B at a frequency offset -45 kHz. The gains on the front-ends are adjusted such that they are within receiver dynamic range.

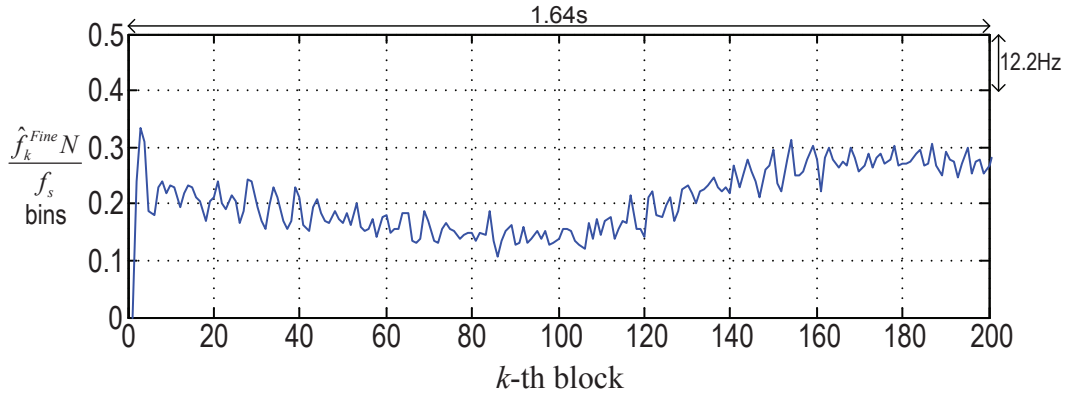


Fig. 7.14: Fine frequency tracking by \hat{f}_k^{Fine} . $f_s=0.5$ Msamples/s, $N=4096$.

Fig. 7.14 shows \hat{f}_k^{Fine} 's fine frequency tracking of the aggregated local oscillator drifts. As estimated, the coarse frequency correction module has reduced the frequency offset to about 0.25 bins ($0.25f_s/N$ Hz). The ripples seen in the figure are primarily due to $\text{RMSE}(\hat{f}_k^{Fine})$ caused by the interference effect of the desired signal

in the fine frequency estimation algorithm.

7.5 Summary

- The chapter describes the use of complex envelopes to model the reverse IM3 problem that occurs when a large jamming signal from one jammer mixes at the output of a second colocated jammer's power amplifier. The reverse IM3 product may fall on the desired receive channel of a colocated receiver and cause interference. The chapter discusses in full a postdistortion cancellation system that uses multiple receiver front-ends to regenerate and adaptively cancel the reverse IM3 product. The multiple receiver front-ends avoid the need for extremely high sample rates that would be necessary to cover both jammers and the corrupt desired signal in a single unit.
- A novel two stage frequency correction scheme is proposed to remove frequency offsets, introduced by the multi-front-end receiver architecture. The correction scheme uses an FFT for coarse correction, and signal correlation for fine frequency tracking. The feedback fine correction scheme can track frequency offset drifts well outside the coarse correction capability.
- Mathematical analysis and simulations were used to comprehensively characterize the system. It is shown that the desired signal acts as noise for the frequency correction scheme and for the estimation of the cancellation coefficient. Averaging is used to improve the accuracy of the estimates. The output SIR (SIR_o) was shown to be dependent on the equivalent number of uncorrelated samples (N_s) in the averaging block. This is equal to the number of samples (N) in the block, divided by the over sampling rate (OSR) of the modulation, and multiplied by a factor (η) that is dependent on the modulation parameters of the signals. Spectral convolution is used to derive the factor η .
- The maximum SIR improvement possible was shown to be $(N_s - SIR_y)$ dB. Therefore, it is recommended to switch OFF the canceling circuit when $SIR_y <$

N_s .

- The chapter demonstrated a working prototype of the postdistortion cancellation system. Jammers at frequencies 477MHz and 922MHz caused a reverse IM3 product at 1367MHz which is within the GPS² satellite band. The frequency correction and cancellation algorithm with an oversampling rate OSR=64, a data block size of $N = 4096$ and an FFT size of $M = 8192$ -points achieved an 18dB output SIR that is in close agreement with the simulation and analytical results. The input SIR was 2dB indicating a 16dB reduction in the reverse IM3 distortion.

²GPS signals are very low level and are particularly sensitive to noise and distortion.

Chapter 8

Conclusion

The thesis aimed at providing a comprehensive solution for base station receivers operating in a colocated setting. Chapter 1 gave an overview of the forward intermodulation and the reverse intermodulation products that originate when base station transceivers are placed at close proximity to one another. Forward intermodulation products are generated when large jamming signals mix within the victim receiver, these are common and modeled by the receiver's IP3. High powered jamming signals regardless of their frequency may also cause receiver desensitization. Reverse intermodulation products are generated when strong jamming signals from one transmitter feed in the reverse direction through the antenna system and mix in the output stage of a second transmitter's power amplifier.

A controlled laboratory setup was used in chapter 2 to verify the presence of reverse intermodulation products using in a colocated setting. Interference from the dominant reverse IM3 product did not comply with the general idea of backing off by 1dB to get 3dB reduction; it was proportional to the level of reverse signal coupling into the power amplifier's output port. Further, a practical experiment demonstrated receiver desensitization.

Chapter 4 proposed a reference antenna based adaptive cancellation system that mitigates forward IM3 products and desensitization by reducing the jamming signals before they hit the receiver circuits. The practicality of such a system depends on understanding how the cancellation loop and its components effect the overall

system performance. A dynamic range analysis of the system was carried out. It was demonstrated that the adaptive cancellation system improved the overall IP3 of the system, however, this was achieved at the expense of additional noise added by the components of the cancellation loop. The system IP3 ($IP3_T$) and noise factor (F_T) expression that were derived concludes that the coupling gain (C) of the cancellation coupler is a compromise between achieving higher IP3 values and lower noise figures.

Chapter 5 used a novel signal-to-interference-and-noise ratio (SINR) analysis to maximize SINR by optimizing C . The optimum coupling gain expression was then used to define a design jamming level X_d for a given coupler. Depending on the properties of the cancellation loop components, X_d characterized the SINR performance of the system into two regions, the noise-dominated region (for $X < X_d$), and the distortion-dominated region (for $X > X_d$). It was understood that the efficiency of the jammer cancellation system is maximized when operating in the distortion-dominated region. The plateaued noise-dominated region directed switching OFF the cancellation path when significant jammers are not present. Chapter 5 also demonstrated a prototype of the cancellation system under a controlled setting, i.e., a directly fed reference antenna. An automated cancellation loop reduced the jamming signals by 46dB in 8.4ms. The prototype achieved a significant 42dB SINR improvement over the basic “do-nothing” system at $X_d = -4.6\text{dBm}$.

Chapter 6 addressed the key challenge of implementing an over-the-air prototype of the adaptive cancellation system, i.e., the reference antenna picks up a copy of the desired signal and results in self-cancellation. The demonstrated prototype places the reference antenna close to the aggressor jammer antennas, thus, achieving a higher interference-to-signal ratio on the reference path. After gain-phase adjustment in the reference path there is negligible desired signal cancellation in the primary path. The over-the-air prototype achieved a 25dB reduction in jammer level, eliminating all distortion products within the receiver. The desired signal had a small self-cancellation of 0.3dB. The compromise was a 5dB increase in the receiver’s noise figure.

Although reducing the jammers before they hit the receiver front-end mitigates internally generated distortions, it does not reduce the reverse IM3 products that are generated at the output of the colocated transmitters. Chapter 7 proposed a postdistortion cancellation scheme for the victim receiver. The scheme used the fundamental jammers in a distortion regeneration circuit to synthesize an estimate of the reverse IM3. The postdistortion cancellation scheme then used the estimate to mitigate the interfering reverse IM3. A multi-front-end receiver architecture was used to ensure tracking of out-of-band jammers without the need for extremely high sampling frequencies. However, this led to frequency offsets between the estimate and the reverse IM3 product. To overcome this, the proposed scheme used a two part novel frequency offset correction technique, an FFT for coarse correction and signal correlation for fine frequency tracking. A feedback fine frequency tracking scheme was also devised to track frequency drifts beyond the coarse correction capability. It was understood that the desired signal acted as noise to the FFT function, hence, requiring larger M -point FFTs at higher input signal-to-interference ratios (SIR_y). The fine frequency correction used a block processing scheme. The maximum SIR improvement in dB was given by $N_s(\text{dB}) - SIR_y(\text{dB})$ where N_s is the number of uncorrelated samples in a block, suggesting a shutdown of the canceling circuit when $SIR_y > N_s$. Finally, a working prototype was demonstrated to achieve 16dB cancellation of the interfering reverse IM3, using a block length $N = 4096$ and an $M = 8192$ -point FFT.

8.1 Future Work

8.1.1 Multi-loop Adaptive Cancellation

The proposed system in chapters 4-6 used a single cancellation loop and is only capable of mitigating jamming signals radiating from a single aggressor jammer antenna. However, a colocated setting is likely to have more than one jammer. Future work would involve the implementation of a multi-loop adaptive cancellation system that is capable of mitigating jamming signals from multiple colocated jammers. It

would be interesting to look into the practicality of convergence algorithms for such multi-loop cancellation.

8.1.2 Cognitive Sensing and Jammer Selection

The prototype of the postdistortion cancellation system in chapter 7 was manually tuned to the jammer frequencies. In future work, the automation of such a system would require major contributions in cognitive sensing and jammer selection.

Appendix A

The Modulation Parameter Factor

η

The variance of the signal ϕ'_k from the correlation of $\hat{\mathbf{u}}''_k$ with \mathbf{s}_k (the desired signal component in \mathbf{y}_k) is obtained by calculating the power spectrum $P(f)$ of the signal $(\mathbf{s}_k \hat{\mathbf{u}}''_k)$ and then multiplying it with the power frequency response of the averaging function. An N -point averaging filter has a low pass frequency response, with an effective power bandwidth of f_s/N (where f_s is the sampling frequency). We make an approximate solution for the case where all signals have the same bandwidth of f_s/OSR and a rectangular spectral shape. If the desired signal \mathbf{s}_k with spectrum $S(f)$ was passed through the averaging filter, its variance would be reduced by $\eta N/OSR$, where $\eta = 1$.

The spectrum $P(f)$ is a convolution of $S(f)$ with the spectrum $\hat{U}(f)$ (of the IM3 distortion signal $\hat{\mathbf{u}}''_k$), which itself is a triple convolution of the spectrums $A(f)$, $A(f)$ and $B(f)$ (of the fundamental jammer signals a and b). i.e. $P(f) = S(f) * \hat{U}(f) = S(f) * A(f) * A(f) * B(f)$. There are 4 convolved terms. We note that the convolution of two unit rectangular signals (power spectral density=1, bandwidth=1) is triangular in shape (magnitude=1, bandwidth=2), and the convolution of two triangles give a signal with a magnitude spectrum of $2/3$ at the center of the band (at DC). Since N is large, the averaging filter bandwidth is very small and we assume a constant spectrum of $P(0)$ over its bandwidth. The variance is, therefore, reduced

by $(9/4)N/OSR$, giving $\eta = 9/4$. Of course, the magnitude of $A(f)$ and $B(f)$ also has an effect on the variance, but this is accounted for by the normalization when ϕ'_k goes to $\hat{\rho}_k$.

Appendix B

The Variance of \hat{f}_k^{Fine} due to Frequency Offset

The linear phase shift of θ across the block in the second term in (7.51) produces an orthogonal error ϵ_k in ϕ_k , the mean of which is zero. For small θ ,

$$\bar{\epsilon}_k = \frac{1}{N} \sum_1^N \rho \hat{u}_{n,k} \hat{u}_{n,k}^* \left(\frac{\theta}{2} - \frac{\theta n}{N} \right) e^{-j\psi_k} = 0. \quad (\text{B.1})$$

We now split the summation into 2 parts (Fig. B.1). The mean for the first and second $N/2$ samples is $\bar{\epsilon}_{k,1} = \left(\frac{\theta}{4}\right) \rho \sigma_u^2 e^{-j\psi_k}$ and $\bar{\epsilon}_{k,2} = \left(-\frac{\theta}{4}\right) \rho \sigma_u^2 e^{-j\psi_k}$ respectively. The variance for both halves are,

$$\sigma_{\epsilon_{k,1}}^2 = \sigma_{\epsilon_{k,2}}^2 = \frac{2}{N} \sum_1^{N/2} \rho^2 \sigma_u^4 \left\{ \left(\frac{\theta}{2} - \frac{\theta n}{N} \right) - \left(\frac{\theta}{4} \right) \right\}^2 = \frac{\theta^2}{48} \rho^2 \sigma_u^4. \quad (\text{B.2})$$

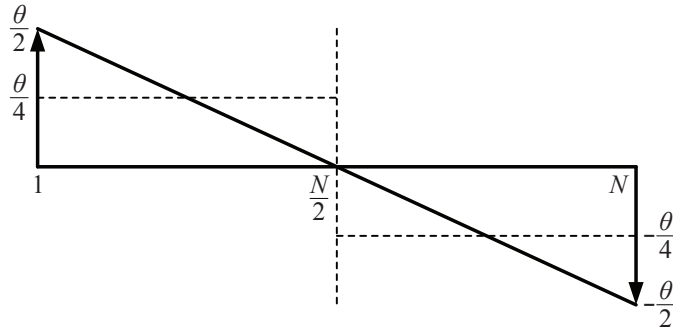


Fig. B.1: Linear phase $\theta (= 2\pi f^{Fine} N/f_s)$ across a block.

When we average over all N samples the mean goes to zero and the variance becomes $\sigma_{\epsilon_k}^2 = \frac{\theta^2}{48N_s} \rho^2 \sigma_{\dot{u}}^4$. We then substitute for θ as per 7.46, and change back to a phase error $\sigma_{\angle\phi_k}^2 = \tan^{-1} \left(\sigma_{\epsilon_k}^2 / |\bar{\phi}_k|^2 \right)$ by using the small angle approximation. The phase error variance is doubled after the subtraction of (7.33) to give \hat{f}_k^{Fine} . Thus, the variance of \hat{f}_k^{Fine} due to the second term in (7.51) becomes

$$\sigma_{\hat{f}_{k,2}^{Fine}}^2 = \frac{\left(f^{Fine}\right)^2}{24N_s}. \quad (\text{B.3})$$

References

- [1] M. Minges, “Key Trends in the Development of the Mobile Sector,” *Information and Communications for Development 2012: Maximizing Mobile*. Washington, D.C.: The World Bank, 2012.
- [2] K. Allsebrook and C. Ribble, “VHF cosite interference challenges and solutions for the United States Marine Corps’ expeditionary fighting vehicle program,” in *Proc. IEEE Military Communications Conference*, 2004.
- [3] F. German , K. Annamalai, M. Young , M. C. Miller, “Simulation and Data Management for Cosite Interference Prediction,” in *Proc. IEEE International Symposium on Electromagnetic Compatibility*, July 2010.
- [4] I. Demirkiran, D. D. Weiner, A. Drozd and I. Kasperovich, “Knowledge-based Approach to Interference Mitigation for EMC of Transceivers on Unmanned Aircraft,” in *Proc. IEEE International Symposium on Electromagnetic Compatibility*, July 2010.
- [5] J. J. Gavan and M. B. Shulman, “Effects of Desensitization on Mobile Radio System Performance, Part I: Quantitative Analysis,” *IEEE Transactions on Vehicular Technology*, vol. VT-33, no. 4, pp. 285-290, November 1984.
- [6] B. Razavi, *RF Microelectronics*. Upper Saddle River, NJ: Prentice Hall, 1998, pp. 11-53.

-
- [7] B. Razavi, "Design Considerations for Direct-Conversion Receivers," *IEEE Transactions on Circuit and Systems II: Analog and Digital Signal Processing*, vol. 44, no. 6, June 1997.
- [8] J. B. Johnson, "Thermal Agitation of Electricity in Conductors," *Physical Review*, vol. 32, pp. 971-99, July 1928.
- [9] H. T. Friis, "Noise Figures of Radio Receivers," in *Proc. of the IRE*, vol. 32, no. 7, pp. 419-422, July 1944.
- [10] IRE Subcommittee 7.9 on Noise, "Description of the Noise Performance of Amplifiers and Receiving Systems," in *Proc. of the IEEE*, vol. 51, no. 3, pp. 436-442, March 1963.
- [11] P. Vizmuller, *RF Design Guide: Systems, Circuits, and Equations*, Boston : Artech House, Incorporated, 1995.
- [12] P. L. Lui, "Passive Intermodulation Interference in Communication Systems," *Electronics and Communication Engineering Journal*, June 1990.
- [13] V. Golikov, S. Hienonen, P. Vainikainen, "Passive Intermodulation Distortion Measurements in Mobile Communication Antennas," in *Proc. Vehicular Technology Conference*, vol.4, pp. 2623-2625, 2001 .
- [14] S. S. Soliman, M. D. Srinath, *Continuous and Discrete Signals and Systems*, 2nd Ed. Upper Saddle River, NJ: Prentice Hall, 1998.
- [15] S. Ahmed and M. Faulkner, "Interference Issues at Co-located Base Stations and an Adaptive Cancellation Solution," in *Proc. Electromagnetic Compatibility Symposium and Exhibition Melbourne*, September 2010.
- [16] Mini-Circuits. ZHL-42 Amplifier. *Data Sheet*. [Online]. Available: <http://www.minicircuits.com/pdfs/ZHL-42.pdf>
- [17] W. Guthrie and D. Hanson. (2005, June 13). Co-Location Interference Mitigation. *White Paper*. Netcom Inc., USA. <http://www.netcominc.com>

- [18] Alain Roussel, Charles W. T. Nicholls, and Jim S. Wight, "Frequency Agile RF Feedforward Noise Cancellation System," in *Proc. IEEE Radio and Wireless Symposium*, 2008.
- [19] J. Zhu, A. Waltho, X. Yang, X. Guo, "Multi-Radio Coexistence: Challenges and Opportunities," in *Proc. 16th International Conference on Computer Communications and Networks (ICCCN)*, pp. 358-364, 13-16 August, 2007.
- [20] X. Yang, H. Liu, X. Guo, "Bluetooth Coexistence with 4G Broadband Wireless Networks," in *Proc. IEEE Communications Society Conference on Sensor Mesh and Ad Hoc Communications and Networks (SECON)*, pp. 1-9, June 2010.
- [21] B. Xavier, L. Christensen, "Cellular/WiFi Multi-mode Systems," in *Proc. IEEE Radio and Wireless Symposium*, pp. 3-6, 17-19 January, 2006.
- [22] H. Thomas, W. Kodim, R. Gloeckler, H. Dingfelder, "Transmitter Leakage Cancellation Circuit for Co-Located GPS Receiver," European Patent 1 091 497, 11 April 2001.
- [23] R. J. McConnell, R. Tso, "Method and Apparatus for Reducing GPS Receiver Jamming during Transmission in a Wireless Receiver," U.S. Patent 6 961 019, 1 Nov 2005.
- [24] A. Raghavan, E. Gebara, E. M. Tentzeris and J. Laskar, "Analysis and Design of an Interference Canceller for Collocated Radios," *IEEE Transactions on Microwave Theory and Techniques*, vol. 53, no. 11, November 2005.
- [25] S. Kannangara and M. Faulkner, "Adaptive Duplexer for Multiband Transceiver," in *Proc. Radio and Wireless Conference (RAWCON)*, pp. 381-384, 10-13 August, 2003.

-
- [26] B. Widrow, J. R. Glover, J. M. McCool, J. Kaunitz, C. S. Williams, R. H. Hearn, J. R. Zeidler, E. Dong, Jr., and R. C. Goodlin, "Adaptive noise canceling: Principles and applications," *Proc. IEEE*, vol. 63, no. 12, pp. 1692-1716, 1975.
- [27] B. Widrow and S.D. Stearns, *Adaptive Signal Processing*. Englewood Cliffs, NJ 07632: Prentice Hall, 1985.
- [28] A. Katz, D. McGee, C. Brinton and J. Qiu, "Sensitivity and Mitigation of Reverse IMD in Power Amplifiers," in *Proc. IEEE Topical Conference on Power Amplifiers for Wireless and Radio Applications (PAWR)*, January 2011.
- [29] T. Nojima, T. Konno, "Cuber Predistortion Linearizer for Relay Equipment in 800 MHz Band Land Mobile Telephone System," *IEEE Transactions on Vehicular Technology*, vol. 34, no. 4, pp. 169-177, November 1985.
- [30] H. Matsubara, K. Ishihara, N. Miyadai, T. Nojima, "A Novel 3rd-and-5th-Order Predistortion Circuit for 2 GHz Band W-CDMA Amplifier," in *Proc. Asia-Pacific Microwave Conference (APMC)*, pp. 1-4, 11-14 December 2007.
- [31] T. Rahkonen, T. Kankaala, M. Neitola, "A Programmable Analog Polynomial Predistortion Circuit for Linearising Radio Transmitters," in *Proc. 24th European Solid-State Circuits Conference*, pp. 276-279, 22-24 September 1998.
- [32] S. P. Stapleton, F. C. Costescu, "An Adaptive Predistorter for a Power Amplifier Based on Adjacent Channel Emissions," *IEEE Transactions on Vehicular Technology*, vol. 41, no. 1, pp. 49-56, 1992.
- [33] G. Baudoin, P. Jardin, "Adaptive Polynomial Pre-distortion for Linearization of Power Amplifiers in Wireless Communications and WLAN," in *Proc. International Conference on Trends in Communications (EUROCON)*, pp. 157-160, 4-7 July, 2001.

- [34] F. H. Raab, P. Asbeck, S. Cripps, P. B. Kenington, Z. B. Povovich, N. Potheary, J. F. Sevic and N. O. Sokal “RF and Microwave Power Amplifier and Transmitter Technologies- Part 4,” *High Frequency Electronics*, November 2003.
- [35] M. Faulkner, “DC Offset and IM2 Removal in Direct Conversion Receivers,” *IEE Proc. Communication*, vol. 149, no. 3, pp. 179-184, June 2002.
- [36] E. A. Keehr, A. Hajimiri, “Equalization of Third-Order Intermodulation Products in Wideband Direct Conversion Receivers,” *IEEE Journal of Solid-State Circuits*, vol. 43, no. 12, pp. 2853 - 2867, December 2008.
- [37] E. A. Keehr, A. Hajimiri, “Successive Regeneration and Adaptive Cancellation of Higher Order Intermodulation Products in RF Receivers,” *IEEE Transactions on Microwave Theory and Techniques*, vol. 59, no. 5, pp. 1379 - 1396, March 2011.
- [38] M. Valkama, A. S. H. Ghadam, L. Anttila, M. Renfors, “Advanced Digital Signal Processing Techniques for Compensation of Nonlinear Distortion in Wideband Multicarrier Radio Receivers,” *IEEE Transactions on Microwave Theory and Techniques*, vol. 54, no. 6, pp. 2356 - 2366, June 2006.
- [39] Ettus Research LLC. Universal Software Radio Peripheral. *Product Details*. [Online]. Available: <https://www.ettus.com/product/details/USRP-PKG>
- [40] Ettus Research LLC. WBX 50-2200MHz Rx/Tx. *Product Details*. [Online]. Available: <https://www.ettus.com/product/details/WBX>
- [41] S. Ahmed and M. Faulkner, “An Adaptive Cancellation System for a Colocated Receiver and its Dynamic Range,” in *Proc. IEEE Radio and Wireless Symposium*, January 2011.
- [42] S. Ahmed and M. Faulkner, “Optimized Interference Canceling for Colocated Base Station Transceivers,” *IEEE Transactions on Vehicular Technology*, vol. 60, no. 9, pp. 4175-4183, October 2011.

-
- [43] Hittite Microwave Corporation. HMC630LP3E Vector Modulator. *Data Sheet*. [Online]. Available: http://www.hittite.com/content/documents/data_sheet/hmc630lp3.pdf
- [44] Mini-Circuits. Monolithic Amplifier ERA-3. *Data Sheet*. [Online]. Available: <http://www.minicircuits.com/pdfs/ERA-3+.pdf>
- [45] L. C. Godara, "Application of Antenna Arrays to Mobile Communications, Part II: Beam-Forming and Direction-of-Arrival Considerations," in *Proceedings of the IEEE*, vol. 85, no. 8, pp. 1195-1245, August 1997.
- [46] H. Krim and M. Viberg, "Two Decades of Array Signal Processing Research: The Parametric Approach," *IEEE Signal Processing Magazine*, vol. 13, no. 4, pp. 67-94, July 1996.
- [47] S. M. Kuo and D. R. Morgan, "Active Noise Control: A Tutorial Review," in *Proceedings of the IEEE*, vol. 87, no. 6, pp. 943-973, June 1999.
- [48] C. A. Balanis, *Antenna theory: Analysis and Design*. 2nd Edition. USA: John Wiley & Sons, Inc., 1996, pp. 151.
- [49] Mini-Circuits. ZX60-33LN-S+ Low Noise Amplifier. *Data Sheet*. [Online]. Available: <http://www.minicircuits.com/pdfs/ZX60-33LN+.pdf>
- [50] J. Armstrong, "Analysis of New and Existing Methods of Reducing Inter-carrier Interference Due to Carrier Frequency Offset in OFDM," *IEEE Transactions on Communications*, vol. 47, no. 3, pp. 365-369, March 1999.
- [51] B. Ai, Z. Yang, C. Pan, J. Ge, Y. Wang, Z. Lu, "On the Synchronization Techniques for Wireless OFDM Systems," *IEEE Transactions on Broadcasting*, vol. 52, no. 2, pp. 236-244, June 2006.
- [52] Y. Yao, G. B. Giannakis, "Blind Carrier Frequency Offset Estimation in SISO, MIMO, and Multiuser OFDM Systems," *IEEE Transactions on Communications*, vol. 53, no. 1, pp. 173-183, January 2005.

REFERENCES

- [53] J. J. Busgang, "Crosscorrelation Functions of Amplitude Distorted Gaussian Signals," Research Laboratory of Electronics, M. I. T., Cambridge, MA, Technical Report no. 216, March 1952.